Abstracts of the Annual Meeting of Planetary Geologic Mappers, Tucson, AZ 2007

Edited by Leslie F. Bleamaster III[1], Tracy K.P. Gregg[2], Kenneth L. Tanaka[3], and R. Stephen Saunders[4]

[1] Planetary Science Institute, 1700 E. Ft. Lowell Rd., Suite 106, Tucson, AZ 85719.

[2] The State University of New York at Buffalo, Department of Geology, 710 Natural Sciences Complex, Buffalo, NY 14260.

[3] U.S. Geological Survey, 2255 N. Gemini Drive, Flagstaff, AZ 86001.

[4] NASA Headquarters, Office of Space Science, 300 E. Street SW, Washington, DC 20546.

Open-File Report 2007–1233

U.S. Department of the Interior
U.S. Geological Survey

U.S. Department of the Interior
DIRK KEMPTHORNE, Secretary

U.S. Geological Survey
Mark D. Myers, Director

U.S. Geological Survey, Reston, Virginia 2007

For product and ordering information:
World Wide Web: http://www.usgs.gov/pubprod
Telephone: 1-888-ASK-USGS

For more information on the USGS—the Federal source for science about the Earth,
its natural and living resources, natural hazards, and the environment:
World Wide Web: http://www.usgs.gov
Telephone: 1-888-ASK-USGS

Report of the Annual Mappers Meeting
Planetary Science Institute
Tucson, Arizona
June 28 and 29, 2007

Approximately 22 people attended this year's mappers meeting, and many more submitted abstracts and maps *in absentia*. The 2007 meeting was convened by Tracy Gregg, Les Bleamaster, Steve Saunders, and Ken Tanaka and was hosted by David Crown and Les Bleamaster of the Planetary Science Institute (PSI) in Tucson, Arizona. Oral presentations and poster discussions took place on Thursday, June 28 and Friday, June 29. This year's meeting also included a unique opportunity to visit the operations centers of two active Mars missions; field trips to the University of Arizona took place on Thursday and Friday afternoons.

Outgoing Geologic Mapping Subcommittee (GEMS) chairperson, Tracy Gregg, commenced the meeting with an introduction and David Crown followed with a discussion of logistics and the PSI facility; Steve Saunders (Planetary Geology and Geophysics Discipline Scientist) then provided a brief program update. Science presentations kicked off with Venus mapper Vicki Hansen and graduate students Eric Tharalson and Bhairavi Shankar of the University of Minnesota, Duluth, showing a 3-D animation of the global distribution of tesserae and discussing the implications, a progress report for V-45 quadrangle mapping, and a brief discussion of circular lows. Les Bleamaster (PSI) followed with a progress report on mapping of the V-50 quadrangle and the 1:10M Helen Planitia quadrangle. David Crown (PSI) concluded the Venus presentations with a discussion of progress made on the V-30 quadrangle. The remainder of Thursday's presentations jumped around the Solar System including Mars, Io, and Earth. Ken Tanaka of the U.S. Geological Survey (USGS) began the afternoon with a general discussion of the status of the planetary mapping program at USGS. Buck Janes (University of Arizona) provided background information about the Mars Odyssey Gamma Ray Spectrometer (GRS) and presented some new element maps, which may be useful for geologic mapping. Dave Williams of Arizona State University reported on the progress of his global Io map and James Dohm (University of Arizona) discussed results of terrestrial remote mapping studies. Thursday afternoon, the mappers were given a tour of the High Resolution Imaging Science Experiment (HiRISE) operations facility and were given some basic information about how the images are obtained, processed, and publicly released.

With official GEMS transition completed at lunch on Thursday, incoming GEMS chair Leslie Bleamaster took the reigns of Friday's meeting. Science presentations began with Ken Tanaka discussing 1:20M-scale global and 1:2M-scale polar mapping of Mars. Jim Zimbelman (Smithsonian Institution) described his 1:1M Medusae Fossae map (MC-8 SE), which is nearing completion, and new mapping (MC-16 NW and MC-23 NW) to further evaluate the Medusae Fossae. Brent Garry, also of the Smithsonian Institution, presented work on Ascraeus Mons. Peter Mouginis-Mark (University of Hawai‘i) reported progress on his 1:200K and larger maps of Tooting crater and of the Olympus Mons summit caldera. Laszlo Keszthelyi (USGS) presented mapping of Athabasca

Valles, with much of the credit going to Windy Jaeger. Jim Skinner (USGS) introduced a new mapping project including nine MTM quadrangles in the Utopia Planitia region. Tracy Gregg finished off the day's science presentations with discussion of Hesperia Planum. After discussion was complete, the group once again traveled to the University of Arizona - this time for a tour of the Mars Phoenix operations center. Principal Investigator Peter Smith beamed as he led mappers through the multi-million dollar facility.

A main topic of discussion throughout the entire meeting was that of nomenclature, specifically how to classify the individual depressions at the tops of volcanoes. Paterae, as has been used for Mars, Venus, and Io, was suggested, but introduces several problems with the classical and literal usage of the term over the past few decades. The group proposed that crater, like it is used for terrestrial volcanoes, would be the most appropriate term and suggested that GEMS, along with Jenny Blue (USGS), approach the IAU to discuss this issue further.

The next mappers meeting will be held in Flagstaff, at the U.S. Geological Survey, tentatively on June 19 and 20, 2008.

CONTENTS

Venus

Galilean Satellites

Global Geologic Map of Europa
T. Doggett, P. Figueredo, R. Greeley, T. Hare, E. Kolb, D. Senske, K. Tanaka, and S. Weiser

The Global Geologic Map of Ganymede
G.W. Patterson, J.W. Head, G.C. Collins, R.T. Pappalardo, L.M. Procter, and B.K. Lucchitta

The Global Geologic Map of Io: Approach and Mapping Status
D.A. Williams, L.P. Keszthelyi, P.E. Geissler, W.L. Jaeger, T.L. Becker, D.A. Crown, P.M. Schenk, and J.A. Rathbun

Moon

Use of Clementine UVVIS and NIR Data for Lunar Geologic Mapping
L.R. Gaddis

Remote Sensing Studies of Copernicus Rays: Implications for the Calibration of the Lunar Stratigraphic Column
B.R. Hawke, T.A. Giguere, L.R. Gaddis, B.A. Campbell, D.T. Blewett, J.M. Boyce, J.J. Gillis-Davis, P.G. Lucey, C.A. Peterson, M.S. Robinson, and G.A. Smith

Mars

Geology of MTM Quadrangles -40277, -40272, -45277, and -45272, Eastern Hellas Planitia, Mars
L.F. Bleamaster III and D.A. Crown

Geologic Map of MTM 35337, 40337, and 45337 Quadrangles, Deuteronilus Mensae Region of Mars
F.C. Chuang and D.A. Crown

Mapping Margaritifer Terra: MTMs -15017, -20002, -20007, -20017, -20022, -25002, -25007
C.M. Fortezzo, K.K. Williams and J.A. Grant

Mapping Hesperia Planum, Mars
T.K.P. Gregg and D.A. Crown

Hydrologic and Volcanic Evolution of Athabasca Valles, Mars: The First Step to Geologic Mapping at 1:500,000 Scale
L. Keszthelyi, W. Jaeger, and K. Tanaka

Geologic Mapping of the Martian Impact Crater Tooting
P. Mouginis-Mark

Geologic Mapping of the Olympus Mons Caldera
P. Mouginis-Mark

Final Map Results of the Olympia Cavi Region of Mars (MTM 85200): Geologic Units and History
J.A. Skinner, Jr. and K. Herkenhoff

Geology of the Southern Utopia Planitia Highland-Lowland Boundary Plain: Current Understanding and First Year Mapping Plan
J.A. Skinner, Jr., K.L. Tanaka, and T.M. Hare

New Global Geologic Map of Mars
K.L. Tanaka, J.M. Dohm, T.M. Hare, R.P. Irwin III, E.J. Kolb, and J.A. Skinner, Jr.

Recent Geologic Mapping Results for the Polar Regions of Mars
K.L. Tanaka and E.J. Kolb

Margaritifer Terra Quadrangles -20012 and -25012: Reviewed and Submitted
S.A. Wilson, J.A. Grant, and C.M. Fortezzo

Geologic Mapping of the Medusae Fossae Formation on Mars (MC-8 SE)
J.R. Zimbelman

Other

Remote Geologic Mapping of Lunar Crater Volcanic Field, Nye County, Nevada: a Test for Planetary Geologic Reconnaissance
J.M. Dohm, K.L. Tanaka, J.A. Skinner, Jr., L.A. Crumpler, and T.M. Hare

Geoscience Data Visualization Systems Applied to Planetary Geological Mapping
J.W. Head, Prabhat, A.S. Forsberg, A.T. Basilevsky, M.A. Ivanov, J.L. Dickson, C.I. Fassett, J.S. Levy, G.A. Morgan, and P.S. Kumar

GEOLOGIC MAPS OF SHIMTI TESSERA (V-11) AND VELLAMO PLANITIA (V-12), VENUS

J.C. Aubele, New Mexico Museum of Natural History & Science, Albuquerque, NM jayne.aubele@ state.nm.us

Introduction. Two quadrangles in the Niobe Planitia region have been mapped as part of the Venus geologic mapping effort. Shimti Tessera (V-11) and Vellamo Planitia (V-12) are adjacent quadrangles located in the northern hemisphere of Venus. V-11 extends from 25° to 50° N and 90° to 120° E, and V-12 extends from 25° to 50° N and 120° to 150° E.

Shimti Tessera (V-11). This quadrangle includes Tilli-Hanum Planitia in the north, a portion of Akkruva Colles in its northeast quadrant, and Niobe Planitia in its southeast and south-central regions. Shimti and Kutue Tesserae cover portions of the central and southeastern part of the quadrangle. Three named coronae within the quad are: Eurynome Corona, Metra Corona, and Maa-Ema Corona. Near the northern boundary of the quad are two named volcanic centers: Kurukulla Mons and Hiei Chu Patera (mapping has shown that flows originating from the patera clearly overlay material associated with Kurukulla Mons). Named impact craters include: Manzolini, Antonina, Irina, Vallija, Moses, and Cather, and several additional unnamed impact craters have been mapped within the quad. Medeina Chasma enters from the WNW, Friagabi Fossae enters from the north, and Uni Dorsa extends NNW-SSE across the boundary between V-11 and-V12.

Vellamo Planitia (V-12). Akkruva Colles also extends across the V-11 and V-12 boundary to form the extreme northwestern portion of V-12. Ananke Tessera occurs in the north-central portion of the quad; however, most of V-12 consists of lowland plains – Vellamo Planitia in the northeast and Llorona Planitia in the southeast. Two named coronae within the quadrangle are: Boann Corona and Cauteovan Corona. Named impact craters include: Vallija (on the boundary between V-11 and V-12, Nijinskaya, MacDonald, Kollwitz, Regina, Taglioni, Polina, Almeida, Irene, Laura, Valentina, and Barto. Nephele Dorsa is oriented north-south in Vellamo Planitia and and Frigg Dorsa occurs in the extreme northeast corner of the quad.

Description of Stratigraphic Units.

Tessera. In both V-11 and V-12, Tessera material (t) is interpreted to be the stratigraphically oldest unit, and is embayed by other units. Tessera material is radar bright and consists of at least two sets of intersecting ridges and grooves; it has been referred to as complex ridged terrain [1,2].

Densely lineated plains material (pdl), identical to the unit defined by Ivanov & Head in V-13 [3], is a minor unit in V-12 but covers more area within V-11, and appears to be spatially associated with tessera in most cases. This unit is characterized by parallel and subparallel lineaments (dominantly fractures) that are generally aligned in a single direction. Mapping of V-11 provides strong observational evidence that pdl may be interpreted to be partially flooded or resurfaced margins of tessera terrain.

Ridged and grooved plains material (prg), identical to the unit defined in V-13 [3], is characterized by sets of relatively broad ridges, arranged in linear belts. As Ivanov and Head stated: "although defined by structural elements (arches and ridges), this unit exhibits consistent characteristics and stratigraphic relationships and can be mapped as a material unit" [3]. In both V-11 and V-12, this unit is of minor areal extent and includes Uni Dorsa, Nephele Dorsa, and Frigg Dorsa.

Shield plains material (psh). During analysis of the Venera 15/16 data [1], some regions on Venus were recognized as consisting of extensive areas of small hills interpreted to be volcanoes, and were given the feature name "colles" (defined as an area of small hills or knobs) by the Venus nomenclature subcommittee of the I.A.U. During initial analysis of the Venera data and subsequent analysis of Magellan [4], these regions were confirmed as areas of abundant small, predominantly shield-type, volcanoes occurring over extensive areas rather than in the well-defined, relatively small, local clusters called shield fields. One of these regions is Akkruva Colles, first described by Schaber [5] as a region of abundant small volcanoes.

Quadrangle V-12 was mapped and reports were presented in the mid-late 1990s [6]. The reports included the description and interpretation of a new unit in V-12, the "shield plains" or "Akkruva shield plains," designated as psh in the original map (mid-90s) and in the current submitted map. The geologic unit described from V-12 is a plains unit which contains almost all of the small volcanoes in the Ananke Tessera area. The type example of this unit is located at 43N, 131.5E, and consists of an *average* density of small volcanoes numbering $4500/10^6 km^2$ in association with plains material of intermediate radar backscatter. Unit Psh exhibits consistent characteristics and stratigraphic relationships within V-12, consistently overlying tessera in this region and directly and consistently overlain and embayed by wrinkle ridged plains material. It is interpreted as a distinctive plains unit erupted by, or in association with, small volcanoes, and a useful local to regional stratigraphic marker. Mapping of V-11 has extended the significance and extent of the unit; it has been mapped over an area of $2.3X10^6 km^2$ in V-11 and V-12. Other mappers have also identified the continuation of this shield plains unit into adjoining quadrangles [3,7]. Hansen's description of a thin, locally discontinuous layer that is lace-like in appearance [7] is an apt description of the unit as mapped. Ivanov and

Head [3] have shown that the unit is much more extensive areally than was initially assumed.

Wrinkle ridged plains material (pwr) covers much of V-12 and V-11; the unit is characterized by relatively homogeneous plains material with few associated small volcanoes and many wrinkle ridges in parallel or orthogonal patterns. The plains are analogous to the ridged unit on Mars [8] and interpreted to be regional volcanic plains subsequently deformed by ridge structure.

In V-12, two units of pwr can be defined, both of which are younger than the shield plains (psh), with the lower unit (pwr_1) mottled to radar bright and the upper unit (pwr_2) radar dark. This is not consistent with the plains units mapped in adjacent quadrangles V-4 and V-13 [3] and may be a local stratigraphic relationship, where (pwr_2) in V-12 is correlative with (pwr_1) mapped regionally in surrounding quads.

Wrinkle ridged plains material in V-11 is also consistently younger than psh but is difficult to divide into two consistent and well-defined units. In V-11, wrinkle ridged plains has been mapped as a complex unit consisting of regional radar dark to intermediate plains and local radar bright contributions from local volcanic centers.

Lobate plains material (pl) and *digitate plains material (pd)* form local units, in both V-11 and V-12, primarily associated with mapped volcanic centers, including Hiei Chu Patera and an unnamed and newly mapped patera at 25°N, 115°E. These units are characterized by plains with sinuous to lobate to digitate radar bright patterns interpreted to be volcanic flow fields that postdate the emplacement of pwr. A flow field has also been identified in association with a cluster of small shields located between Shimti Tessera and Eurynome Corona at 27.5°N, 95°E.

Streaked plains material (pst) in V-12 is interpreted to be aeolian aggradational or degradational resurfacing of the pre-existing plains terrain (pwr_1)

Impact craters have been mapped, where possible, by two units: undivided crater floor, wall, rim and continuous ejecta (c); and outflow deposits (cf). Several craters are characterized by radar dark material or a circular pattern of radar dark and bright material.

In most cases, the *coronae* in both quads are defined solely by structural lineations; however, Boann Corona in V-12 and an unnamed and newly mapped corona-like structure at 27°N, 141° are partially delineated by mappable patches of densely lineated plains material (pdl).

Observations of Akkruva Shield Plains, V-11 and V-12. The Akkruva shield plains material is characterized by abundant small shield-shaped hills ranging from a few kilometers in diameter to approximately 20 km, and associated plains apparently formed by coalesced point-source eruptions. Ten (10) larger volcanic edifices, classified as intermediate volcanoes, occur within the Akkruva shield plains, but the majority of the hundreds to thousands of individual edifices are small and relatively consistent in diameter-range. Shields commonly occur in clusters, giving the unit a locally hilly texture. In fact, the preliminary map of V-12 called this unit "hilly mottled plains material." Individual shields are radar dark or radar bright, circular features, with or without a central pit. At times, they are defined by a "halo" of flank material encircled by younger ridged plains material surrounding an individual edifice or by a network of structural ridges surrounding an edifice. Evidence for structural deformation after emplacement occurs in V-11 where a small fracture visibly cuts through one of the shield edifices. A cluster of shields at 37°N, 96°E in V-11 is clearly covered, but still visible in outline, beneath a radar bright surficial material associated with a dark "spot" impact crater. An opportunity to observe and test the differences between shield plains and shield fields also exists in V-11. One cluster of shields in the southwest corner of the quad has an associated flow field, but otherwise appears to be in the same stratigraphic position with respect to tessera as is the shield plains unit.

The entire unit is extensive, crossing the boundary between V-11 and V-12, and covering much of Tilli-Hanum Planitia and eastern Niobe Planitia. In V-12, it covers much of the region between 120° and 130°E for the entire latitude range of the quad and in V-11, it covers a wedge shaped region from 50°N, 105°E to 25°N, 120°E and then extends along the entire southern boundary of the quad and into adjacent quadrangle V-23. Patches of shield plains occur in the same stratigraphic position, always above the basal terrains, in western V-11 and eastern V-12. Similar map relations exist across V-3, V-4, V-13, V-23 and V-24 [3,7]. Mapping of these patches provides evidence for a regional shield plains unit in this particular region of Venus that is extensive and continuous, but intermittently exposed beneath younger plains units.

V-11 and V-12 provided the original definition and type example of the unit that has been subsequently also mapped by others as shield plains material. The completed geologic maps of V-11 and V-12 can now provide additional data to better understand this unit.

[1] Barsukov&others (1986) JGR 91; Basilevsky&others (1986) JGR 91 [2] Solomon&others (1992) JGR 91 [3]Ivanov&Head (2004) Geol Map of V-4, I-2792; Ivanov&Head (2005), Geol Map of V-13, I-2870; Ivanov&Head (in press) Geol Map of V-3 [4]Guest et al. (1992) *JGR* 97; Head et al. (1992) *JGR 97*; Crumpler et al. (1989) *Sci 246*; Aubele&Slyuta (1990) *EMP, 50/51*; Garvin&Williams (1990), *GRL17*; Aubele&Crumpler (1992) *International Colloquium on Venus*, LPI Contrib. 789; Aubele (1993) *LPSC24*; Crumpler et al (1997) *in Venus II* UofA Press; Crumpler&Aubele (2000) *in* H. Sigurdsson et al. *Encyl of Volcanology* Academic Press [5]Schaber (1988) LPSC19 [6]Aubele (1997) *GSA Abst. 29, no. 6,* A-138; Aubele (1996) *LPSC 27*, 49; Aubele (1995) *LPSC 26*, 59; Aubele (1994) *LPSC 25, 45*; Aubele (1993) *GSA Abst. 25*, A-221 [7]Hansen (2005) *GSA Bull 117*, no.5/6; Hansen (2003) *LPSC* 34; Hansen (in press) Geol Map of V-23; Lang&Hansen (in press) Geol Map of V-24 [8] Scott&Tanaka (1986) Geologic Map of the Western Hemisphere Mars, USGS Map I-1802-A

GEOLOGY OF THE WESTERN PART OF THE V-36 THETIS REGIO QUADRANGLE. A. T. Basilevsky[1,2] and J. W. Head[2], [1]Vernadsky Institute of Geochemistry and Analytical Chemistry, RAS, Moscow, Russia, atbas@geokhi.ru, [2]Department of Geological Sciences, Brown University, Providence RI 02912 USA.

Introduction: This work is a continuation of the photogeologic mapping of the V-36 quadrangle, that is part of the USGS 1:5M planetary mapping project [1]. Here we report on mapping of the western half of this quadrangle.

Mapping Results: As a result of mapping, eleven material stratigraphic units and three structural units have been identified and mapped. The material units include (from older to younger): tessera terrain material (tt), material of densely fractured plains (pdf), material of fractured and ridged plains (pfr), material of shield plains (psh), material of plains with wrinkle ridges (pwr), material of smooth plains of intermediate brightness (psi), material of radar-dark smooth plains (psd), material of lineated plains (pli), material of lobate plains (plo), material of craters having no radar-dark haloes (c1), and material of craters having clear dark haloes (c2).

The morphologies of the material units in the study area are generally similar to those observed in other regions of Venus [2]. The youngest units are lobate plains (plo) which here typically look less lobate than in other areas of the planet. Close to them in age are smooth plains which are indeed smooth and represented by the two varieties mentioned above. Lineated plains (pli) are densely fractured in a geometrically regular way. Plains with wrinkle ridges, being morphologically similar to those observed in other regions, here occupy unusually small areas. Shield (psh) plains here are also not abundant. Locally they show wrinkle ridging. Fractured and ridged plains (pfr), which form the so-called ridge belts in other regions, are observed as isolated areas of clusters of ridged plains surrounded by other units. Densely fractured plains (pdf) are present in relatively small areas in association with coronae and corona-like features. Tessera terrain (tt) is dissected by structures oriented in two or more directions. Structures are so densely packed that the morphology (and thus nature) of the precursor terrain are not known.

Structural units include tessera transitional terrain (ttt), fracture belts (fb) and rifted terrain (rt). Tessera transitional terrain was first identified and mapped by [4] as areas of fractured and ridged plains (pfr) and densely fractured plains (pdf) deformed by transverse faults that made it formally resemble tessera terrain (tt). The obvious difference between units tt and ttt is the recognizable morphology of precursor terrain of unit ttt. Fracture belts are probably ancient rift zones [3]. Rifted terrain (rt), as in other regions of Venus, is so saturated with faults that according to the recommendation of [1] it should be mapped as a structural unit.

The lower crater material unit is represented by 5 craters, one of which, Mariko, is superposed on rifted terrain. The upper unit is represented by one splotch in the northwestern part of the mapped part of quadrangle.

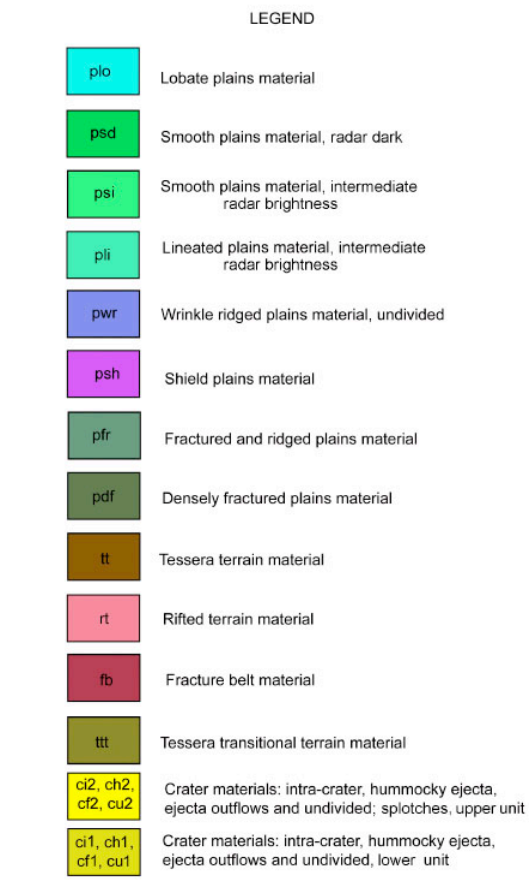

Conclusions: Our mapping analysis and results show that although the mapped units are generally similar to those observed in other regions of the planet, some of them have unusual areal abundances that imply unique aspects of the geologic history of this region. In particular, the unusually high abundance of rifted terrain (rt) and tessera transitional terrain (ttt) have interesting implications and require additional studies.

References: [1] Tanaka K. (1994) USGS Open File Report 94-438. [2] Basilevsky A. T. & Head J. W. (2000) Planet. Space Sci., 48, 75-111. [3] Banerdt et al. (1997) in Venus II, U. Arizona Press, 901-930. [4] Ivanov M. A. & Head J. W. (2001) JGR, 106, 17,515-17,556.

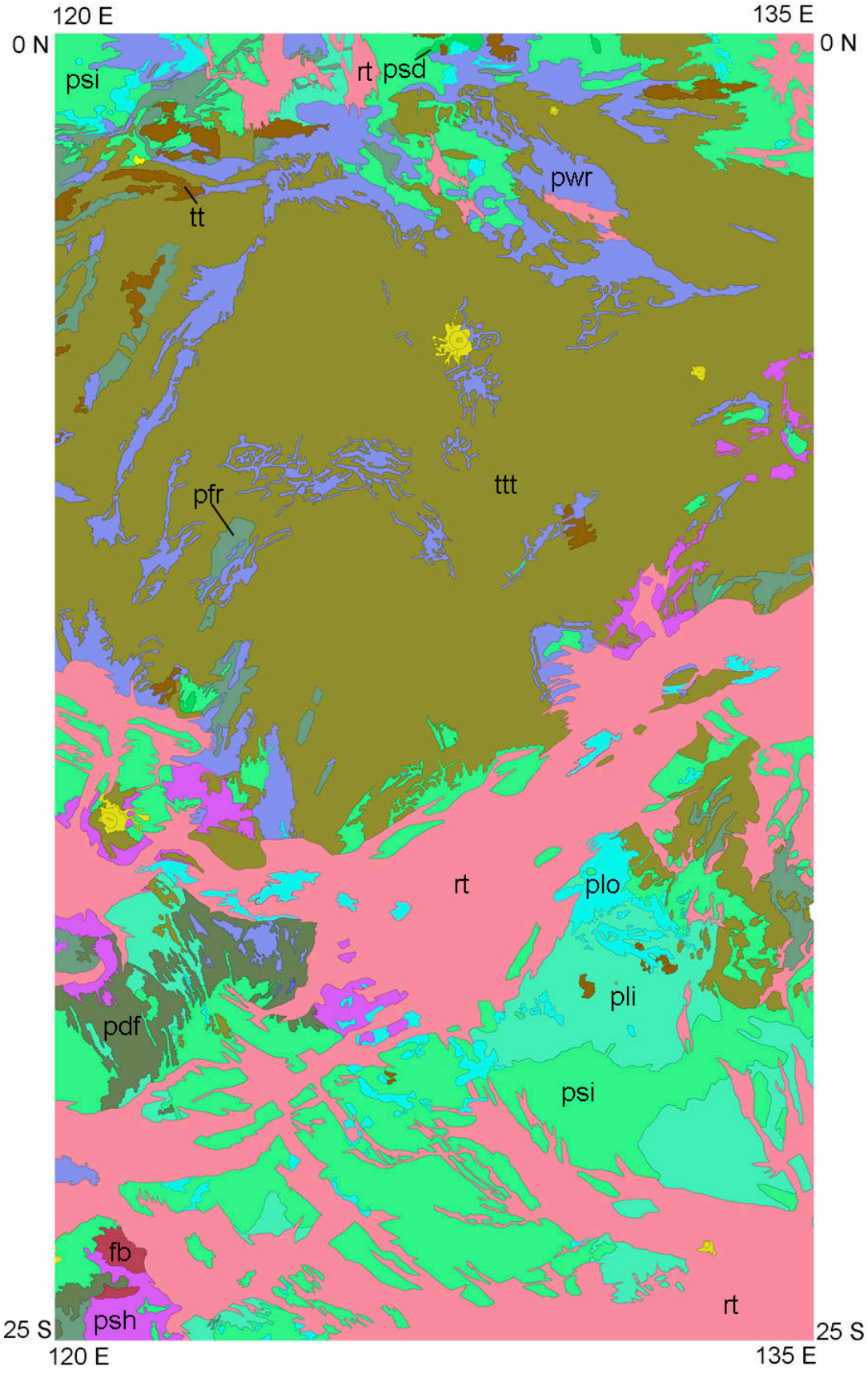
120 E
135 E
0 N
0 N
psi
rt
psd
pwr
tt
ttt
pfr
rt
plo
pli
pdf
psi
fb
psh
rt
25 S
25 S
120 E
135 E

GEOLOGIC MAPPING OF ISABELLA QUADRANGLE (V-50) AND HELEN PLANITIA, VENUS. Leslie F. Bleamaster III, Planetary Science Institute, corporate address - 1700 E. Ft. Lowell Rd., Suite 106, Tucson, AZ 85719; mailing - 3635 Mill Meadow Dr., San Antonio, TX 78247; lbleamasPSI@satx.rr.com

Introduction. The Isabella Quadrangle (25-50°S, 180-210°E – Figure 1) lies to the south of the eastern extent of the Diana-Dali Chasmata system and Atla Regio, which contains the volcanoes Sapas, Maat and Ozza Montes. Isabella Quadrangle is host to numerous coronae and small volcanic centers (paterae and shield fields), focused (Aditi and Sirona Dorsa) and distributed (penetrative north-south trending wrinkle ridges) contractional deformation, and radial and linear extensional structures, all of which contribute materials to and/or deform the expansive surrounding plains (Nsomeka and Wawalag Planitiae). Specific questions posed for geologic mapping of the V-50 quadrangle include: 1) What and where are the source locations for the regionally dominant plains materials (e.g., coronae, paterae, shield fields, rifts and fissures)? 2) What is the relationship, if any, between focused (deformation belts) and distributed (wrinkle ridges) contractional strain and local/regional volcanism? 3) What role does structural reactivation play in deformation belt and wrinkle ridge development? 4) What are the spatial and temporal relationships between craters with outflows and volcanic constructs, and to what extent are crater outflows directly related to impact processes versus post-impact modification?

In addition to V-50, this project is mapping Helen Planitia at 1:10M-scale (0-57°S/180-300°E – Figure 2), which covers over 70 million square kilometers (approximately 1/8th) of the surface of Venus, expresses 10 kilometers of relief from the highlands of Atla and Phoebe Regiones to the depths of Parga Chasmata and vast Helen lowlands, and exposes areas representing the entirety of Venus' preserved geologic history as determined by Average Surface Model Ages (ASMA) [1 and 2]. Geologic mapping will afford the opportunity to synthesize previous mapping efforts and place existing geologic interpretations V-39, V-40, and V-59 [3 - 5], and the diversity of other features into a coherent geologic history in order to help address the geodynamical and thermal evolution of the region across several physiographic provinces, a substantial number of which may be indicative of recent and/or present activity (three volcanic rises, two major chasmata, hundreds of coronae and paterae, and thousands of small volcanic constructs) [1, 6, and 7].

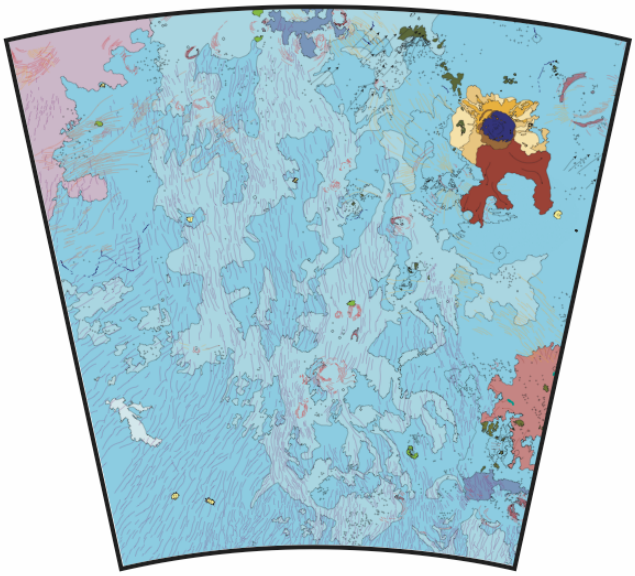

Figure 1. V-50, Isabella Quadrangle (25-50°S, 180-210°E). Mapping in progress.

Isabella Quadrangle (V-50). Isabella Quadrangle is dominated by regional plains (blues above), which have tentatively been divided into two members (regional plains, members a and b) based on unimpressive backscatter variations, which result in very inconsistent mottled characteristics of both members. The regional plains have been deformed by penetrative north-trending wrinkle ridges and east-striking fractures, and several broad north-trending topographic undulations, suggesting that both members were in place prior to east-west shortening. Most noteworthy is that member b (lighter backscatter, light blue above) lacks channel forms (canali), and is found on the trailing side of some wind blown features and topographic obstacles. It will be important to comprehensively address the spatial relationship between these two regional plains members and the preservation of channel forms, shield edifices, wrinkle ridges and their orientations, wind-blown features, all SAR

cycles, topography, reflectivity, and emissivity. Further evaluation will help determine if the member a and b boundary as currently delineated is a true unit contact or just a radar facies boundary related to surficial deposits of a mobile material.

Helen Planitia. Current efforts are focused on mapping the distribution and orientation of structural trends and flow morphologies, and the demarcation of flow unit boundaries based on primary and secondary surface morphologies. To date, several hundred radial and circular features (both digitate and lobate flow fields and fracture, fault, and ridge suites) have been documented and match closely the existing coronae and/or volcanic landform databases [8 and 9]; however, not all correspond directly with defined Type I or Type II coronae, or other named volcanic landforms.

The majority of these radial/circular features lie within a few hundred kilometers of the Parga Chasmata rift system (see below), marking a southeast trending line of relatively young volcano-tectonic activity. Although some very localized embayment and crosscutting relationships display clear relative age relations between centers of activity, the majority of Parga Chasmata volcanism and tectonism overlaps in time from Atla Regio in the west to Themis Regio in the east, extending ~10,000 linear kilometers. Atla and Themis Regiones (rift-dominated and coronae-dominated volcanic rises, respectively [10]) lie in characteristically different ASMA regions (Atla-young; Themis-intermediate); however, preliminary mapping has not revealed any significant 'stratigraphic' support for these model age differences.

References: [1] Phillips, R.J. and Izenberg, N.R. (1995) *Geophys. Res. Lett., 22,* 1517-1520. [2] Hansen, V.L. and Young, D.A. (in press) *GSA Special Paper.* [3] Brian, A.W. et al., (2005) *USGS Sci. Inv. Map 2813.* [4] Chapman, M.G. (1999) *USGS Geo. Inv. Sers. I-2613.* [5] Johnson, J.R. et al., (1999) *USGS Geo. Inv. Sers. I-2610.* [6] Herrick R.R., and Phillips, R.J. (1994) *Icarus, 111,* 387-416. [7] Price and Suppe (1994) *Nature, 372,* 756-759. [8] Crumpler L.S. et al., (1997) in *Venus II,* 697-756. [9] Stofan E.R. et al., (2001) *Geophys. Res. Lett., 28,* 4267-4270. [10] Smrekar, S.E., et al., (1997) in *Venus II*, 8445-878.

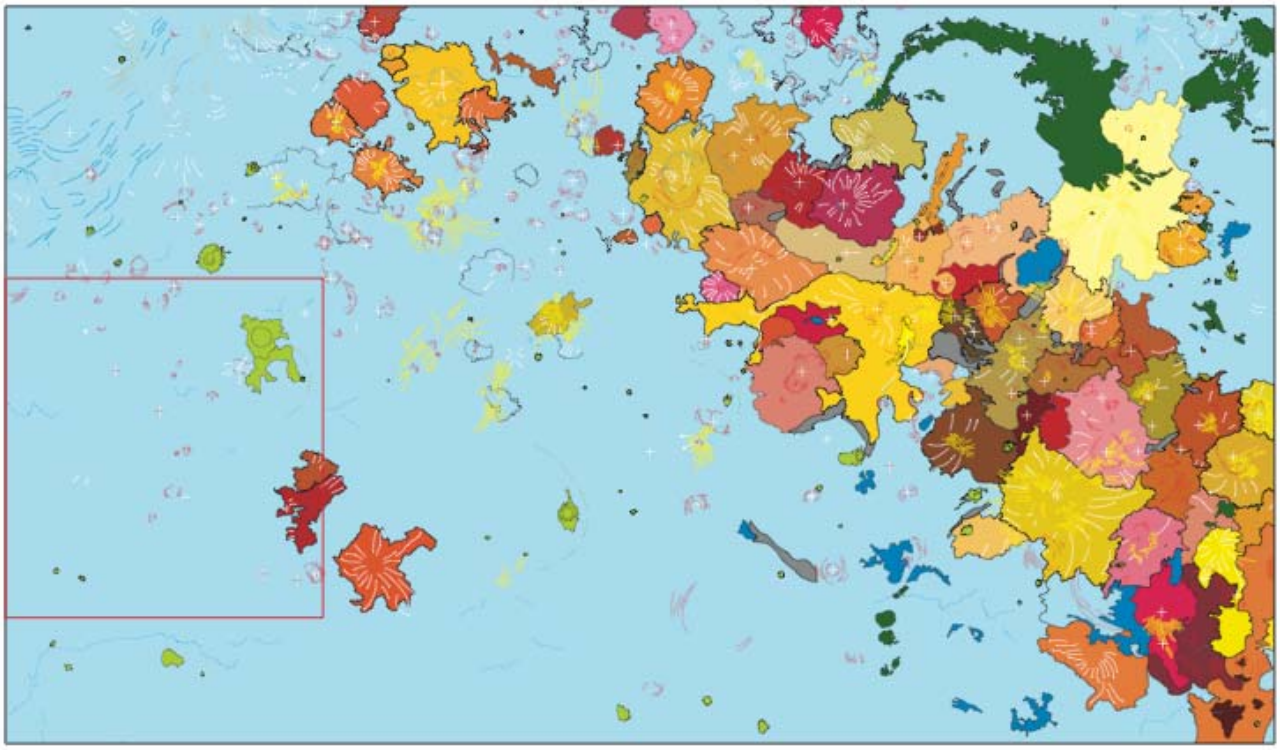

Figure 2. Preliminary geologic map of the Helen Planitia Regional Study Area (0-57°S, 180-300°E; 1:10M-scale). Volcanic flows and deformation related to Parga Chasmata dominate the eastern portion of the map area (browns, reds, oranges, and yellows) and embay/crosscut Phoebe Regio (green) in the northeast. Background blue has not been mapped at this scale. Red box to the west delineates 1:5M-scale V-50 quadrangle boundary (Figure 1).

GLOBAL MAPPING OF VENUS' RIBBON TESSERA TERRAIN: PRELIMINARY RESULTS.

V. L. Hansen[1], T. Nordberg[1] and, I. López[2], [1]Department of Geological Sciences, University of Minnesota Duluth, Duluth, MN 55812; [2]Área de Geología, Escuela Superior de Ciencias Experimentales y Tecnología. Universidad Rey Juan Carlos, 28933. Móstoles, Madrid, Spain (vhansen@d.umn.edu)

Introduction: Venus displays a rich variety of exogenic and endogenic structures that provide clues to its history. Currently, widely accepted hypotheses that dominate textbooks and popular science call for a globally extensive catastrophic volcanic flooding event to bury 100-80% of Venus' surface with 1-3 km lava in 10 to 100 m.y. time. Flooding would create a crater-free global surface in the form of lowland plains, effectively erasing (through burial) the recorded geologic history prior to flooding at ~750 Ma. Subsequent to flooding, colliding bolides created the suite of ~970 well preserved impact craters, which display a near random distribution across Venus. Catastrophic volcanic resurfacing hypotheses call for an ~1-3 km thick layer in order to bury pre-existing impact craters; this prediction is tested through global mapping of ribbon tessera terrain, and construction of isopach surfaces. Ribbon tessera terrain reportedly formed as a globally extensive layer prior to catastrophic flooding.

Such a map will allow us to identify global patterns of tessera-terrain outcrops and fabric patterns in order to identify local, regional or global patterns. Such patterns will provide clues to tessera terrain formation. In addition this database will allow us to test such hypotheses as global to near global catastrophic resurfacing as tessera terrain should form the basal layer for widespread flooding. Ribbon-terrain characterizes highland plateaus, but it also occurs in small to large kipukas scattered across much of the Venusian lowlands.

Method: Using NASA Magellan SAR images we are creating a geologic map of ribbon tessera terrain at a global scale. Tessera terrain outcrops and structural patterns (ribbons and folds) are mapped across individual georeferenced VMap quadrangles using linked data files in an Adobe Illustrator environment. We transfer the results to the ArcGlobe GIS environment using Map Publisher. Once in the ArcGlobe GIS environment data is projected global allowing us to discount projection issues and observe outcrop and structural patterns across VMap boundaries. In addition the data can be compared to other global data sets.

Data layers include USGS VMap SAR image bases, and synthetic stereo images (created by combining USGS SAR images and Magellan altimetry using macros developed by D.A. Young). SAR and synthetic stereo images are consulted in both normal and inverted modes. Most VMap quadrangles were examined by each of the co-authors for ribbon tessera terrain identification. To date we do not have SAR data for V-62, the south pole region, and we lack synthetic stereo for V-1, the north pole region. Despite the lack of synthetic stereo data for the north pole, we have been able to conduct ribbon tessera terrain mapping and this region is included on the global map.

The global tessera map is a work in progress. Tessera terrain on all VMAPs have been identified and transferred to the ArcGlobe environment. Numerous boundary mismatches are currently being addressed, while the map of ribbon and fold trends is in progress. About twenty five percent of the VMap quadrangles have structural trends mapped, with the northern hemisphere receiving the most attention to date.

Results to date: Perhaps the most striking result is the uneven global distribution of ribbon tessera terrain, with the second most striking result being the detailed patterns that might emerge from this style of mapping.

Tessera terrain is distributed across the northern hemisphere in large to small outcrops. The region of Lakshmi Planum marks the single largest region that is relatively tessera free (we are still debating whether small exposures within Lakshmi represent ribbon tessera terrain or not). In places the outcrops mark bead-like necklaces tracing out arcs and circular features 1200-1800 km in diameter. Elsewhere tessera outcrops as quite large extensive regions. Despite the high concentration of tessera terrain only Fortuna and Tellus Tesserae occur across a north polar centered view, as recognized crustal plateaus.

The southern hemisphere view is strikingly different. Crustal plateau Alpha Regio lies along

the perimeter of a south pole centered global view, and elsewhere tessera terrain occurs as small outcrops in chains of clusters, but representing only a small percent of the southern hemisphere surface.

The eastern and western hemisphere views are also quite different from one another. The eastern hemisphere (1-180°) is dominated by crustal plateaus Tellus Tesserae, and W. Ovda, E. Ovda and Thetis Regiones, and an extensive circular tract of ribbon tessera west of W. Ovda. Elsewhere tessera exposures define arcs to circular chains, as well as scattered to clustered groups. Although exposures are more dominate in the northern hemisphere in this view, there are exposures across the southern hemisphere. The western hemisphere (180-360°) lacks the obvious crustal plateaus and associated huge tracts of tessera terrain; tessera chains and numerous small, scattered and regionally dispersed outcrops of tessera mark this view.

Globally three styles of outcrop patterns emerge from the data to date: 1) large quasi-circular tracts of tessera similar to crustal plateaus, although not preserved as elevated plateaus; 2) long curvilinear arcs, 100s to 1000+ km long with varying widths up to 250-400 km; the arcs in general have long aspect ratios, in strong contrast with the more blob-like tracts; and 3) small scattered, yet grouped exposures as small as tens of km^2, yet occurring across regional areas covering over 2 to 3 million km^2.

Across the global view cross-cutting relations seem likely given the intersecting or overlapping nature of the outcrop arcs. The addition of structural trends to the global map will provide further constraints to identify temporal patterns and relations that might exist. Structural mapping to date indicates that tessera structural fabrics generally parallel the arcuate outcrops with fold ridges parallel to the arc, and ribbon trends typically normal to the arc. Across the dispersed small outcrops, structural patterns are consistent between outcrops across extensive regions.

Although SAR data strictly constrain only surface geometry, the patterns preserved in SAR images can be used to construct three-dimensional views in the same way that terrestrial map patterns reflect subsurface rock patterns. The dispersed nature of small isolate outcrops, taken together with the detailed digitate contact between tessera terrain and cover material can allow us to project regional subsurface slopes of tessera terrain and cover material. Based on relations gleaned from dispersed outcrops within V-23, we calculated a moderately steep slope between underlying ribbon tessera and cover material. We used a particularly steep slope in order to maximize the estimate of cover material. Using this slope (0.4°) we created global isopach surfaces marking the projected location of 1 km and 3 km-thick cover layer above the ribbon tessera terrain. In most places the slopes are significantly shallower, and thus the isopach surfaces represent a conservative view of those regions of Venus that could harbor cover above ribbon tessera thicker than 1 km (and 3 km). Given that volcanic catastrophic resurfacing hypotheses call for 1-3 km thick flows emplaced above ribbon tessera terrain, this analysis should provide a valid test of the catastrophic volcanic resurfacing.

Isopach surfaces for 1 and 3 km of cover above tessera terrain indicate that portion and distribution of the surface of Venus that could harbor buried impact craters would not result in Venus' current near random impact crater distribution. Visual inspection indicates that less than 50 percent of the northern hemisphere (polar view) could have >1 km thick cover above a basal tessera terrain layer (tessera terrain need not exist everywhere in the subsurface, in this case the 'cover' would exceed 1 km); similarly the eastern hemisphere view indicates >50 percent surface covered by 1-km flows. In contrast, the southern and western hemispheres show significantly more burial possible, with perhaps 90 percent of the southern hemisphere (south pole view) capable of burial beneath 1-km, and 60-70 percent of the western hemisphere. The western hemisphere includes volcanic rises Atla, Beta and Themis Regiones, which might well contribute to more significant burial of basal tessera terrain. Small isolated exposures of ribbon tessera terrain across this region suggest that tessera originally existed across large regions, and has been subsequently buried or otherwise removed. Both the low amounts of regions in the northern and eastern hemisphere that could be buried, and the striking

global differences indicate that catastrophic resurfacing hypotheses are incompatible with the global ribbon tessera terrain mapping. Mapping of structural trends within ribbon terrain may provide critical clues to tessera terrain formation. Ribbon and fold trends mapped to date indicate coherent patterns across and between isolated tessera outcrops, providing strong evidence that Venus likely preserves a geologic record (and history) that extends further back in time than widely appreciated.

GLOBAL GEOLOGICAL MAP OF VENUS: PRELIMINARY RESULTS. M. A. Ivanov, Vernadsky Institute, RAS, Moscow, Russia (Mikhail_Ivanov@brown.edu).

Introduction: The Magellan SAR images provide sufficient data to compile a geological map of nearly the entire surface of Venus. Such a global and self-consistent map would serve as an important document to address many key questions in the geologic history of Venus. 1) What units/structures characterize the surface [1-3]? 2) What volcanic/tectonic regimes do they represent [4-7]? 3) Did these regimes occur globally or locally [8-11]? 4) What are the relative time relationships among the units [8]? 5) Are these relationships consistent regionally or globally [8-10]? 6) What is the absolute timing of formation of the units [12-14]? 7) What is the history of the long-wavelength topography and geoid? 7) What model(s) of heat loss and lithospheric evolution [15-21] does this history represent? The ongoing USGS program of Venus mapping has already resulted in a series of published maps at the scale 1:5M [e.g. 22-30]. These maps have a patch-like distribution, however, and are being compiled by authors with different mapping philosophies that are not always in agreement with each other in terms of mapped units and their relationships. Here the preliminary results of global geological mapping of Venus at the scale 1:10M is presented, representing the current status of a global mapping project. The map represents a contiguous area extending from 82.5°N to 22.9°S and comprises ~70% of the planet. The new map permits one to address some of the questions raised above.

Mapping procedure: For the initial mapping analyses, images of high resolution (C1-MIDR and F-MIDR) were used to define units [1,9,11]. The map was then compiled on C2-MIDR sheets, the resolution of which permits identifying the basic characteristics of previously defined units. The higher resolution images were again used during the mapping to clarify geologic relationships. When the map was completed, its quality was checked using published USGS maps [e.g., 22-30] and the catalogue of impact craters [31]. The results suggest that the mapping on the C2-base provided a high-quality map product.

Units and structures: A set of material units and tectonic structures describes the geological configurations throughout the map area (Fig. 1). The complete stratigraphic column consists of the following units (from older to younger): *Tessera* (t) displays multiple sets of tectonic structures. *Densely lineated plains* (pdl) are dissected by numerous subparallel narrow and short lineaments. *Ridged plains* (pr) commonly form elongated belts of ridges. *Mountain belts* (mt) resemble ridge belts and occur around Lakshmi Planum. *Shield plains* (psh) have numerous small volcanic edifices on the surface. *Regional plains* were divided into the lower (pr_1) and the upper (pr_2) units. The lower unit has uniform and relatively low radar albedo; the upper unit is brighter and often forms flow-like occurrences. *Shield clusters* (sc) are morphologically similar to psh but occur as small patches that postdate regional plains. *Smooth plains* (ps) have uniform and low radar albedo and occur near impact craters and at distinct volcanic centers. *Lobate plains* (pl) form fields of lava flows that are typically undeformed by tectonic structures and are associated with major volcanic centers.

Specific structural assemblages accompany the material units: *Tessera-forming structures* (ridges and grooves), *ridge belts*, *groove belts* (structural unit gb), *wrinkle ridges*, and *rift zones* (structural unit rt). The tessera-forming structures and ridge belts predate vast plains units such as psh and rp_1. Groove belts postdate tessera and ridge belts. Shield plains and regional plains mostly embay groove belts. In places, groove belts appear to form contemporaneously with the vast plains units. Wrinkle ridges deform all material units predating smooth and lobate plains. Rift zones appear to be contemporaneous with sc, pl, and ps and cut older units.

Crater statistics: Two factors, the atmosphere screening [32-34] and the observational bias [35], appear to affect the statistics of the smaller (<16 km) craters. For the larger craters these factors are negligible and the larger craters were used to estimate the crater density on mapped units. The shape and size of occurrences of units may also affect the crater statistics on Venus where the total number of craters is small. To minimize influence of this factor the crater density on large and contiguous units that have quasi-equidimensional occurrences was estimated. These units are: t, psh, rp_1, rp_2, pl, and rt; together, they cover ~84% of the surface. The mean densities (craters per $10^6 km^2$) of craters on these units are as follow: tessera: 1.046 (±0.158, one σ); shield plains: 1.004 (±0.126); regional plains, lower unit: 0.982 (±0.103); regional plains, upper unit: 0.614 (±0.140); lobate plains: 0.547 (±0.144); rifts: 0.609 (±0.173). The mean density of craters in the map area (all units) is 0.938 (±0.054). If the mean crater density corresponds to the mean surface age, T [19], then the ages of the above units as fractions of T are: tessera: 1.11T, shield plains: 1.07T, regional plains, lower unit: 1.05T, regional plains, upper unit: 0.67T, lobate plains: 0.58T, rifts: 0.67T.

These results are consistent with the mapped stratigraphic relationships and indicate that there are two groups of units: The older units (t, psh, rp1) are densely clustered around 1.1T and the younger units (rp2, pl, rt) were formed around 0.6T. The exposed area

of the older units is ~59% of the map area (the true area must be larger) and the younger units cover ~25% of the surface. Depending upon the estimates of the absolute value of T (from 750 Ma [36] through 500 Ma [37] to 300 Ma [38]), it is possible to estimate the duration of specific periods in the observable geologic history of Venus. The older units appear to form during a relatively short time, from 45 m.y (T = 750 Ma) to 18 m.y (T = 300 Ma). The minimum integrated resurfacing rate (both volcanic and tectonic) at this time was from ~4.2 to ~10.4 km^2/y. The younger units spanned a longer time and the integrated resurfacing rate during their formation was from ~1.2 to ~3.0 km^2/y. The large time gap (from 285 to 114 m.y.) between the two groups of units and the significant drop in the resurfacing rates suggest that the older and the younger units correspond to two different geodynamic regimes that were probably related to different patterns of mantle convection and lithospheric properties.

References: 1) Basilevsky, A.T. and J.W. Head, *PSS,* 43, 1523, 1995; 2) Basilevsky, A.T. and J.W. Head, *PSS*, 48, 75, 2000; 3) DeShon, H.R. et al., *JGR,* 105, 6983, 2000; 4) Head, J.W. et al., *JGR,* 97, 13153, 1992; 5) Solomon, S.C. et al., *JGR,* 97, 13199, 1992; 6) Squyres, S.W. et al., *JGR,* 97, 13579, 1992; 7) Stofan, E.R. et al., *JGR,* 97, 13347, 1992; 8) Guest, J.E., and E.R. Stofan, *Icarus,* 139, 56, 1999; 9) Basilevsky, A.T., et al., *in: Venus II, S.W. Bougher et al. eds., Univ. Arizona Press* 1047, 1997; 10) Head, J.W. and A.T. Basilevsky, *Geology,* 26, 35, 1998; 11) Ivanov, M.A. and J.W. Head, *JGR*, 106, 17515, 2001; 12) Price, M. and J. Suppe, *Nature,* 372, 756, 1994; 13) Price, M. et al., *JGR,* 101, 4657, 1996; 14) Namiki, N. and S.C. Solomon, *Science,* 265, 929, 1994; 15) Parmentier, E.M. and P.C. Hess, *GRL*, 19, 2015, 1992; 16) Head, J.W. et al., *PSS*, 42, 803, 1994; 17) Turcotte, D.L., *JGR*, 98, 127061, 1993; 18) Arkani-Hamed, J. and M.N. Toksoz, *PEPI*, 34, 232, 1984; 19) Solomon, S.C, *LPSC (Abstr.), XXIV,* 1331, 1993; 20) Phillips R.J. and V.L. Hansen, *Science*, 279, 1492, 1998; 21) Solomatov, S.V. and L.-N. Moresi, *JGR,* 101, 4737, 1996; 22) Bender, K.C., et al., *USGS Map I-2620*, 2000; 23) Rosenberg, E. and G.E. McGill, *USGS Map I-2721*, 2001; 24) Ivanov, M.A. and J.W. Head, *USGS Map I-2684*, 2001; 25) Ivanov, M.A. and J.W. Head, *USGS Map I-2792*, 2003; 26) Ivanov, M.A. and J.W. Head, *USGS Map 2870*, 2005; 27) Bridges, N.T. and G.E. McGill, *USGS Map I-2747*, 2002; 28) Campbell, B.A. and P.G. Campbell, *USGS Map I-2743*, 2002; 29) Hansen, V.L. and H.R. DeShon, *USGS Map I-2752*, 2002; 30) Brian, A.W., et al., *USGS Map 2813*, 2005; 31) Schaber, G.G.et al., *USGS OFR 98-104*, 1998; 32) Phillips, R.J., et al., *JGR,* 97, 15923, 1992; 33) Ivanov, B.A., et al., *JGR ,* 97, 16167, 1992; 34) Herrick, R.R. and R.J. Phillips, *Icarus,* 112, 253, 1994; 35) Ivanov, M.A. and A.T. Basilevsky, *GRL,* 20, 2579, 1993; 36) McKinnon, W.B., et al., *in: Venus II, S.W. Bougher et al. eds., Univ. Arizona Press,* 1014, 1997; 37) Schaber, G.G., et al., *JGR,* 97, 13257, 1992; 38) Strom, R.G., et al., *JGR,* 99, 10899, 1994.

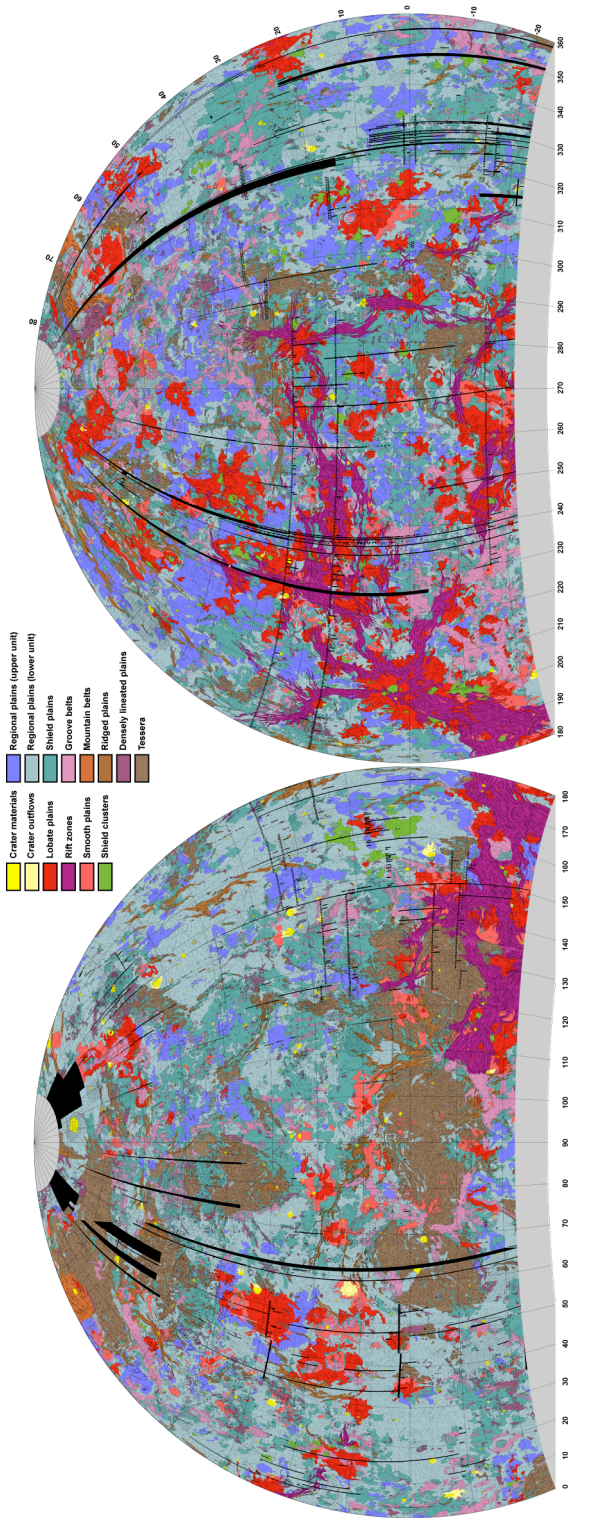

Fig. 1. Geological map of Venus. Scale is ~1:10M; Lambert equal-area projection.

GEOLOGIC HISTORY OF THE LAVINIA PLANITIA/LADA TERRA REGION, VENUS: RESULTS OF MAPPING IN THE V-55, V-61, AND V-56 QUADRANGLES. M. A. Ivanov[1,2] and J. W. Head[2]; [1]Vernadsky Institute, RAS, Moscow 119991, Russia (mikhail_ivanov@brown.edu), [2]Brown University, Providence, RI 02912, USA, [3] (james_head@brown.edu).

Introduction: Lada Terra (~300-90°E, 55-80°S, V-61 and V-56) is a region of midlands (0-2 km above MPR) that is dominated by a large dome-shaped structure. Lada hosts many coronae interconnected by belts of graben and large complexes of lava flows [1-5]. The lowland of Lavinia Planitia (~330-0°E, 25-55°S, V-55) is to the N of Lada Terra. Deformational belts of ridges and grooves and vast mildly deformed plains characterize the floor of Lavinia [6]. The pattern of deformation, topography, and gravity signature are consistent with mantle downwelling under Lavinia [6-8] and with mantle upwelling in the region of Lada Terra [9]. Thus, Lada Terra and Lavinia Planitia apparently represent contrasting geodynamic provinces, the history of which may be coupled [4]. Here we summarize results of the geological mapping in three (V-55 [10], V-61 [11], and V-56, in progress) quadrangles that cover the Lavinia/Lada region. The main goal of our study was to establish the timing and sequence of events during formation and evolution of these regions and reconstruct the major episodes of Lada Terra/Lavinia Planitia geologic history.

Topographic configuration of Lavinia Planitia and Lada Terra: Lavinia Planitia is a large basin ~1500 km across and is as deep as ~1.5 km below MPR. The deepest portion of the basin is at its S edge. The major portion of Lada Terra is within midlands. The most prominent topographic feature of Lada Terra is a broad (~1000 km) symmetric swell, the summit of which is at elevation ~3.5 km. Two regional-scale topographic features (1000s of km long, 100s of km wide, 1-2 km amplitude), an elongated depression, and a topographic ridge, concentrically outline the swell of Lada from the north and east.

Units, structures, and their stratigraphic relationships: In our mapping, we used traditional methods of unit definition [12,13] modified for radar data [14]. On this basis [14-18], we defined units and structures and mapped relations between them using F/C1-MIDR images and altimetry data. All mapped quadrangles display similar sets of material and tectonic units. Consistent age relationships allow broad stratigraphic correlations among the units. The oldest unit is *tessera (t)*, which is deformed by intersecting ridges and grooves [19-25] and embayed by less deformed materials. *Densely lineated plains (pdl)* are cut by densely packed lineaments and embay tesserae where these units are in contact. Broad (5-10 km) ridges arranged in linear belts commonly deform *ridged plains (pr)*. The belts predominantly occur on the floor of Lavinia Planitia. Abundant small (a few km) shield-like features characterize *shield plains (psh)*. The unit occurs mostly in Lavinia Planitia where it embays ridged plains. *Regional plains (rp)* consist of two units. The lower unit (rp_1) has relatively low radar backscatter and preferentially occurs in the lowlands surrounding Lada Terra. The upper unit (rp_2) has a higher radar albedo and, sometimes, lobate boundaries. Both units embay shield plains. *Lobate plains (pl)* have lobate and digitate boundaries and internal flow-like features. *Smooth plains (ps)* display morphologically smooth surfaces with uniform radar albedo. *Shield clusters (sc)* form groups of small shields similar to those of psh but with flow-like features. Materials of ps, pl, and sc preferentially occur in central Lada and embay the majority of tectonic structures.

The older contractional structures in the map area are the ridges that deform ridged plains (pr). Shield plains and regional plains embay the ridges. The younger contractional features are wrinkle ridges that deform regional plains and other older units and are embayed by ps and pl. Fractures and graben in the studied region are typically collected in zones of extensional structures, groove belts and rift zones. *Groove belts (gb)* preferentially occur on the floor of Lavinia Planitia where they cut ridges of the unit pr and are embayed by shield plains and regional plains. *Rift zones (rt)* are concentrated in Lada Terra and appear to be contemporaneous with the youngest plains units (pl, ps, sc).

Discussion and conclusions: The V-55, V-61, and V-56 quadrangles cover a region that consists of two provinces, Lavinia Planitia and Lada Terra, contrasting in gravity, topography, and overall geologic history. The deformational zones of ridge belts populate the floor of Lavinia and the most prominent belts preferentially occur at the deepest portion of the lowland. The important characteristic of the basin is the absence of young deformation and volcanic materials postdating wrinkle ridges. The general topographic configuration of Lavinia Planitia and the radial pattern and topographic position of the belts of ridges are consistent with formation of the belts due to subsidence of the Lavinia basin [7]. The stratigraphic position of the belts implies that the subsidence has largely occurred relatively early and the topographic asymmetry of Lavinia suggests that the locus of the subsidence was near its S and E edges. The vast plains (psh, rp_1, and rp_2) were emplaced on the floor of the lowland when it already was largely formed.

In contrast to Lavinia, Lada Terra is an elevated region dominated by the swell and characterized by abundant young volcanism (pl) and young extensional deformation (rt). The summit of the swell is one of the most important sources of young lavas that flow down the slopes of the swell [12,26]. Magellan gravity data

[27,28] show that the swell is characterized by significant geoid height (~40 m). The geological, topographic, and gravity characteristics are consistent with mantle upwelling [9] in central Lada. The stratigraphic position of the most abundant units in Lada Terra (pl) means that this latest upwelling largely postdated the subsidence in Lavinia Planitia.

The geologic history of the region of Lavinia Planitia and Lada Terra appears to consist of two major phases. The earlier phase corresponds to formation of the vast basin in Lavinia, development of deformational belts on its floor, and near-contemporary formation of marginal groove belts. Later, during the phase of broad updoming, massive volcanism and extensional tectonics occurred in Lada Terra largely postdating formation of Lavinia and the groove belts. The close geographic position of Lavinia Planitia and Lada Terra, their overall topographic configuration, and general sequence of events in these regions suggest a genetically linked evolution [4]. In this model, the downwelling in Lavinia occurred together with marginal extension in Lada, followed by younger rifting and volcanism in Lada Terra.

References: 1) Stofan, E.R. et al., *JGR,* 97, 13347, 1992; 2) Crumpler, L.S. and J. Aubele, *in: Encycl. of Volcanoes,* 727, 2000; 3) Roberts, K.M., et al., *JGR,* 97, 15991, 1992; 4) Magee, K.M. and J.W. Head, *JGR,* 100, 1527, 1995; 5) Baer, G. et al., *JGR,* 99, 8355, 1994; 6) Squyres, S.W. et al., *JGR,* 97, 13579, 1992; 7) Bindschadler, D.L. et al., *JGR,* 97, 13495, 1992; 8) Simons, M., et al., *GJI,* 131, 24, 1997; 9) Kiefer, W.S. and B.H. Hager, *JGR,* 96, 20947, 1991; 10) Ivanov, M.A. and J.W. Head, *USGS Geol. Inv. Ser., Map I-2684,* 2001; 11) Ivanov, M.A. and J.W. Head, *USGS Geol. Inv. Ser.,* 2006; 12) Code of Stratigraphic Nomenclature, *AAPGB*, 45, 645, 1961; 13) Wilhelms, D.E., *in: Planetary Mapping,* 208, 1990; 14) Tanaka, K.L., *USGS OFR 94-438*, 50, 1994; 15) Basilevsky, A.T. and J.W. Head, *EMP,* 66, 285, 1995; 16) Basilevsky, A.T. and J.W. Head, *PPS,* 43, 1523, 1995; 17) Basilevsky, A.T. et al., *in: Venus II* 1047-1086, 1997; 18) Ivanov, M.A. and J. W. Head, *JGR,* 106, 17515, 2001; 19) Barsukov, V.L. et al., *JGR,* 91, D399, 1986; 20) Basilevsky, A.T., et al., *JGR,* 91, D399, 1986; 21) Bindschadler, D.L. and J.W. Head, *JGR,* 96, 5889, 1991; 22) Sukhanov, A.L., *in*: *Venus Geology, Geochemistry, and Geophysics*, 82, 1992; 23) Solomon, S.C. et al., *JGR,* 97, 13199, 1992; 24) Ivanov, M.A. and J. W. Head, *JGR,* 101, 14861, 1996; 25) Hansen, V.L. and J.J. Willis, *Icarus*, 123,296, 1996; 26) Bridges, N.T. and G.E. McGill, *USGS Geol. Inv. Ser., Map I-2747,* 2002, 27) Konopliv, A.S., et al., *GRL,* 20, 2403, 1993, 28) Konopliv, A.S. and W.L. Sjogren, *Icarus,* 112, 42, 1994.

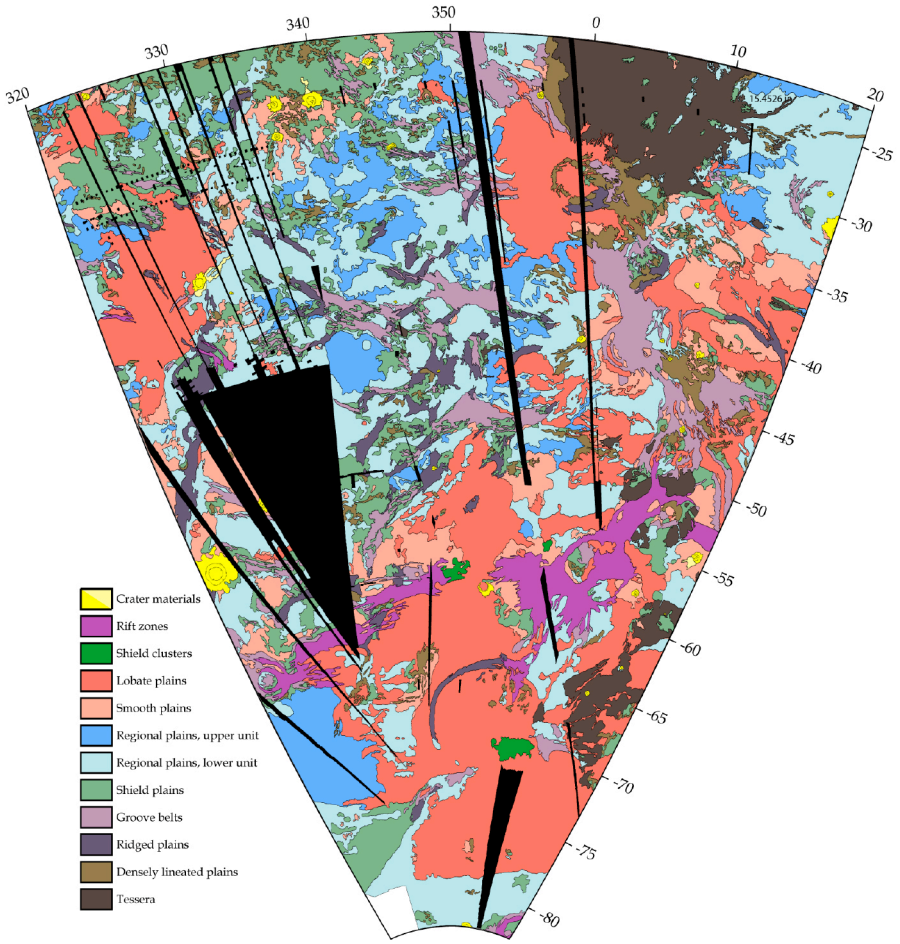

Fig. 1. Geological map of the Lavinia Planitia/Lada Terra region. Lambert equal-area projection.

THE FREDEGONDE (V-57) QUADRANGLE, VENUS: PRELIMINARY RESULTS, M. A. Ivanov[1,2] and J. W. Head[2]
[1]Vernadsky Institute, RAS, Moscow, Russia, mikhail_ivanov@brown.edu; [2]Brown University, Providence, RI, USA, james_head@brown.edu

Introduction: The most significant topographic province on Venus (~80%) are midlands (0-2 km above MPR, [1,2]) that display the richest variety of features [3-12]. The sequence of terrains, units, and structures in the midlands are crucially important in the understanding of the time and modes of formation of this topographic province. The Fredegonde quadrangle (V-57, 50-75°S, 60-120°E) in the southern hemisphere of Venus is a typical region of midlands that exposes abundant features characterizing this province. The area of the map is also in contact with the upland of Lada Terra to the W and the lowland of Aino Planitia to the NE and, thus, may portray characteristics of the transitions from the midlands to the other major topographic provinces of Venus, lowlands and highlands. Here we report on the preliminary results of geologic mapping in the V-57 quadrangle and describe major features, units, and structures exposed in the map area, and outline the main episodes of the geologic history of this region.

Major geologic and topographic features of the V-57 area: The Fredegonde quadrangle (Fig. 1) covers the eastern portion of Lada Terra, which is within the midlands. The most prominent features in the map area are several large and small coronae organized into chains of circular structures interconnected by swarms of extensional structures, grooves and graben. The largest corona chain includes four coronae (Ilyana, Ambar-ona, Dunne-Musun, and Triglava Coronae) and extends in a NNE direction for several thousands of km through the central portion of the quadrangle. The second chain occurs in the NW corner of the map area. It includes two coronae (Shyv-Amashe and Marzyana Coronae) embedded within a broad deformational zone of extensional structures consisting of Geyaguga and Xaratanga Chasmata. The corona-groove chains resemble in many aspects the corona-rift zones at the margins of large equidimensional basins such as Lavinia (V-55) and Atalanta (V-4) Planitiae [13,14]. Subordinate structural zones within the V-57 area are fragments of belts of contractional ridges (Oshumare Dorsa) that occur centrally. The corona-groove chains and belts of ridges represent broad (100s km wide) and relatively low (100s m up to a kilometer high) topographic ridges. Broad and shallow (100s km across, 100s m deep) basin-like features of Mugazo, Alma-Merghen, Laimdota Planitiae occur between the corona-groove chains. Mildly deformed plains units cover the surface of the basins.

Material and structural units and their relationships: The variety of material and structural units that make up the surface of the V-57 quadrangle can be divided into three groups of different relative ages (Fig. 1). (I) The first group of oldest units consists of two material units, densely lineated plains (pdl) and ridged plains (pr), and one structural unit of groove belts (gb). Unit pdl occurs as small outliers in the central area of the map area. Ridged plains are exposed in fragments of the belts of ridges (Oshumare Dorsa). Groove belts consist of dense swarms of fractures and graben that interconnect coronae within the corona-groove chains. All units of this group form either local (pdl) or regionally important elevated areas (pr and gb) that are embayed by vast plains units. (II) The second group consists of two material units, shield plains (psh) and regional plains (rp). These units occur at the middle stratigraphic level and cover the majority of the quadrangle. Abundant small shield- and cone-like features (interpreted to be small volcanoes [15-17]) characterize the surface of shield plains. The volcanoes appear to be sources of the locally adjacent plains material. Regional plains have morphologically smooth surfaces and uniform radar backscatter. Sources of these plains material are not obvious. Wrinkle ridges deform both units of this group and sometimes occur in the older units. Shield plains and regional plains occur at relatively low topographic levels and fill the topographic basins. (III) The third group forms the top of the regional stratigraphic column and consists of two material units of smooth plains (ps) and lobate plains (pl). Smooth plains have uniform and preferentially low radar albedo and lobate plains are characterized by lobate and digitate boundaries. Both units are tectonically undeformed and embay most tectonic structures including wrinkle ridges. Lobate plains are spatially associated with some coronae (e.g. Dunne-Musun) of the corona-groove chains. Individual flows of this unit extend down the regional slopes and partly fill the basin-like topographic lows.

Summary: The results of our preliminary mapping in the V-57 quadrangle (Fig. 1) allow reconstruction of the major episodes of the geologic and topographic evolution of the eastern portion of Lada Terra [18]. Tectonic deformation apparently prevailed during the early stages of the history. The most prominent tectonic features were formed early on and are currently exposed as deformational belts of ridges and the corona-groove chains. The relationships between the older contractional and extensional structures suggest that the ridge belts are older and the corona-groove chains are younger features. The tectonic components of coronae (annulae, fracturing in the core, etc.) appear to be quasi-synchronous with the linear segments of the groove swarms that connect the coronae. The vast

plains of the second group of units, however, broadly embay the corona-groove complexes and, thus, appear to be younger. During the earlier episodes of the regional geologic history, the most important topographic features, the broad topographic ridges and the basins, were formed.

During the middle and late periods of the geologic history, volcanic activity dominated in the region and the vast plains units were emplaced. These plains, now moderately deformed by tectonic structures filled the broad basin-like topographic features but left the older topographic ridges (ridge belts and corona-groove chains) exposed. Such a topographic distribution of shield plains and regional plains suggests that the overall topographic configuration of the midlands within the map area was established prior to emplacement of the units from the middle stratigraphic level. The youngest lobate plains sometimes represent a volcanic component of some coronae (e.g. Dunne-Musun). This association of the younger volcanic materials with the older tectonic structures suggests that some coronae were either 1) reactivated later, 2) their volcanic activity was delayed until the later stages, or 3) formational activity continued, but volcanism represents a late phase. The flow direction of lobate plains (from the broad topographic ridges toward the floor of the basins) suggests, however, that the general topographic shape of the region within the V-57 quadrangle remained stable until the latest stages of the geologic history in this area.

References: 1) Masursky, H., et al., *JGR*, 85, 8232, 1980, 2) Pettengill, G.H., et al., *JGR*, 85, 8261, 1980, 3) Ford, P.G. and G.H. Petttengill, *JGR*, 97, 13103, 1992, 4) Barsukov, V.L., et al., *JGR*, 91, D399, 1986, 5) Frank, S.L. and J.W. Head, *EMP*, 50/51, 421, 1990, 6) Basilevsky, A.T. and J.W. Head, *PSS*, 48, 75, 2000, 7) Basilevsky, A.T. and J.W. Head, *JGR*, 105, 24583, 2000, 8) Stofan, E.R., et al., *Icarus*, 152, 75, 2001, 9) Bleamaster, L.F. and V.L. Hansen, *JGR*, 109, doi: 10.1029/2003JE002193, 2004, 10) Nunes, D.C., et al., *JGR*, 109, doi: 10.1029/2003JE002119, 2004, 11) Young, D.A. and V.L. Hansen, *JGR*, 110, doi: 10.1029/2004JE00 1965, 2005, 12) Herrick, R.R., et al., *JGR*, 110, doi: 10.1029/ 2004JE002283, 2005, 13) Ivanov, M.A. and J.W. Head, *USGS Map I-2684*, 2001, 14) Ivanov, M.A. and J.W. Head, *USGS Map I-2792*, 2004, 15) Aubele J.C., *LPSC XXVI*, 59, 1995, 16) Addington, E.A., *Icarus*, 149, 16, 2001, 17) Ivanov, M.A. and J.W. Head, *JGR*, 109, doi:10.1029/ 2004 JE002252, 2004, 18) Kumar, S. and J.W. Head, this volume.

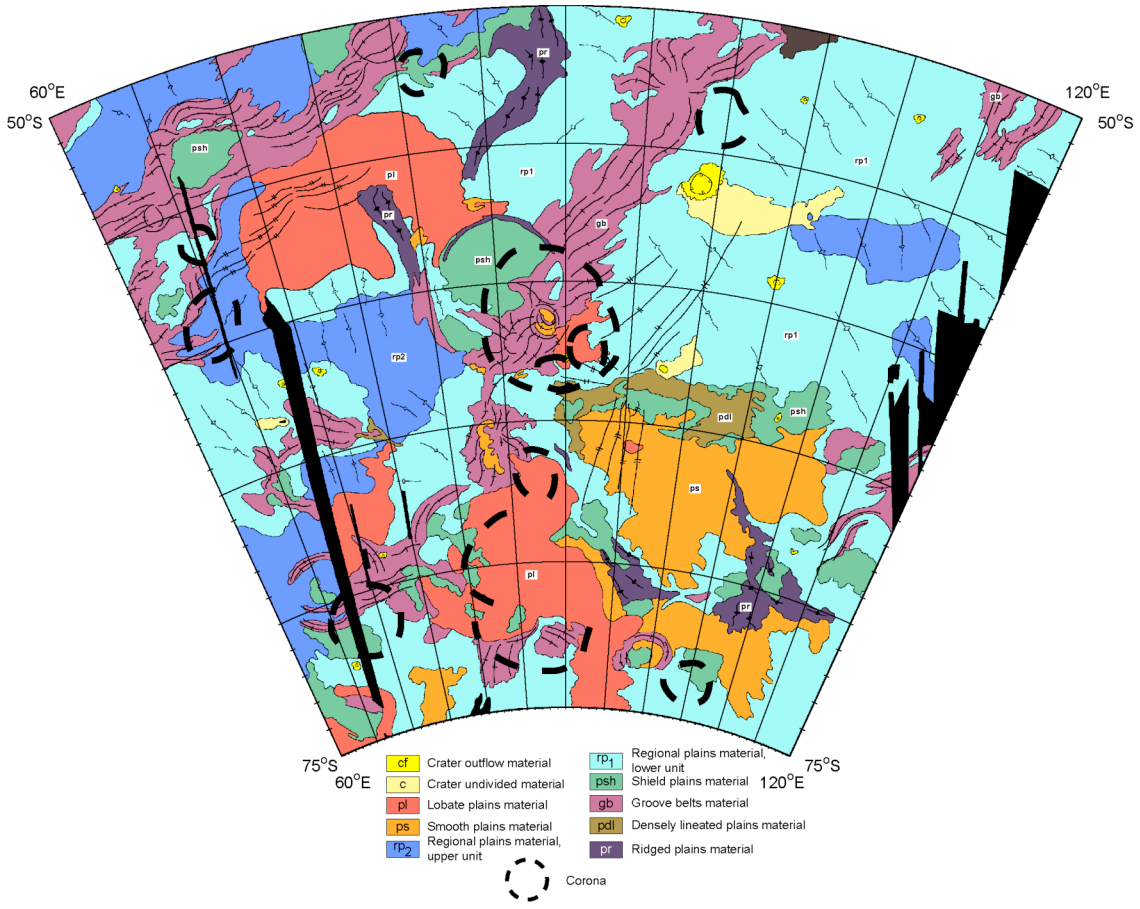

Fig. 1. Preliminary geological map of the Fredegonde (V-57) quadrangle.

THE V-7 QUADRANGLE: SEQUENCE OF EVENTS DURING FORMATION OF LAKSHMI PLANUM, VENUS.

M. A. Ivanov[1,2] and J. W. Head[2] ; [1]Vernadsky Institute, RAS, Moscow, Russia, mikhail_ivanov@brown.edu; [2]Brown University, Providence, RI, USA, james_head@brown.edu

1. Introduction: Lakshmi Planum (western Ishtar Terra) represents a unique class of highlands on Venus: It is a high-standing volcanic plateau (3-4 km above MPR), which is surrounded by the highest Venusian mountain ranges that are 7-10 km high [1-7]. Lakshmi Planum is the key feature of the V-7 quadrangle (50-75°N, 300-360°E). Two classes of models were proposed to explain the unique topographic and morphologic characteristics of western Ishtar Terra. In the first, this feature is considered as a result of mantle upwelling followed by formation and collapse of a large dome [6, 8-10]. In the second, Lakshmi Planum is explained by a mantle downwelling and collision of terrains against a foreland in the core of Lakshmi [11-16]. The sequence of events during the formation of Lakshmi plays a crucial role in the assessment of both models. The first class of models predicts a general progression of events from inside out whereas the alternative model would be consistent with the opposite direction of the geologic activity, the older relative age of the mountain ranges, and younger volcanic activity in the central area of the plateau. Here we describe the set of mapped units and structures and outline the apparent sequence of events during formation of Lakshmi Planum based on the results of the mapping of the V-7 area.

2. Material units: Eleven material units make up the surface of the V-7 quadrangle (Fig.1). (1) Tessera (t) is exposed inside and outside Lakshmi Planum and appears to be the oldest material because it is embayed by most of the other units in the map area. (2) Densely lineated plains (pdl) postdate tessera and form one of the oldest units. Patches of pdl occur outside Lakshmi Planum. (3) Ridged plains (pr) postdate pdl and occur outside Lakshmi. (4) Shield plains (psh) display abundant small (a few km) shield-shaped features interpreted to be small volcanoes. The unit embays the previous ones and occurs predominantly within the lowlands around Lakshmi. (5) Pitted and grooved material (pgm) displays small pits and is cut by broad and shallow grooves with scalloped edges. The unit occurs inside Lakshmi in spatial association with the mountain ranges. (6) Regional plains (rp) have a smooth surface, which is cut by wrinkle ridges. This is the most widespread unit and occurs inside and outside of Lakshmi Planum. (7) Lower unit of lobate plains (pl_1) is also deformed by wrinkle ridges but has lobate boundaries and higher radar albedo than regional plains. The unit occurs both inside and outside Lakshmi. (8) Upper unit of lobate plains (pl_2) is characterized by lobate flows that embay most tectonic structures including wrinkle ridges. The unit forms flow complexes outside Lakshmi and surround Colette and Sacajawea Paterae inside the plateau. (9) Smooth plains (ps) have uniform and low radar albedo. Material of unit ps embays wrinkle ridges. The largest occurrence of the unit is in the southern portion of Lakshmi Planum. (10) Impact craters (c) and (11) crater outflow deposits (cf) are peppered throughout the quadrangle without any preferential concentrations.

3. Structures (Fig.1): Extensional structures. In places, extensional structures (fractures and graben) are closely spaced and obscure underlying terrain. These concentrations form belts (groove belts, gb) that extend for hundreds of kilometers mostly within the southern regional slope of Lakshmi Planum where they cut the units pdl and pr and are embayed by shield plains and regional plains. Contractional structures. Several types and scales of contractional features are observed within the quadrangle. Wrinkle ridges mildly deform shield plains and regional plains. Broader and more linear ridges dominate ridged plains (pr), which are largely equivalent to the ridge belts of [17,18]. The most important occurrences of contractional structures in the map area are mountain belts (unit mt) that surround the interior of Lakshmi Planum and consist of densely spaced ridges 5-15 km wide and tens of km long. Regional plains inside and outside Lakshmi usually embay the ridges.

4. Discussion and conclusions There are three major physiographic provinces in the map area: the exterior of Lakshmi Planum, the interior of Lakshmi, and the surrounding mountain ranges. The exterior of Lakshmi displays abundant tectonized units that predate regional plains (t, pdl, gb, pr, Fig. 1) suggesting that tectonic deformation dominated in this region during the earlier episodes of the geologic history. The oldest unit in the interior of Lakshmi is tessera and the heavily tectonized units such as pdl, pr, and gb are almost absent there (Fig. 1). This suggests a possible gap in the tectonic/stratigraphic sequence from tessera to regional plains in the interior of Lakshmi Planum. The outliers of tessera are scattered throughout the interior probably because the suite of the younger plains units there is relatively thin. The important feature of the interior is the absence of either ridges or ridge belts that indicates virtual lack of contractional deformation there. The absolute majority of contractional deformation is concentrated within the mountain belts (Fig. 1). The oldest unit embaying the ranges is regional plains. Thus, the mountain belts formed relatively early during the geologic history of the region. Regional plains and the younger plains units occur both inside and outside Lakshmi. The state of

their deformation units indicates that tectonic activity responsible for the deformation of such units as pdl, pr, and gb and formation of the mountain ranges mostly ceased by the time of emplacements of the vast plains (psh, rp, pl_1, pl_2, ps).

The general sequence of events documented within the V-7 quadrangle indicates that tectonism dominated during the earlier episodes of the geologic history before emplacement of shield plains and regional plains. The major deformational belts, including the mountain ranges, formed during this period. The concentration of the tectonized units outside Lakshmi and their absence in the Lakshmi interior suggests the general progression of tectonic events oriented from outside toward the planum, which is consistent with the formation of the western Ishtar Terra due to large-scale horizontal convergence, underthrusting, imbrication, and folding [13,14,16,19]. The major plains units were emplaced, and preserved their morphological identity at a time when tectonic deformation had largely waned and the general topographic configuration of the region was established. The youngest activity in the region was related to volcanism through a few distinct volcanic centers inside and outside Lakshmi.

References: 1) Masursky, H., et al., *JGR*, 85, 8232, 1980, 2) Pettengill, G.H., et al., *JGR*, 85, 8261, 1980, 3) Basilevsky, A.T., et al., *JGR.,* 91, D399, 1986, 4) Barsukov, V.L. et al., *JGR,* 91, D399, 1986, 5) Sukhanov, A.L., et al., *USGS Map I-2059*, 1989, 6) Pronin, A.A. *In: Venus Geology, Geochemistry, and Geophysics,* 68-81, 1992. 7) Kaula, W.M., et al., *JGR.,* 97, 16085, 1992, 8) Pronin, A.A., *Geotectonics,* 20, 271, 1986, 9) Grimm, R.E. and R.J. Phillips, *GRL,* 17, 1349, 1990, 10) Grimm, R.E. and R.J. Phillips, *JGR,* 96, 8305, 1991, 11) Vorder Bruegge, R.W. and J.W. Head, *GRL,* 16, 699, 1989, 12) Vorder Bruegge, R.W. and J.W. Head, *Geology,* 19, 885, 1991, 13) Head, J.W., *Geology,* 18, 99, 1990, 14) Roberts, K.M. and J.W. Head, *GRL,* 17, 1341, 1990, 15) Bindschadler, D.L., et al., *GRL,* 17, 1345, 1990, 16) Keep, M. and V.L. Hansen, *JGR.,* 99, 26015, 1994, 17) Solomon, S.C., et al., *JGR*, 97, 13199, 1992, 18) Squyres, S.W., et al., *JGR*, 97, 13579, 1992, 19) Vorder Bruegge, R.W. and J.W. Head, *EMP,* 50/51, 251, 1990.

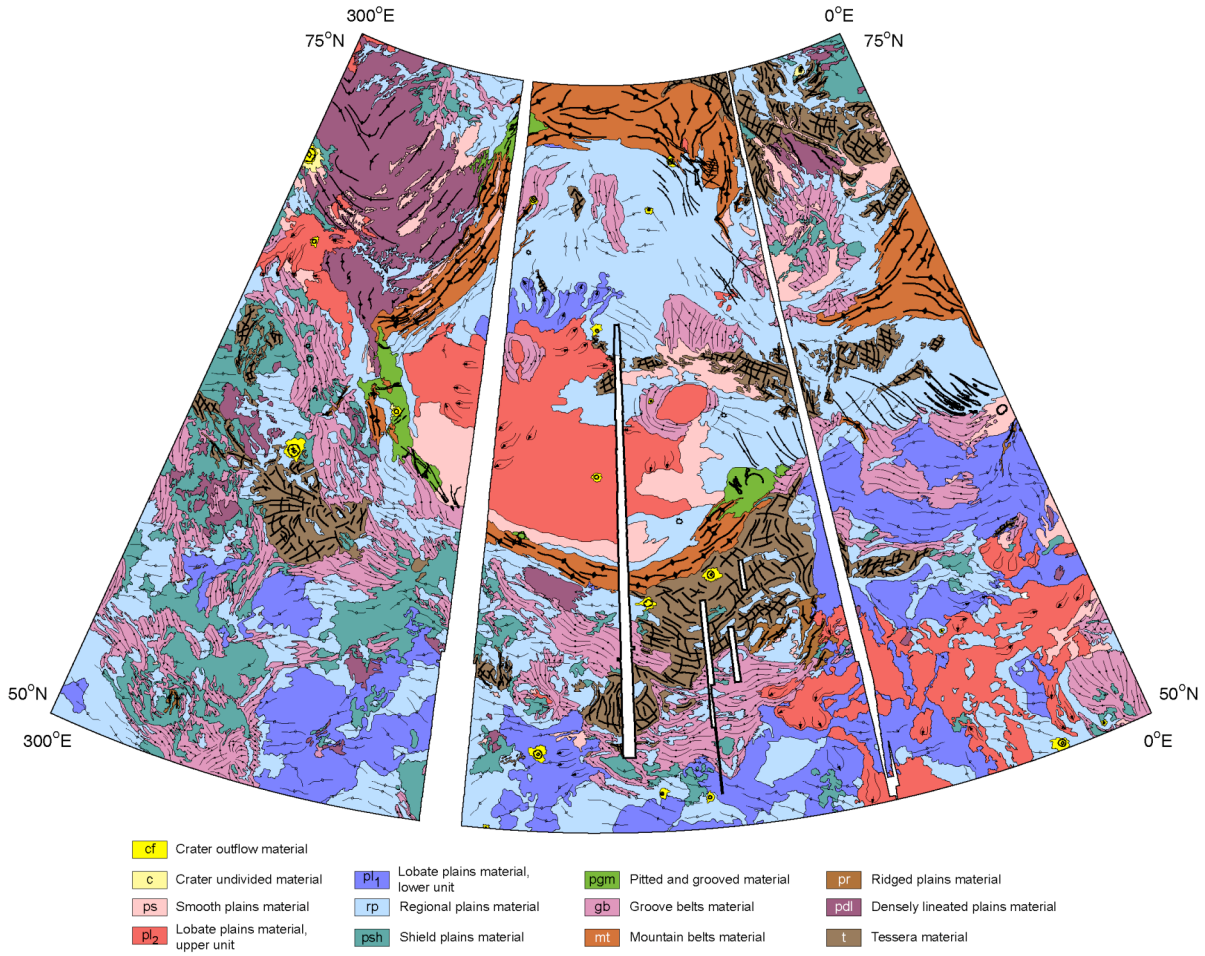

Fig. 1 Geological map of the Lakshmi Planum (V-7) quadrangle.

GEOLOGICAL MAPPING OF THE LADA TERRA (V-56) QUADRANGLE, VENUS: PRELIMINARY OBSERVATIONS,

P. Senthil Kumar[1,2] and James W. Head[2], [1]National Geophysical Research Institute, Hyderabad 500007, India, senthilngri@yahoo.com; [2]Department of Geological Sciences, Brown University, Providence, RI 02912, USA, james_head@brown.edu.

Introduction: Geological mapping of the V-56 quadrangle (Fig. 1) reveals various tectonic and volcanic processes in Lada Terra that consist of tesserae, regional extensional belts, coronae, volcanic plains and impact craters. This study aims to map the spatial distribution of different material units, deformational features or lineament patterns and impact crater materials. In addition, we also establish the relative age relationships (e.g., overlapping or cross-cutting relationship) between them, in order to reconstruct the geologic history. Basically, this quadrangle addresses how coronae evolved in association with regional extensional belts, in addition to evolution of tesserae, regional plains and impact craters, which are also significant geological units of Lada Terra.

Geologic mapping: We used 250-m-per-pixel Magellan SAR images to prepare a geologic map in a scale of 1:5,000,000. Wherever necessary, full-resolution (75-m-per-pixel) images are used for fine details. This quadrangle is bordered by Kaiwan Fluctus (V-44) [1] and Agnesi (V-45) [2] quadrangles in the north; Mylitta Fluctus (V-61) [3,4], Fredegonde (V-57) [5] and Hurston (V-62) [2] quadrangles in the west, east, and south, respectively. From the geologic mapping, we report on the distribution of the following material and structural units, and reconstruct the geologic history.

Material and structural units: The oldest known material units are tesserae. They are radar bright areas characterized by multiple orientations of lineaments; two sets are dominant: NNW-SSE and ESE-WNW oriented lineaments. Tightly spaced ridges and troughs generally characterize tesserae. The third dominant lineaments are NNE-SSW and NNW-SSE oriented long rift zones, namely, Chang Xi Chasmata and Seo-Ne Chasma; but these are apparently restricted to the Cocomama Tessera. In the northeastern part of the quadrangle, terrains (TLT, Fig. 1) similar to tessera are found. They have NNE-SSW to NE-SW oriented ridges, which are cut by ESE-SNW to NW-SE oriented troughs. The spacing of these structures is greater than the structures of the tessera. The tessera units contain intra-tessera basins, which are filled by lava flows of different ages; most of them are derived from the units outside the tessera, and a few are from intra-tessera volcanism.

Regional plains units embay the tessera terrain; they have wrinkle ridges and a few young fracture systems. The oldest known plains (but younger than tessera) are lineated (LP, Fig. 1), and are closely associated with shield plains (unit 5, Fig. 1) and the tessera. The LP is characterized by tightly spaced, NNW-SSE oriented fractures, which are also common in the tessera. Two types of shield plains are present: a few occur in the pre-regional plains areas, while others occur in the core of coronae and adjoining areas.

The older regional plains (unit 4, Fig. 1) are cut by two regional extensional belts [6]: (1) NNW-SSE trending, 6000-km long and 50-200 km wide, Alpha-Lada (AL) belt, and (2) NNE-SSW trending, 2000 km long and 300 km wide, Derceto-Quetzalpetlatl (DQ) belt. These two belts are composed of fractures, rift basins and strike-slip zones. The DQ belt is punctured by Sarpanitum, Eithinoha and Quetzalpetlatl Coronae, while the Otygen, Demvamvit and Okhin-Tengri Coronae occur along the AL belt. A few coronae have a circular central dome and outer concentric depression; they are defined by fractures, rift basins and ridge belts. Asymmetric and multiple coronae also occur in the southern part of the AL belt. Two other extensional belts branch from the AL belt. Dyamenyuo and Toyo-uke Coronae and Loo-wit and Kshumay Montes puncture these extensional belts. At many places, corona structures cut across the regional extensional belts, while at other places, the extensional belts cross the corona structures. There is a clear overlapping time relationship, as the one affects the formation of the other. Corona volcanism and tectonics are also closely related to one another. Lava flows erupt along the corona fractures, for example, in the Ethinoha Corona. Lava flows emanating from coronae travel several hundred kilometers. Volcanism is also related to shield volcanoes in many places.

The DQ and AL belts separate the plains units of Lavinia Planitia, Aibarchin Planitia and Mugazo Planitia, where lava flows are abundant; principally there are four plain units, of which the oldest one appears to be common to all the planitia units. Most of the younger units are locally derived from the coronae. The regional plains occurring to the east of Otygen Corona have undergone intense fracturing and emplacement of dykes after post corona-extensional belt deformation. These fractures occur in two directions: ENE-WSW and NW-SE. It appears that they represent the latest deformation, and could probably be related the terrain uplift, as is evident in many terrestrial examples.

Impact craters are the youngest geologic units, except for one that is affected by the extensional belt deformation and the other embayed by regional plains. Most impact craters show complex geometry and a few

are bowl-shaped. Many complex craters show run-out flows characteristic of oblique impacts. Further detailed mapping is underway to reconstruct the complete geologic history of this quadrangle in near future.

Acknowledgements: We thank Misha Ivanov for his help while initiating this mapping project, and Jay Dickson and Prabhat while working with the virtual wall image facility.

References: [1] Bridges, N.T., and McGill, M.E., *USGS Scientific Investigations Map I-2747,* 2002. [2] http://astrogeology.usgs.gov/Projects/PlanetaryMapping/MapStatus/VenusStatus/Venus_Status.html. [3] Ivanov, M.A., and Head, J.W., *USGS Scientific Investigations Map 2920,* 2006. [4] Ivanov, M.A., and Head, J.W., this volume. [5] Ivanov, M.A., et al., this volume. [6] Baer, G., et al., *J. Geophys. Res*., 99, 8335-8369, 1994.

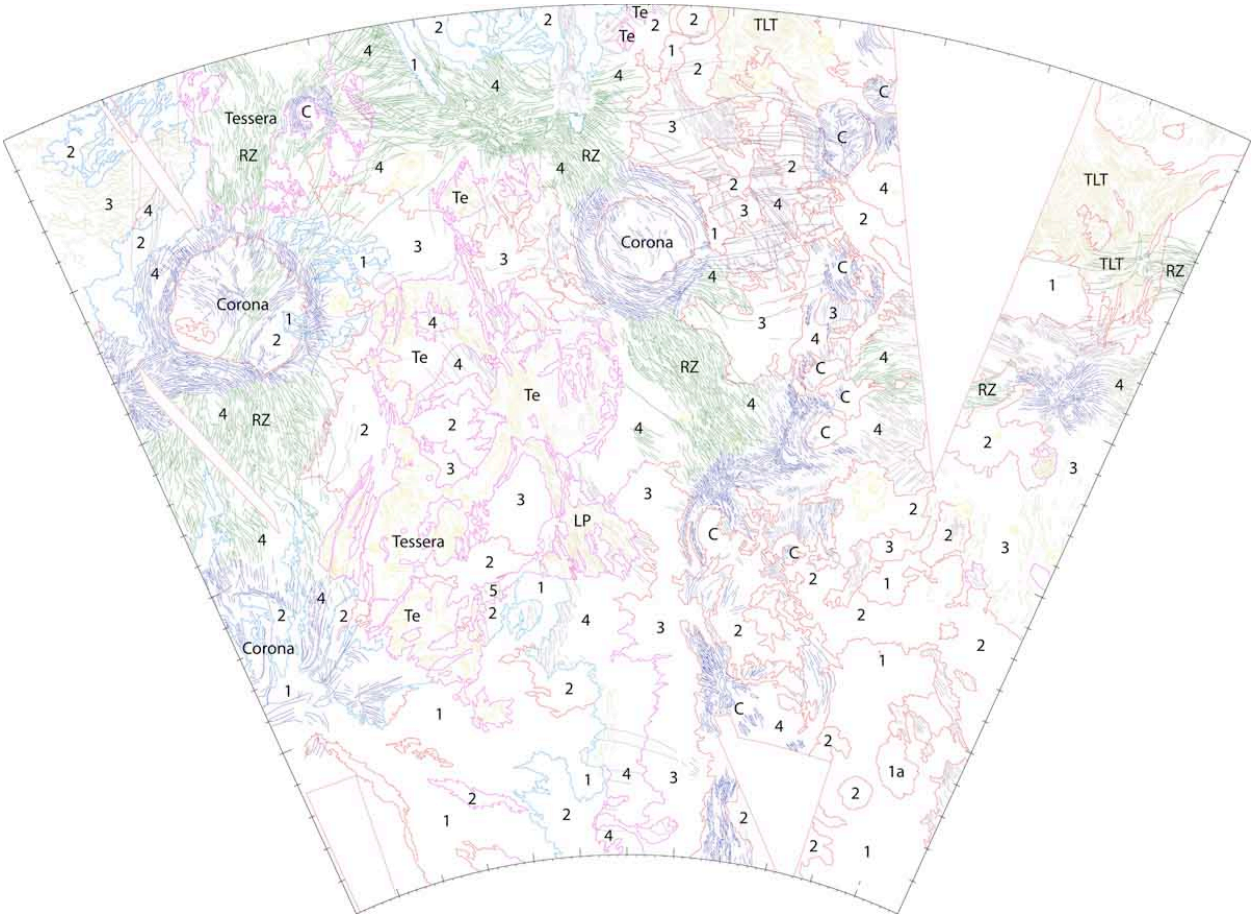

Fig. 1. Preliminary geological sketch map of V-56 Lada Terra quadrangle (50°S-75°S; 0°E-60°E): Material units (from older to younger): tessera terrain (Te), tessera-like terrain (TLT), lineated plains (LP), plain units from 5 to 1 and impact craters. Lineament patterns defining the tessera (Te) extensional belts (RZ) and coronae (C) are shown in different colors: greenish yellow–tessera, green–extensional belts; dark blue–coronae. Many of the plains units (3 to 1) are related to volcanism of coronae.

PRELIMINARY GLOBAL SURVEY OF CIRCULAR LOWS, A SUBSET OF VENUSIAN CORONAE. B. Shankar[1] and V. L. Hansen[1], [1]Department of Geological Sciences, University of Minnesota Duluth, Duluth, MN 55812 (shank075@d.umn.edu; vhansen@d.umn.edu).

Introduction: Venus preserves over 500 coronae, most of which occur in chains (68%) or clusters (21%) spatially associated with mesoland chasmata and highland volcanic rises, respectively [1-8]. Coronae range in diameter from 60-1100 km (~200-km diameter median [4, 5]). Many workers accept that coronae represent the surface expression of endogenic diapirs [e.g., 2, 4, 9-14], although other hypotheses have been proposed, including formation as volcanic caldera and by exogenic impactors [e.g., 2, 15-29]. The wide range in character of coronae might indicate that not all coronae formed by similar processes. We investigate the formation of a subset of coronae, herein called circular lows, through detailed mapping of individual circular lows, regional mapping of circular lows in V-45, and a global survey of circular lows.

Background: Were all coronae created equally? That is, did all coronae form by a similar mechanism? Can a claim of similar genetic formation be robustly supported? The spatial association of corona chains and corona clusters with chasmata and volcanic rises, respectively, favors endogenic formation for these two broad groups of coronae. Many of these coronae also display radial fractures and concentric structures (called radial concentric coronae [4]), as well as associated flows that are consistent with endogenic genesis [e.g., 4-5, 10, 12, 29]. But ~11% of coronae occur as relatively isolated features in Venus' lowland [4-5]. In contrast to chained and clustered coronae, lowland/isolated coronae lack compelling spatial evidence for endogenic formation. Lowland/isolated coronae do not, so far as has been recognized, define geometric patterns among coronae, nor do they correlate spatially with other geological features. Morphologic and structural characteristics might also set lowland/isolated coronae apart from 'typical' coronae that occur in chains and clusters. Some lowland/isolated coronae lack significant fracture annuli, and/or associated flows [5]; these differences could reflect post-formation burial or different mechanisms of formation. The subset of lowland/isolated coronae might be divisible into two distinct morphologic types (not including stealth coronae of Stofan et al. [5]): (a) features marked by positive topography and radial fractures (radial lowland coronae, herein; although the morphology of these coronae appears to be similar to radial concentric coronae of Stofan et al. [4], we use radial lowland coronae herein to specify their lowland location), and (b) features marked by circular basins (negative topography relative to surroundings) with morphology akin to sunken amphitheaters (coronae types 4 or 8 of Smrekar and Stofan [6]; circular lows, herein).

Methods: We are in the process of conducting a global survey of circular lows. We use Magellan SAR and altimetry data for all the Vmap quadrangles (V-1 to V-62), in addition to synthetic stereo images for V-2 to V-61 as circular lows are best recognized in synthetic stereo imagery. The polar quadrangles, V-1 and V-62, do not have synthetic stereo images. This data base allows us to conduct a global survey to identify all circular features with negative topographic signatures. We have previously constructed synthetic stereo images for each of the Venus VMap quadrangles, except the polar regions, using the USGS VMap SAR image base and Magellan altimetry data following the procedure outlined by Kirk et al. [31] using macros developed by D.A. Young.

Adobe Illustrator™ allows layer transparency which enables concurrent consideration of altimetry and SAR data, as is crucial for circular low identification. Circular lows are most readily visible in synthetic stereo imagery, but these images do not allow us to easily quantify relative heights of rims, or interior depths, which can be gained from contoured altimetry data. D.A. Young also developed macros that allow us to contour altimetry data so VMap synthetic stereo imagery and contoured altimetry are easily overlain and compared in Abode Illustrator™.

Global survey data is collected on georeferenced VMap images using Adobe Illustrator; full resolution SAR images are imported from USGS Map-a-Planet as required. Survey results are tabulated such that individual circular low locations and characteristics can be plotted globally in order to allow comparison with other global data bases. All information will be complied on the USGS VMap bases. Map Publisher™ software enables us to reproject

mapping in an ArcGlobe GIS™ environment, in order to make comparisons with other global data sets including: coronae, impact craters, ridge belts, tessera terrain, tectonic provinces, etc. We have found that the method of data collection and reprojection of the data, rather than reprojection of image data, allows us to consider the highest resolution data in such a project.

We are mapping circular low locations using ArcGlobe GIS™ so that we can compare spatial locations of circular lows with one another and with global scale geomorphic features across Venus. In addition, we examine individual circular lows through VMap data analysis in order to determine a range of criteria including: location, tectonic setting, host terrain, shape (ellipticity), diameter, topographic profiles, annuli character (width, degree spread, structural character), presence and extent of radial fractures, location and extent of flows, presence of rim, and interior features. We will compare circular lows to the global database of ribbon tessera that are independently generated and still in progress. We expect that other criteria may emerge during the course of the global survey.

Preliminary results: To date we have identified 67 potential circular lows that range in diameter from 30-375 km (~125 km diameter median). Although most circular lows are circular, a few are elliptical in shape. Circular lows are relatively equally distributed throughout the planet. They appear equally in the northern and southern hemispheres, although the latitudes between 125°E and 202°E host only a few (three) circular lows.

Circular lows commonly occur as relatively isolated features. However, they can occur in near proximity to one another. For example, six circular lows occur on either side of Gegute Tessera, north of Aphrodite Terra (~15^{o}N/120^{o}E). A group of three circular lows occur around at 53^{o}S/290^{o}E.

Topographically, circular lows dominantly occur within the lowlands; however they avoid the deepest lowland basins. Seven circular lows occur in highlands locations including: three in Lakshmi Planum, one each in Atla and Ovda Regiones, and two in western Ovda Regio. Six circular lows may occur within the region between Atla Regio and Atahensik Corona; these features might, however, reflect regional topographic complexity, rather than specific morphological features.

Tectonically, circular lows do not occur in chasma-corona chains except as previously noted. They also do not occur in volcanic rises.

References: [1] J.W. Head et al. JGR, 97 13153-13198 (1992). [2] S.W. Squyres et al. JGR, 97 13611-13634 (1992). [3] K.M. Roberts & J.W. Head GRL, 20, 1111-1114 (1993). [4] E.R. Stofan et al. JGR, 97, 13347-13378 (1992). [5] E.R. Stofan et al. GRL, 28 4267-4270 (2001). [6] S.E. Smrekar & E.R. Stofan Sci., 277 1289-1294 (1997). [7] S.E. Smrekar & E.R. Stofan Icarus, 139 (1) 100 (1999). [8] J.E. DeLaughter & D.M. Jurdy Icarus, 139 (1) 81 (1999). [9] D.M. Janes et al. JGR, 97 16055-16068 (1992). [10] E.R. Stofan et al. in, *Venus II*, 931-968, Univ. AZ Press (1997). [11] D.M. Koch JGR, 99 2035–2052 (1994). [12] D.M. Janes & S.W. Squyres JGR, 100 (E10) 21,173-21,187 (1995). [13] D.M..Koch & M. Manga GRL, 23 225-228 (1996). [14] V.L .Hansen Geol. Soc. Amer. Bull., 115 1040-1052 (2003). [15] V.L. Barsukov et al. Geokhimia, 12 1811-1820 (1984). [17] D.B. Campbell & B. Burns Science, 204 1424-1427 (1979). [18] R.A.F. Grieve & J.W. Head, Episodes, 4(2) 3-9 (1981). [19] J.W. Head & S.C. Solomon Science, 213 62-76 (1981). [20] H. Masursky et al. JGR, 85 8232-8260 (1980). [21] G.G. Schaber & J.M. Boyce Impact and explosion cratering—Planetary and terrestrial implications: New York, Pergamon Press, 603-612 (1977). [22] O.V. Nikolayeva et al. Geochemistry International, 23(9) 1-11 (1986). [23] O.V. Nikolayeva LPSC, 24 1083-1084 (1993). [24] R. Greeley Planetary Landscapes; 2nd ed., Allen & Unwin, London (1987). [25] W.B. Hamilton, Geol. Soc. Am., C-2 597-614, (1993). [26] W.B. Hamilton, GSA Spec. Paper 388, 781-814 (2005). [27] P.H. Schultz LPSC, 24 1255-1255 (1993). [28] C. Vita-Finzi et al., GSA Spec. Paper 388, 815-824 (2005). [29] V.E. Hamilton & E.R. Stofan Icarus, 121 (1) 171 (1996). [30] R.L. Kirk et al. JGR, 97 16371-16380 (1992).

UPDATE ON MAPPING OF QUADRANGLES V-28, V-52 AND V-19. E.R. Stofan[1, 2], J.E. Guest[2], A.W. Brian[2] and P.M. Martin[3], [1]Proxemy Research (20528 Farcroft Lane, Laytonsville, MD 20882, ellen@proxemy.com), [2] Department of Earth Sciences, University College London WC1E 6BT, [3]Department of Earth Sciences, Durham University DH1 3LE.

Introduction: Although extensive mapping of the surface of Venus and continued analysis of Magellan data have allowed a more complete understanding of the venusian surface, controversy remains over the evolution the surface [e.g., 1, 2]. We are finalizing maps of three quadrangles, which will add to this ongoing scientific debate. Quadrangle V-28, in revision, covers an area along Hecate Chasma. V-53, in revision, covers a portion of Parga Chasmata and Themis Regio. Quadrangle V-19, to be submitted fall 2007, covers the northern margin of western Eistla Regio and Sedna Planitia.

V-28: We identified nine plains materials units in V-28. V-28 has a variety of mappable volcanic landforms including several large shield volcanoes (Nazit Mons, Polik-mana Mons, Kono Mons, and Xochiquetzal Mons), numerous intermediate volcanoes, abundant small volcanic edifices and a large flow field. Few of the edifies are in contact with each other. Eighteen coronae, ranging in size from 125 to 525 km, are located in V-28, as well as flows from a nineteenth corona, Miti, located outside the quadrangle. Of the eighteen coronae, ten have associated mappable deposits. Three outcrops of materials with two or more dominant fracture and/or ridge orientations were mapped as tessera. Thirteen impact craters are in the V-28 quadrangle. Two of the craters, Nuriet and Higgins, have very unusual morphology, with an indistinct, irregular crater and outflow-like deposits. Eight have at least partial dark floors.

The geologic history of V-28 is dominated by formation of rifts, volcanism and corona formation. We can identify no regional-scale plains units; the numerous plains units appear to be local units. Identifying different plains units in and near the rift is extremely difficult, owing to the intensity of the fracturing. Therefore, we do not feel overly confident of the age relationship or continuity of plains units mapped in the immediate vicinity of the rift.

The large number of small and intermediate volcanoes in V-28 illustrates the typical abundant volcanism within the BAT region (Beta-Atla-Themis) [3]. Edifice fields are thought to be relatively young based on superposition relationships, and all plains units, particularly those south of the rift, tend to have anomalously high concentrations of small edifices. Individual small edifices, both within edifice fields and within plains units, appear to span a relatively long period of time, based on cross-cutting relationships with local structures. The earliest history of this quadrangle is preserved in deformed plains units and tessera on either side of the rift. The amount of time represented by these units, and whether they represent earlier episodes of rift formation in this region, is not clear. Later plains units of relatively limited aerial extent were formed by volcanic processes. These units were subsequently rifted. Volcanism and corona formation occurred prior to, during and after rift formation.

On Venus, only ~17% of the total population of impact craters are either volcanically embayed and/or tectonized (Schaber et al., 1992). In V-28, 38% of craters are embayed or tectonized. In addition, several other craters have a somewhat ambiguous relationship with surrounding units. We also do not include in the embayed population the number of dark floored craters; therefore, we would argue that the 38% is likely to be an underestimate. Detailed mapping clearly is likely to raise the number of tectonized and embayed craters on Venus. Despite this, the V-28 region clearly contains an anomalous number of modified craters.

V-53: We have identified seven plains materials units within V-53. None of the plains units are analogous to regional-scale plains units mapped in other quadrangles. Eleven units associated with nine named volcanic edifices have been mapped, including those associated with the large volcanoes Chloris Mons, Mielikki Mons and Tefnut Mons. Multiple materials units associated with unnamed or unknown sources have also been mapped and combined into a single unit: a volcanic center unit (unit vc) and edifice field unit (unit ef). Most of the volcanic flow units are not in contact with each other, or with consistent plains or corona units, making an overall volcanic stratigraphy difficult to determine.

Nineteen named coronae have associated flow materials units, along with units associated with three unnamed coronae. In addition, twelve impact craters are in the V-53 quadrangle. They range in diameter from 11- 52 km. Four are superposed on the mottled plains unit; the crater Kitna is superposed on the Themis fractured plains, and Aksentyeva crater is superposed on the Themis lobate plains. The craters Jocelyn and Elza are superposed on flows from Obiemi Corona. The 52 km diameter crater Kenny is clearly embayed by flows from Abeona Mons.

Two craters, Peck and Bernadette, have a complex relationship with the surrounding units. Peck appears to be superposed on unit pdf, but its ejecta has been fractured and embayed, and its interior embayed by later flows that occurred within pdf. We interpret it to

have formed during the apparently protracted evolution of unit pdf. The crater Bernadette is supposed on Nzambi Corona flows, but it is also embayed by small, difficult to map, later Nzambi flows.

The earliest geologic activity in V-53 is recorded by plains units pdf and pl, suggesting that the region has been subjected to multiple episodes of plains forming volcanism and deformation, culminating in the current (ongoing?) activity of Parga Chasmata and Themis Regio. The large number of plains units, coronae and volcanoes in V-53 results in a very horizontal stratigraphic column, as few units are in direct contact. The bulk of the geologic activity is related to uplift, volcanism and corona formation at Themis Regio, and the rifting of Parga Chasmata. All of this activity overlapped in time; the duration of the activity is unknown.

V-19: We have mapped seven plains units in the V-19 quadrangle. One of these plains units (Sedna homogeneous plains) is a much larger scale unit than those mapped in the two chasma-related quadrangles. Twelve flow units associated with five coronae (Nissaba, Purandhi, Idem-Kuva, Tutelina and Mesca) have been delineated. Idem-Kuva and Nissaba units are interfingered; other corona units are not in contact. Flow units associated with eight volcanoes were mapped, including flows from Gula and Sif Montes. Intermediate scale edifices mapped include Toci Tholus, Sachs Patera, Evaki Tholus, and Bunzi Mons. In addition, volcanic center and edifice field units were mapped. In the northern portion of the quadrangle are flow units associated with Neago Flūctus.

Tectonic features in V-19 include Manzan-Gurme Tesserae, Zorile Dorsa, and Karra-māhte Fossae. The dorsa and tessera units are embayed by later plains units and thus form mappable units, while faults of the fossa cut the plains.

The early history of the quadrangle is characterized by tectonic deformation of volcanism (tessera and dorsa formation and plains volcanism). The bulk of the history of the quadrangle is characterized by interfingered, large – and intermediate- scale plains units and corona formation, with activity associated with Eistla Regio (volcanism, corona formation) occurring in the later part of the history of V-19.

Discussion: Two end-member models have been proposed for Venus: a directional model in which specific types of features formed globally at specific times (e.g., 2), and a non-directional model in which types of geologic features form over the range of observable Venus history (~ 750 my) [1, 4]. An exception to the non-directional model is tessera; the majority of tessera plateaus seem to predate the plains that immediately surround them (e.g., 5, 6). All of the quadrangles contain fragments of tessera; theories for these fragments range from an old, widespread unit that underlies much of the plains [5] to the fragments forming at multiple times by different mechanisms [6]. In all three quadrangles the fragments are in close proximity (~100 km), suggesting that they once formed a larger unit. However, the extent and the origin of this unit and the age of it relative to the other 'old' plains units in the quadrangles are not known.

Plains, volcano and corona units in these quadrangles are more consistent with a non-directional model. We see no evidence here for a widespread episode of resurfacing, with the possible exception of V-19; instead the patch-like, composite character supports incremental resurfacing over time. Small edifices have formed throughout the histories of the quadrangles.

References. [1] Guest J.E. and Stofan E.R. (1999) *Icarus, 139,* 55. [2] Basilevsky A.T. et al. (1997), in *Venus II*, eds. S.W. Bougher, D.M. Hunten, R.J. Phillips, *Univ. of Ariz. Press, Tucson*, 1047. [3] Crumpler, L.S., et al., (1997) in *Venus II*, eds. S.W. Bougher, D. M. Hunten, R.J. Phillips, *Univ. of Ariz. Press, Tucson*, 1047. [4] Stofan E.R. et al., (2005) Icarus, 173, 312-321, 2005. [5] Ivanov, M.A. and Head, J.W., (1996) J. Geophys. Res. v. 101, 14, 861-14,908. [6] Hansen, V.L. and J.J. Willis (1996) Icarus v. 123, 296-312.

PRELIMINARY GEOLOGIC MAP OF AGNESI QUADRANGLE, V-45 (25-50S/30-60E). E. R. Tharalson[1] and V. L. Hansen[1], [1]Department of Geological Sciences, University of Minnesota Duluth, Duluth, MN 55812 (thar0030@d.umn.edu; vhansen@d.umn.edu).

Introduction: We are creating a 1:5 M scale geologic map of Agnesi quadrangle (V-45), in order to understand the evolution of lowland tessera terrain, and to compare the formation of radial lowland coronae, and lowland coronae marked by circular basins, referred to as circular lows. Mapping uses full resolution Magellan SAR data, and altimetry.

V-45 Geology: Agnesi quadrangle (V-45), named for centrally located Agnesi crater, hosts nine coronae and several tracts of tessera terrain and lies within Venus' lowland. The area ranges in altitude from 6050.8 to 6053.5 km, with an average of ~6052 km. V-45 is marked by numerous linear to curvilinear ridges, and several local highs which host Tushita and Xi Wang-mu Tesserae in the east and central region, respectively, and various domical coronae in the NW and SE corners of the map area. Fonueha Planitia, which trends east between WNW-trending Tushita Tesserae ridge to the north and a broad mesoland area to the south, is narrow and relatively poorly defined compared to other Venusian planitiae. In the NW part of the quadrangle curvilinear ridges describe concentric circles with diameters of 900-1200 km. The three nested ridges are 100-75 km wide and hundreds of km long, each separated by 200-100 km basins that parallel the adjacent ridges. These ridges host linear tracts of ribbon tessera terrain, with structural fabric parallel to the ridge crests. The intervening elongate basins parallel tessera fold trends. V-45 also hosts nine lowland coronae, two montes, and 13 'pristine' impact craters. Sezibwa Vallis, in the southwest, hosts long flows up to hundreds of km in length sourced from V-44 to the west. V-45 lacks chasmata, except for the misnamed 'Artio Chasma,' which forms the middle curvilinear ridge, rather than a topographic low. Artio ridge preserves shallowly buried ribbon tessera terrain, with structural fabrics parallel to the ridge axis. Shield-terrain occurs across much of V-45. Regional lineaments trend ENE across the map area. The NE corner preserves the only tract of wrinkle ridges, which trend NNW, perpendicular to ENE-fractures. A data gap ~500-650 km occurs across the south-central part of the map area.

We have focused geologic mapping to date on the coronae and tessera terrain, each of which are briefly described in turn.

V-45 coronae: The coronae include four features (Mama-Allpa, Inanna, Codidon, and Mou-nyamy) marked by topographic domes and radial fracture suites (termed radial coronae, herein) and four (Umay-ene, Xcanil, Zemlika, and a small unnamed corona) represent circular basins (termed circular lows, herein). Ekhe-Burkhan Corona, which straddles the south-central boundary, differs morphologically from both the radial coronae and circular lows. Gurshi Mons (SE corner) displays radial fractures, and appears morphologically similar to the adjacent radial coronae.

The four circular lows from NE to SW, and from largest to smallest include: Umay-ene, Zemlika, Xcanil, and an unnamed corona at ~39S/42.5E (here called CL45A). Umay-ene Corona (~370 km diameter), a double-ringed feature, displays a circular basin marked by two nested circular ridges, with an interior central peak (?). Umay-ene lacks radial fractures, although the surrounding region is cut by closely-spaced NE-trending regional fractures to the east, and ribbon tessera terrain to the west. Zemlika (~250 km diameter), marked by concentric structures and sharp topographic gradients, lacks radial features, and clearly crosscuts and hence post-dates ribbon tessera terrain. Xcanil and CL45A lie in the relatively featureless central V-45, southwest of Zemlika; both features display NE-trending fractures parallel to regional trends, but lack radial fracture suites.

Radial coronae Mama-Allpa (NW corner; ~200 km diameter), Mou-nyamy and Codidon (SE corner; each ~200 km diameter), and Inanna, (central-western V-45; ~200 km diameter) display raised interiors and radial fracture suites common among chained and clustered coronae, such as those along Parga and Hecate Chasmata [Hamilton & Stofan 1996]. Unlike their chained and clustered counterparts

however, these radial coronae lack association with chasmata or volcanic rises. Gurshi Mons, which lies between the two SE radial coronae, appears similar to its neighbors.

The topographic and structural difference between these two coronae subsets, circular lows and radial coronae, begs the question: How are geological histories of radial coronae and circular lows similar and/or different? How might documented differences contribute to differences in the mode of formation of these features? Can the differences be explained within the context of different stages of preservation of a similar mode of formation, or do geohistory differences require different modes or mechanisms of formation?

If all coronae form via diapiric mechanism then circular lows might represent older more evolved coronae in which the interior has subsided and early-formed radial fractures are simply buried from obvious view. If circular lows represent a genetically different type of feature, then we should be able to determine this from detailed geological mapping and geohistory analysis. Circular lows might represent, for example, ancient impact features formed under different rheological conditions, either locally or globally defined. Or perhaps an entirely different hypothesis for the formation of either or both subsets of lowland coronae will emerge from the geological mapping and geohistory analysis.

V-45 lowland tessera terrain: This terrain is divisible into at least two packages, northern tessera and southern tessera. Tessera outcrops, marked by penetratively developed tectonic fabrics occur at the highest altitude, and likely represent the oldest local deformation. Northern tessera host well-defined ribbon and fold fabrics typical of ribbon tessera terrain preserved in crustal plateaus. The southern tessera terrain hosts a similar, but possibly different fabric. The northern tessera terrain ribbons and folds describe regional patterns coherent over 100's of km, yet the patterns show apparent truncation by one another. Locally linear tessera tracts mark asymmetric fabric similar to S-C shear fabrics. Both right-lateral and left-lateral shear directions are preserved. Tessera that lies along the crest of two nested curvilinear ridges record right-lateral shear, as do ENE-trending tessera fabrics to the east. But these regions show apparent cross-cutting relations by WNW-trending Pasom-mana Tesserae ridges, which record apparent left-lateral shear. Xi-Wang-mu Tessera, which outcrops along a NE-trending high along the east boundary records local dextral shear, parallel to the trend of the ridge. Tushita Tesserae, which outcrops along a broad WNW-trending high to the south might record a confluence of NW- and NE-trending tessera fabrics. A region, mapped as flooded, or covered tessera terrain, occurs around much of the northern tessera; lineaments within this region typically parallel the trends of adjacent tessera structural patterns. The covered region commonly hosts numerous small shields, forming a thin veneer above tessera terrain below.

The southern tessera lacks clear ribbon and fold fabrics, yet the penetrative tectonic fabric commonly marked by two or more lineaments trends is typical of tessera terrain. Locally ribbon and fold structures might be delineated with moderate confidence. Southern tessera occurs most extensively in the SW corner associated with Ekhe-Burkhan Corona, and outcrops as kipukas among flows of Sezibwa Vallis, and numerous shields in the region surrounding Tuzandi Mons. A penetrative radial fabric marks Tuzandi Mons reminiscent of tessera terrain, and tectonomagmatic centers preserved within the interior of Artemis (V-48); Tuzandi Mons may have formed synchronously with local tectonic fabric.

Circular lows Umay-ene, Zemlika, and Xcanil clearly crosscut adjacent tessera terrain topography and tectonic fabric. The radial coronae are spatially separate from the tessera, and as such temporal relations are less certain; however, it appears that radial coronae likely post-date tessera formation. The incredibly sharp demarcation of the circular low features (topographic and tectonic) stands in strong contrast to the gradational character (topographic and tectonic) typical of the radial coronae—differences that could reflect: 1) marked difference in strength of the strong layer during feature formation, 2) strain rate of impacting body (endogenic or exogenic), or 3) direction of responsible forces (whether from above or below). Radial coronae and circular lows might reflect different genetic processes.

GEOLOGIC MAPPING OF THE KAWELU PLANITIA (V-16) AND BELLONA FOSSAE (V-15) QUADRANGLES ON VENUS. J. R. Zimbelman, CEPS/NASM, Smithsonian Institution, Washington, D.C. 20013-7012 (zimbelmanj@si.edu).

Introduction: This report summarizes the current status of a Venus mapping project supported by NASA grant NAG5-11743 (the no-cost extension of which ended in April of 2006). Work during this past year has focused almost exclusively on the Kawelu Planitia map, but results from this work have application to the Bellona Fossae map as well.

V-16, Kawelu Planitia: The revised map, text, description of map units (DOMU), correlation of map units (COMU), and figures for V-16 were submitted to the U.S. Geological Survey in March, 2007 (see Figs. 1 and 2). The revisions addressed the major

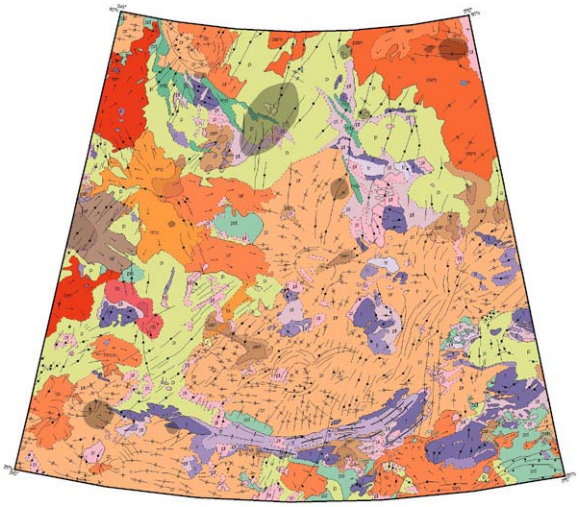

Figure 1. 2007 version of the V-16 geologic map.

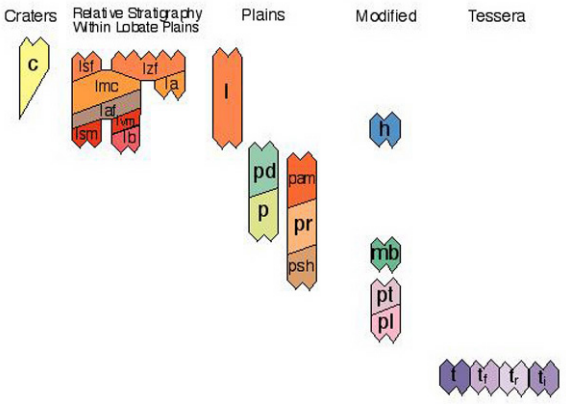

Figure 2. 2007 version of the V-16 COMU.

issues raised by reviewers and incorporated relevant literature that appeared since the map was originally submitted. Unfortunately, U.S.G.S. personnel soon found that the map contact lines did not match up to a digital base map for the quadrangle. After considerable discussion and work with the original map files, it was determined that the root cause appears to be the fact that the map is a composite of several revisions over the years, including major parts that were done on a photo print base rather than on a digital base product. It now appears that at best only a portion of the map line work can be matched to a digital base. We are now attempting to identify how to minimize the amount of new line work that will be required to get the entire map aligned with a digital base map. This is the unfortunate heritage of map work that began in the non-digital mapping era. We will work closely with U.S.G.S. personnel to get this map into an acceptable format as quickly as possible, but the need to redo line work means that this effort likely may take some time.

V-15, Bellona Fossae: Essentially all efforts since the end of the no-cost extension of the mapping grant have gone into preparation of the V-16 materials, described above. The V-15 map (Fig. 3)

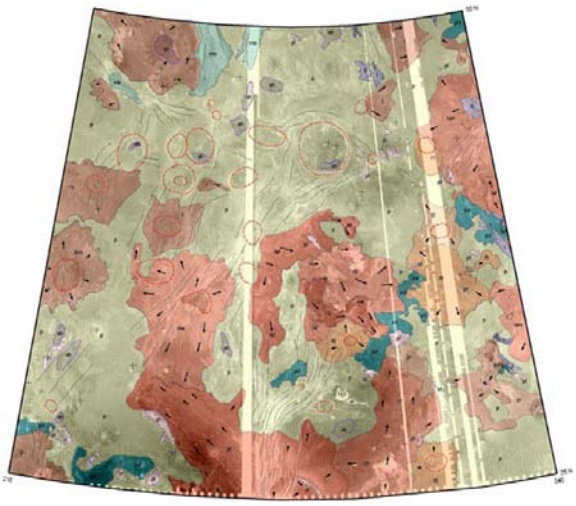

Figure 3. Current version of the V-15 geologic map.

remains the same as what was presented at the 2006 mappers meeting. We do not anticipate major changes being needed to the geology for this map, and it will also benefit greatly from the V-16 materials for text, DOMU, and COMU preparations. We will pursue completion of this map for submission once the V-16 issues have been resolved.

GLOBAL GEOLOGIC MAP OF EUROPA. T. Doggett[1], P. Figueredo[1,*], R. Greeley[1], T. Hare[2], E. Kolb[1], D. Senske[3], K. Tanaka[2] and S. Weiser[1], [1]School of Earth and Space Exploration, Arizona State University, Tempe, AZ, [2]U.S. Geological Survey, Flagstaff, AZ, [3]Jet Propulsion Laboratory, California Institute of Technology, Pasadena, CA, (*currently at the ExxonMobil Research Company, Houston, TX.)

Introduction: Europa, with its indications of a sub-ice ocean, is of keen interest to astrobiology and planetary geology. Knowledge of the global distribution and timing of Europan geologic units is a key step for the synthesis of data from the *Galileo* mission, and for the planning of future missions to the satellite.

The first geologic map of Europa [1] was produced at a hemisphere scale with low resolution *Voyager* data. Following the acquisition of higher resolution data by the *Galileo* mission, researchers have identified surface units and determined sequences of events in relatively small areas of Europa through geologic mapping [2-6] of images at various resolutions acquired by *Galileo*'s Solid State Imaging (SSI) camera [7]. These works [2-6] provided a local to sub-regional perspective and employed different criteria for the determination and naming of units. Unified guidelines for the identification, mapping and naming of Europan geologic units were put forth by [8] and employed in regional-to-hemispheric scale mapping [9,10] which is now being expanded into a global geologic map.

Methodology: A global photomosaic [11] of *Galileo* and *Voyager* data was used as a basemap for mapping in ArcGIS, following suggested methodology of allostratigraphy for planetary mapping [12]. Due caution was exercised given that the mosaic has a resolution varying from 12.6 to 0.23 km per pixel (Fig. 1), as well as variations in illumination and viewing geometry, to avoid making distinctions between units that are artifacts of these variations. In areas of high resolution coverage, contacts were marked as definite, and left as queried in areas of low resolution coverage. The cut-off between these two mapping regimes is a resolution of 1.7km/pixel.

Stratigraphy: The earliest epoch recorded on the current surface of Europa is typified by plains which appeared smooth at *Voyager* resolutions, but were shown to be intensely ridged at *Galileo* resolutions. The following epoch was dominated by the formation of widely spaced, wider lineae, according to a stratigraphic sequence derived for this work. The multi-ring impact crater Callanish sits early in the linea-forming period, while Tyre sits in the later stages. All other impacts appear to be younger than the linea-forming epoch. The most recent epoch includes the formation of chaos units, with implied genetic similarity, but are formally distinct in terms of stratigraphy, and photometric and resolution differences place a caveat on morphological comparisons. The stratigraphy for the youngest, chaos-forming epoch was separated into distinct regional provinces:

(1) The trailing hemisphere equatorial province, dominated by the large chaos blocks of Annwn and Dyfed Regiones, inclusive of the archetypical Conamara Chaos, and the young Pwyll crater, whose rays and secondaries superimpose on the chaos.
(2) The leading hemisphere equatorial province, dominated by the large chaos blocks of Powys and Tara Regiones, appearing as a rough counterpart to Annwn and Dyfed, though in addition to the resolution/photometry caveat, the differences in the space weathering environment between trailing and leading hemispheres almost certainly causes superficial differences in the appearances of the chaos units contrasted between the two provinces.

A dark unit, transected by lineae, is at the base of the stratigraphic sequence of both provinces, roughly centered on the sub-jovian and anti-jovian points respectively. This appears to indicate a phase of chaos formation prior to the linea-forming epoch.
(3) The Argadnel Regio province, distinctive because of its densely packed ridges and bands in circular and semi-circular configurations and maculae such as Thrace and Thera Maculae. Features called micro-chaos [3] in this region are similar to the knobby chaos unit of other regional maps [9, 10].
(4) The north polar province, mostly poorly resolved, with some high resolution images showing ridges super-imposed on chaotic terrain, inferred to be similar to the ridged dark units at the anti- and sub-jovian points.
(5) The south polar province, appears to be another regional-scale block of chaos, albeit poorly resolved.

References: [1] Lucchitta and Soderblom, in *The Satellites of Jupiter*: 521, 1982; [2] Senske et al., *LPSC* XXIX, #1743, 1998; [3] Prockter et al., *JGR., 104*: 16531-16540, 1999; [4] Kadel et al., *JGR*, 105, 22657-22669, 2000; [5] Figueredo et al., *JGR*, 107, 10.1029/2001JE001591, 2002; [6] Kattenhorn, *Icarus*, 157, 490-506, 2002; [7] Belton et al., *Space Science Reviews*, 60, 413-455, 1992; [8] Greeley et al., *JGR*, 105, 22559, 2000; [9] Figueredo and Greeley, *JGR*, 22629-22646, 2000; [10] Figueredo and Greeley, *Icarus*, 167, 287-312, 2004; [11] USGS, I-2757, 2003; [12] Skinner and Tanaka, *LPSC XXXIV*, #2100, 2003.

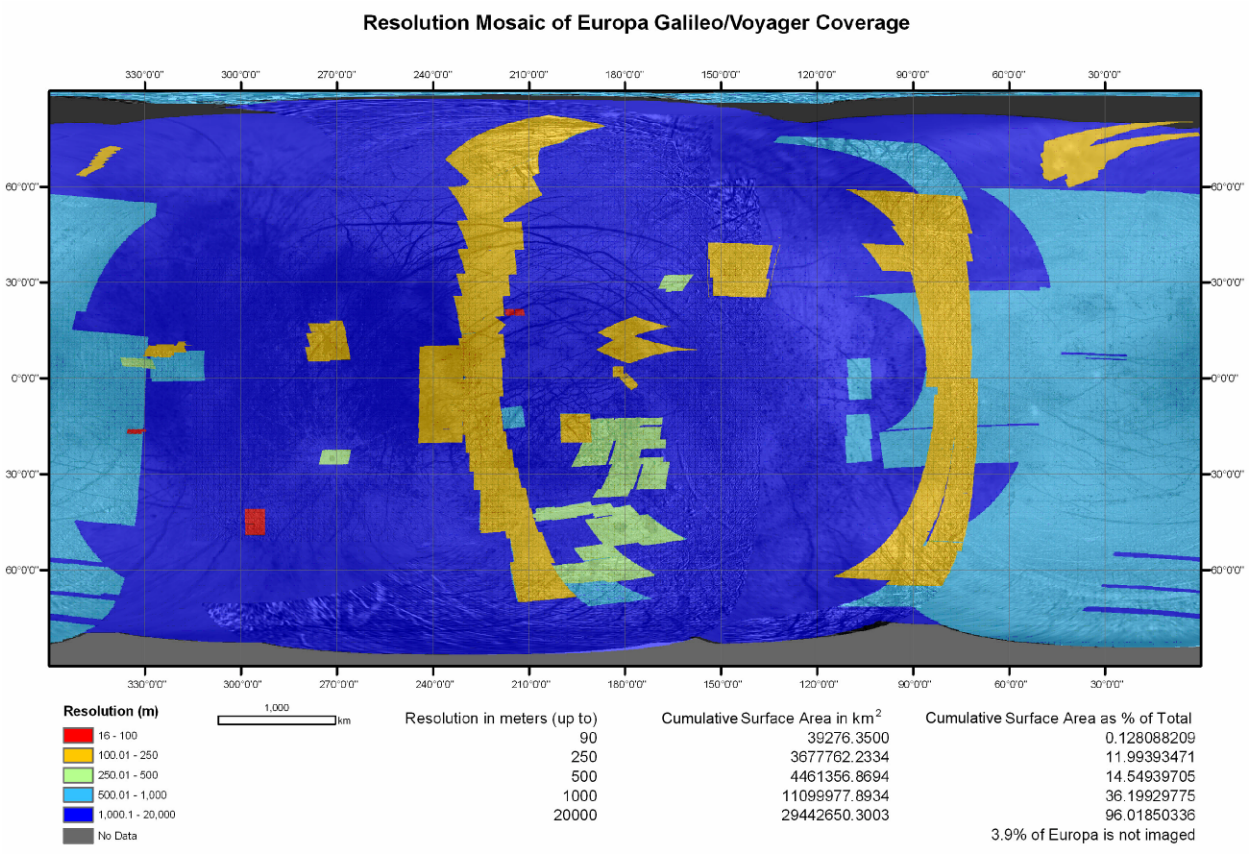

Figure 1: Differences in spatial resolution in the underlying dataset (Galileo/Voyager mosaic) used as base for the global geological map of Europa.

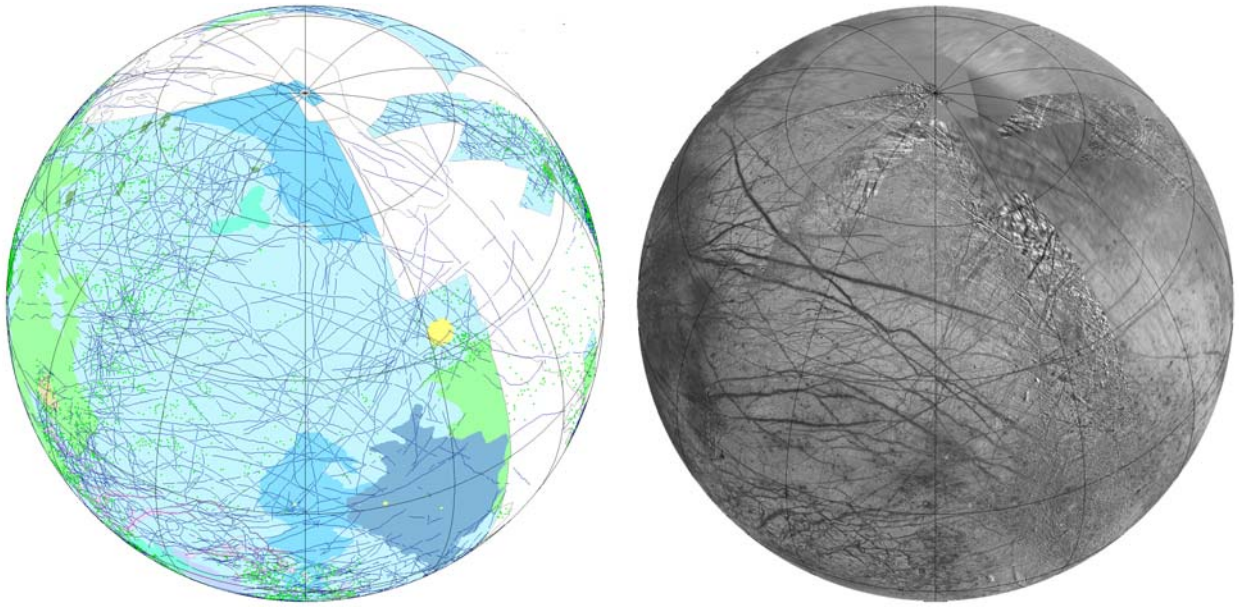

Figure 2: Portion of global geological map of Europa in orthographic projection, centered on northern anti-jovian hemisphere, light blue represents global plains unit, darker blue and green represent disrupted (chaotic units), yellow represents impact craters, dark blue lines represent major lineaments, green dots represent lenticulae.

THE GLOBAL GEOLOGIC MAP OF GANYMEDE. G. Wesley Patterson[1], James W. Head[1], Geoffrey C. Collins[2], Robert T. Pappalardo[3], Louise M. Prockter[4], and Baerbel K. Lucchitta[5], [1]Department of Geological Sciences, Brown University, Providence, RI, 02912 (Gerald_Patterson@brown.edu), [2]Wheaton College, Norton, MA, 02766, [3]Jet Propulsion Laboratory, Pasadena, CA, 91109, [4]Applied Physics Laboratory, Laurel, MD, 20723, [5]USGS, Flagstaff, AZ, 86001.

Introduction: The surface of Ganymede can generally be divided into two material types that exhibit differences in albedo, crater density, and surface morphology. Covering approximately a third of the surface is a lower albedo or dark material that is heavily cratered and commonly modified by the presence of large-scale arcuate fracture systems termed furrows. Crater density suggests dark materials represent the oldest preserved surfaces on Ganymede, though they generally have lower crater densities than neighboring Callisto, suggesting a limited amount of resurfacing [1]. The other two thirds of the surface are covered by vast globe-encircling swaths of a higher relative albedo or light material that has a crater density significantly lower than dark material. These swaths are themselves divided into polygons that range in appearance from relatively smooth to heavily modified by troughs termed grooves, at resolutions > 500 m/pixel. It has been suggested that light material formed predominantly through the modification of dark material by tectonic and cryovolcanic resurfacing processes [2].

The presence of this surface dichotomy leads to a number of fundamental questions about the formation and evolution of the surface of Ganymede. What is the origin of the albedo heterogeneity of the surface? How have dark and light materials evolved through time? What internal forces led to the formation of tectonic structures like furrows and grooves? Does the formation of grooves primarily reflect a local or global stress regime and how has that stress regime changed through time? What are the properties of craters on Ganymede and what are the relative age relationships among geologic features on the surface? Understanding the geological record of Ganymede is crucial to answering these questions.

We have compiled a global geological map of Ganymede that represents the most recent understanding of the satellite on the basis of Galileo mission results. This contribution builds on important previous accomplishments in the study of Ganymede [e.g., 1, 3-9] and will help to provide constraints on models for the formation and evolution of Ganymede and potentially the other the Galilean satellites.

Material units:

Dark material: Dark material is subdivided into three units for the global geologic map: A cratered unit (**dc**), a lineated unit (**dl**), and an undivided unit (**d**). This material has been heavily modified via impact processes (palimpsests, craters, basins, and related furrows), sublimation, mass wasting, and tectonism. Galileo high resolution images suggest that the dark material is composed of a relatively thin dark deposit overlying brighter icy material, and that it has been modified by surface processes such as sublimation, mass wasting, ejecta blanketing, and tectonism [8, 10].

Light material: Light material is subdivided into four units: A grooved unit (**lg**), a subdued unit (**ls**), an irregular unit (**li**), and an undivided unit (**l**). Light material forms swaths that cross-cut the older dark terrain and contain polygons 10s to 100s of kilometers wide, forming an intricate patchwork across the surface. Light material is primarily characterized by the density and orientation of structural grooves that exist within a given polygon. Light materials are interpreted to form from dark material via extensional tectonism, likely initiated along preexisting fractures (such as furrows).

Reticulate terrain: This terrain consists of a single unit (**r**). It is often associated with and surrounded by bright grooved, bright subdued, and/or dark lineated units but can be distinguished from them by its variable albedo and presence of grooves with two dominant directions (typically near-orthogonal to each other). Reticulate terrain appears to represent dark and light material that has been modified by the formation of orthogonal sets of grooves. It has been suggested that the formation of reticulate terrain may be the result of subsequent episodes of extensional tectonism [1,6], or of block rotation within a distributed shear zone [11].

Impact material: Impact material is divided into three subunits: Crater, Palimpsest, and Basin material. These divisions are based on crater diameter, relative age, and differences in morphology.

Crater material is subdivided based on relative albedo contrast with respect to surrounding materials and the presence of rays and continuous ejecta into degraded craters (**c_1**), partially degraded craters (**c_2**), and fresh craters (**c_3**). A crater ejecta unit (**ce**) is also defined. Craters that cannot be categorized in this manner, most often due to resolution effects, constitute a fourth crater material unit: unclassified craters (**cu**).

Palimpsest material is subdivided into four units: old palimpsests (**p_1**), young palimpsests (**p_2**), unclassified palimpsests (**pu**), and palimpsest interior plains (**pi**). The first two are categorized based on their crosscutting relationships with light materials, the third includes all

other palimpsests, and the last represents the interior deposits of some palimpsests.

Basin material represents units describing the ejecta from Gilgamesh basin and is subdivided into two units: Basin rugged material (**br**) and basin smooth material (**bs**).

Stratigraphy:

To determine age relationships among the various mapped units of the global map of Ganymede (Fig. 1), we utilized observed cross-cutting relationships and crater density measurements [12]. The conclusions drawn from these relationships and crater density measurements are broadly supported by previous crater counting efforts based on Voyager data [1,13].

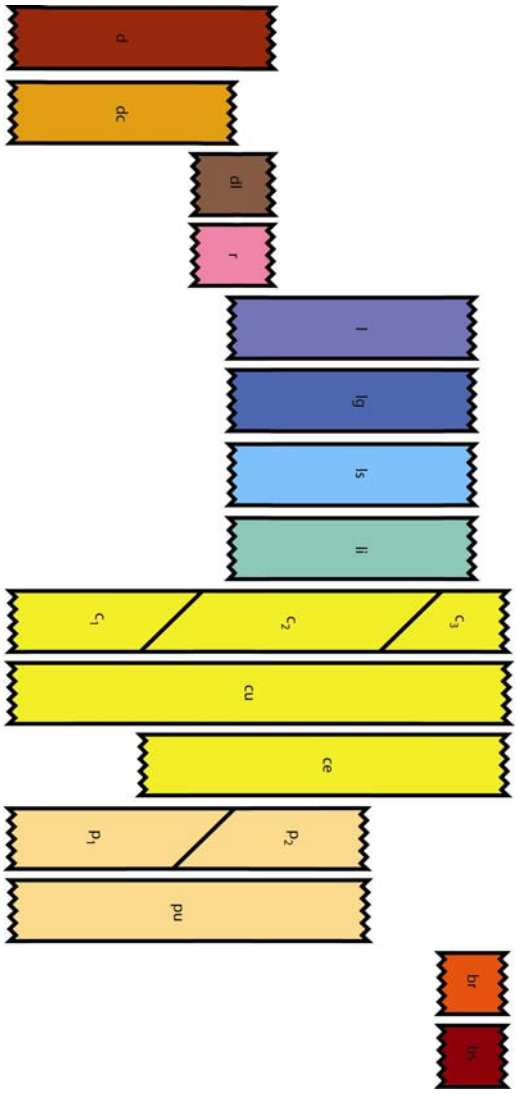

Fig. 1. Correlation chart of Ganymede material units. Younger units are shown above older units; diagonal lines represent transitional or overlapping boundaries; 'saw-tooth' pattern indicates uncertain boundary ages.

References: [1] Shoemaker et al., Sats. of Jupiter, 435, 1982; [2] Pappalardo et al., Jupiter, 363-396; [3] Guest et al., USGS Map I-1934, 1988; [4] Wilhelms, USGS Map I-2242, 1997; [5] Lucchitta et al., USGS Map I-2289, 1992; [6] Lucchitta, Icarus, 44, 481-501, 1980; [7] Pappalardo et al., Icarus, 135, 276-302, 1998; [8] Prockter et al., Icarus, 135, 317-344, 1998; [9] Murchie et al., JGR, 91, E222-E238, 1986; [10] Prockter et al., JGR 105, 22,519-22,540, 2000; [11] Murchie and Head, JGR 93, 8795-8824, 1988; [12] Patterson et al., 38th LPSC, #1098 [13] Murchie et al., Icarus 81, 271-297, 1989.

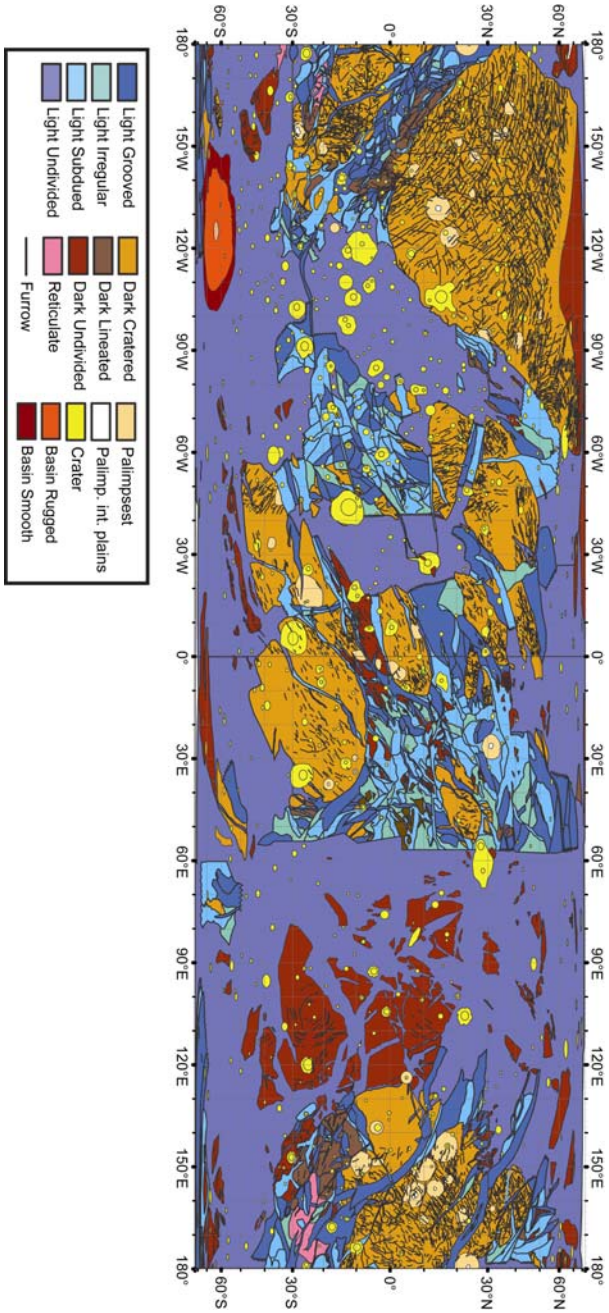

Fig. 2. Preliminary geological map of Ganymede. Unit descriptions are given in the text

THE GLOBAL GEOLOGIC MAP OF IO: APPROACH AND MAPPING STATUS. David A. Williams[1], Laszlo P. Keszthelyi[2], Paul E. Geissler[2], Windy L. Jaeger[2], Tammy L. Becker[2], David A. Crown[3], Paul M. Schenk[4], and Julie A. Rathbun[5]; [1]School of Earth and Space Exploration, Arizona State University, Box 871404, Tempe, Arizona, 85287 (David.Williams@asu.edu); [2]Astrogeology Team, U.S. Geological Survey, Flagstaff, Arizona; [3]Planetary Science Institute, Tucson, Arizona; [4]Lunar and Planetary Institute, Houston, Texas; [5]University of Redlands, Redlands, California.

Introduction: Jupiter's volcanic moon Io is a challenging place to study using typical planetary mapping techniques, because of 1) rapid (in geologic terms) resurfacing from volcanic activity and 2) non-uniform coverage from multiple spacecraft flybys, resulting in a wide range of image resolutions and photometric properties. Nevertheless, because Io's level of volcanic activity makes it unique in our Solar System, it is desirable to map its surface in order to complete a global reconnaissance of its surface features and material units and to understand better its geologic evolution. In this abstract we discuss our approach and progress in producing a global geologic map of Io. For production of our map, we are using a set of combined *Galileo*-*Voyager* global mosaics and ArcGIS software. We are also creating a GIS database to contain all compatible *Galileo*, *Voyager*, and other Io data sets to show surface changes and aid in geologic interpretations.

Background: Io, the innermost Galilean satellite of Jupiter, is the most volcanically active body in the Solar System. Tidal heating produces magma that feeds ~300 active volcanic centers [1-3]. The 1979 *Voyager* flybys observed ~25% of Io's surface at resolutions of <2 km/pixel (the rest at 2-20 km/pixel: [4]), covering mostly the subjovian hemisphere. The *Galileo* mission (1996-2003) included five close flybys of Io, focused mostly on the antijovian hemisphere [5-7], with resolutions between ~10 m/pixel to 20 km/pixel. Previous geologic mapping of Io includes a series of four regional *Voyager*-based maps [8], a *Voyager*-based global map [9], and four *Galileo*-based regional maps [10].

The complementary coverage of Io by *Voyager* and *Galileo* has enabled the production of a series of high quality grayscale and color global mosaics. Our goal is to complement the new mosaics with a corresponding global compilation of geologic understanding at the end of the *Galileo* era. Geologic mapping is a tool that enables the definition and characterization of surface features into process-related material units and structures and places them within their stratigraphic context, allowing recognition of the geologic evolution of an area, region, or planet.

Global Io Mosaics: The USGS Io global mosaics (1 km/pixel nominal resolution) are now the definitive global compilation of image products for Io. They consist of four distinct products: 1) a global mosaic of *Galileo* color images (756nm-green-violet as R-G-B, 4 phase angle); 2) a global mosaic of the best resolution *Galileo* monochrome images; 3) a global mosaic of the best resolution *Voyager* and *Galileo* monochrome images; and 4) a merged product combining *Galileo* color information with the higher resolution monochrome images. Each of these four products is available as an ISIS cube in Sinusoidal, Mercator and Polar Stereographic projections (both north and south pole). An extensive set of ancillary data was developed for all of these mosaics to help users understand the various combinations of data from different sensors, filters, dates, and illumination and viewing geometries. These include footprint plots showing the identity of each of the component images and diagrams that show the incidence, emission, and phase angles, along with the spatial resolutions of the individual frames used.

Strategies for Global Mapping: After analysis of all previous geologic maps and study of the new global mosaics, we developed the following strategy for global mapping. All mapping is done using ArcMap software, part of the ArcGIS package by ESRI:

1) *Map diffuse deposits using Galileo global color data.* This is done because of the wide variety of diffuse deposits on Io (black, yellow, white, red, green), which are thought to represent distinct compositions (silicates, sulfurous materials, SO_2-dominated materials, short-chain sulfur allotropes, products of silicate/sulfur interaction, respectively).

2) *Map mountains, surrounding plateaus, and structural features using various mosaics.* Various image products are used to identify mountains, layered plateaus, and other materials delineated by scarps and other structural features, because they have nearly the same color and texture as background plains and cannot be identified except in images taken during low solar incidence angles.

3) *Map vents and paterae using various mosaics.*

4) *Map lava flow fields using various mosaics.* We first map the outermost boundaries of each flow field around a vent, followed by the addition of more detail (individual lobate flow margins, fresher interior flows) as the available resolution permits. Active or recently active flows are identified by the following criteria: 1) observed surface changes in images obtained at different times; 2) thermal anomalies detected in NIMS data; and/or 3) an observed plume source at or near the flow margins.

5) *Map plains.* The bright plains include everything not mapped in the previous categories, and are thought to consist of silicate crust mantled by various S-

bearing materials [10]. The primary interpatera Plains Material has three subunits based on color (Yellow, White, and Red-Brown); Layered Plains are composed of plateaus separated from surrounding plains by scarps and are thought to be produced by degradational processes [11].

Mapping Progress: We have mapped the polar regions of Io (±57.5 -90) as of May 2007. The following summarizes our results:

In general, Io displays five primary types of morphological units: plains, patera floors, flows, mountains, and diffuse deposits. Plains materials cover ~86% of Io's surface in the polar regions. The greatest percentage (79%) consists of radiation-altered Red-Brown Plains, with lesser amounts of White Plains (SO_2-dominated, 3%) and Bright (yellow) Plains (sulfur-dominated, 2%). Eroded plateaus, or Layered Plains, make up ~3% of the polar regions.

Patera floors have a range of albedos and colors in the polar regions, and are mapped as Bright (presumably sulfur-covered, 0.3%), Dark (presumably silicate-covered, 0.3%), and Undivided (0.8%). There are suggestions of additional paterae in the polar regions, based on albedo and color differences in the mosaics, but confirmation must await more high-resolution coverage. Patera floors range from bright white to yellow-orange to dark black in *Galileo* images, in which the colors suggest various compositions, including mixes of silicates, sulfurous compounds, and relatively pure sulfur dioxide in some cases [12]. Heno Patera (57.1 S, 311.5 W), a 71.1 km diameter patera, has a dark floor and dark flows that surround a circular feature approximately centered on the patera floor. We speculate that this may be the site of an impact that is experiencing modification by volcanism.

There are significant expanses of Bright Lava Flow materials in the polar regions (3% of all mapped polar units), thought to be indicative of sulfur volcanism. The area of the Bright Flows is twice that of the Dark Flows (silicate-dominated, ~1%), although Undivided Flows (units with intermediate albedos and colors) make up another 6% of polar materials. These mapping results suggest that lava flows outside paterae may have a greater role in resurfacing Io than previously thought. Many polar bright flow fields are not directly adjacent to dark flows, perhaps indicative of a significant component of primary sulfur volcanism. Lithologically, Patera Floor materials and Lava Flow materials are probably identical in composition. However, their distinctive geologic settings justifies separating them on the global map.

In the polar regions, Lineated Mountain materials make up about ~2% of the surface. By number there are more mountains identified in the south polar region, due to the better *Voyager* imaging (i.e., need right illumination & resolution). Mottled and Undivided Mountain materials each make up <1% of the polar areas. Lineated Mountain materials are topographically-distinct massifs (relative to layered plains) containing ridges, grooves, scarps, and lineaments on positive-relief edifices. This unit is interpreted as tectonically-disrupted sections of crust containing planar structural features, possibly faults involved in uplift and/or collapse during mountain formation [2]. Massifs with no visible patterns are classified as Undivided. Mottled Mountain materials have smoother surfaces lacking lineations and indicative of mass wasting processes. No volcanic mountains (Tholus, Cone, or Shield materials) were recognized in the polar regions.

The polar regions contain extensive diffuse deposits, which cover 16.5% of the surfaces of other units. White Diffuse deposits are thought to be dominated by SO_2-rich frosts, and make up 64% of all diffuse deposits at the poles. They usually occur at the margins of lava flows or around paterae, but also make up extensive halos around some mountains. Yellow Diffuse deposits are likely composed of some combination of sulfur-rich materials and SO_2, albeit less SO_2 than White deposits. Only 10% of diffuse deposits at the poles are yellow, and these are less extensive than in equatorial regions. Red Diffuse deposits occur as ephemeral mantles around active vents, and make up ~10% of polar diffuse deposits. There are the remnants of two faint red rings in the north polar region, one surrounding Dazhbog Patera (which erupted during the *Galileo* I31 flyby) and one around an unnamed patera at 70 N, 55 W. They have been interpreted as pyroclastic deposits rich in metastable, S_3 and S_4 allotropes, which are red when quenched from magmatic S_2 gas [13], possibly also containing Cl-bearing materials at some vents [14]. Dark Diffuse deposits are interpreted as pyroclastic deposits derived from silicate lavas [15], and cover ~16% of the area of polar units.

A wide range of structural features can be identified in the polar regions of Io, including scarps, ridges, lineaments, and circular depressions (pits and patera rims). The additional low-sun observations and higher resolution of the *Galileo* camera has enabled recognition of these and other structural features over a wider part of Io's surface than was previously possible.

References: [1] *Radebaugh et al*., 2001, *JGR 106*, 33,005-33,020; [2] *Schenk et al*., 2001, *JGR 106*, 33,201-33,222; [3] *Lopes et al*., 2004, *Icarus 169/1*, 140-174; [4] *Smith et al*., 1979a,b, *Science 204*, 951-972, & *Science 206*, 927-950; [5] *McEwen et al*., 2000, *Science 288*, 1193-1198; [6] *Keszthelyi et al*., 2001, *JGR 106*, 33,025-33,052; [7] *Turtle et al*., 2004, *Icarus, 169/1*, 3-28; [8] *Moore, H.J*., 1987, *USGS Map* I-1851, 1:1,003,000; *Greeley, R., et al*., 1988, *USGS Map* I-1949, 1:2,000,000; *Schaber, G.G., et al*., 1989, *USGS Map* I-1980, 1:5,000,000; *Whitford-Stark, J.L., et al.*, 1991, *USGS Map* I-2055, 1:5,000,000; [9] *Crown, D.A., et al*., 1992, *USGS Map* I-2209, 1:15,000,000; [10] *Williams, D.A., et al*., 2002, *JGR* 107, 5068, doi:10.1029/2001JE001821; *Williams, D.A., et al*., 2004, *Icarus* 169, 80-97;

Williams, D.A., et al., 2005, *Icarus* 177, 69-88; *Williams, D.A., et al*., 2007, *Icarus*, *186*, 204-217; [11] *Moore et al*., 2001, *JGR 106*, 33,223-33,240; [12] *Carlson, R.W., et al*., 1997, *GRL 24*, 2479-2482; [13] *Spencer et al.*, 2000, *Science 288*, 1208-1210; [14] *Schmidt & Rodriguez*, 2003, *JGR 108*, 5104, doi: 10.1029/2002JE001988; [15] *Geissler et al*., 1999, *Icarus 140*, 265-282.

USE OF CLEMENTINE UVVIS AND NIR DATA FOR LUNAR GEOLOGIC MAPPING.
Lisa Gaddis, Astrogeology Team, U.S. Geological Survey, Flagstaff, AZ 86001 (lgaddis@usgs.gov).

Introduction: The Clementine global, 11-band mosaic is now available at ~100 m/pixel for 5 ultraviolet-visible (UVVIS) wavelengths (415, 750, 900, 950, and 1000 nm; [1]) and 6 near-infrared (NIR) wavelengths (1100, 1250, 1500, 2000, 2600, and 2780 nm; [2]). The Clementine UVVIS mosaic is available online at the Map-a-Planet (http://www.mapaplanet.org/explorer/moon.html) and the Planetary Image Atlas (http://pds-imaging.jpl.nasa.gov/Missions/Clementine_mission.html) Web sites of the Planetary Data System (PDS). The NIR mosaic is available online at http://astrogeology.usgs.gov/Projects/ClementineNIR/ and it is now being reviewed prior to release by PDS. Although additional processing of these data may yet occur, the data quality is such that first-order analyses can be made [e.g., 3, 4]. These multispectral data are well-suited for use in lunar geologic mapping [e.g., 5].

Color Data for Lunar Mapping: Color information at multiple wavelengths has been used for some time to characterize and map geologic units on Earth [e.g., 6 and references therein]. For the Moon, color information was provided by Earth-based imaging and telescopic data [e.g., 7] and Apollo cameras prior to the Galileo mission and the acquisition of multispectral data by the Solid State Imager (SSI; [8]). In 1994 the NASA/DOD Clementine Mission acquired the first global color data for the Moon using the UVVIS and NIR cameras [9].

Mineralogy: Clementine UVVIS and NIR wavelengths were selected to maximize information on the mineralogy of lunar units (***Figure 1***). Pyroxenes have two absorption bands at these wavelengths, one centered near 1 micron and another near 2 microns; these band centers move to longer wavelengths as Ca and Fe substitute for Mg [e.g., 10]. Olivine has an absorption band centered beyond 1.05 micron that moves as Fe substitutes for Mg [11]. Significant amounts of olivine in lunar soils will broaden the pyroxene absorption at 1 micron and shift it to longer wavelengths. Because olivine lacks a band at 2 microns, the 1 micron absorption in olivine-rich lunar deposits will be strengthened relative to the 2 micron band. The presence of iron-rich volcanic glasses causes ~broad, shallow absorption bands in lunar soils because of the amorphous structure of the glasses [e.g., 12]. As the most abundant opaque mineral in lunar soils, ilmenite lowers their albedo and spectral contrast, and causes the typically red (i.e., sloping toward shorter wavelengths) lunar spectra to become less red [e.g., 13]. The presence of abundant plagioclase increases the albedo and alters other spectral properties of lunar soils.

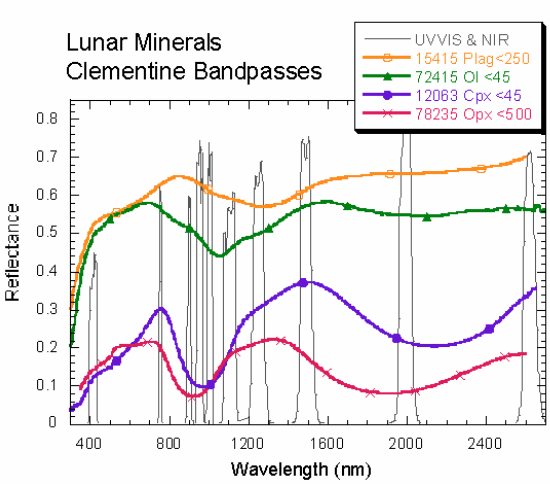

Figure 1. *Laboratory reflectance data for common lunar minerals with Clementine UVVIS and NIR bandpasses superimposed. (after Pieters, Ch. 14, in [7]).*

Maturity: Space weathering on the lunar surface has a significant influence on lunar soils, and causes them to appear more mature with time [e.g., 14, 15]. Comminution, production of agglutinates, and addition of coatings of amorphous silica with submicroscopic metallic iron all act to produce 'mature' lunar soils. Remote spectra of such soils are redder and have lower albedos and lower spectral contrast [16]. To understand the meaning of color variations in analyses of lunar soils, the effects of both maturity and particle size must be considered.

Unit Identification and Characterization: Single-band Clementine images, particularly the 750-nm 'albedo' mosaics, provide first-order compositional information and allow distinction between mare and highland units, low- and high-titanium maria, fresh vs. ancient craters, and some relative age relationships. Soil maturity is a major factor at 750 nm and this has allowed Lucey and others [17] to derive an 'optical maturity' (OMAT) parameter from the UVVIS data at 750 and 950 nm. These OMAT views have been used to determine relative ages of lunar craters [14, 18] and to refine the age of the stratigraphic boundary between the Copernican and Eratosthenian [e.g., 19] epochs on the Moon. Gillis and Lucey [20] note that the 2780 nm NIR data are particularly useful for distinguishing between mare basalt units on the basis of composition and without major soil

maturity effects. Analyses of crater ray brightness and distribution at the 2780 nm wavelength may be especially helpful for relative age assessment of lunar units.

Additional map bases derived from the Clementine data include the UVVIS "standard" color-ratio views (R=750/415; G=750/950; B=415/750) that cancel out the dominant brightness variations of the scene (controlled by albedo variations and topographic shading) and enhance color differences related to soil mineralogy and maturity [e.g., 21]. In these views, lunar highlands, mostly old (~4.5 b.y.) anorthositic rocks, are depicted in shades of red (older) and blue (younger). The lunar maria (~3.9 to ~1 b.y.), mostly iron-rich basaltic materials with varying titanium content, are portrayed in shades of yellow/orange (iron-rich, lower titanium) and blue (iron-rich, higher titanium). Superimposed on and mixed with these materials are those from basins and craters of various ages, ranging from the dark reds and blues of ancient basins to the bright blue rays of younger craters. More sophisticated, Clementine-derived maps include those based on FeO and TiO_2 content [17, 20, 22, 23, 24]. 'Rock type' [25], petrologic [26] and mineral maps [27] have also been derived from Clementine UVVIS data and used to identify and characterize geologic units and features on the Moon.

Visualization and analysis techniques developed for use with terrestrial multi- and hyperspectral data can be used to further characterize and identify geologic units on the Moon with Clementine color data. For example, using spectral scatterplots [e.g., 28] allows segregation of mature and immature lunar soils, and identification of spectral end-members of unique, spatially coherent units. Linear unmixing methods have also been applied to Clementine color data to distinguish compositionally 'pure' units from those of mixed lithologies [e.g., 29]. Geographic Information Systems (GIS) methods have also been applied to the analysis of lunar Clementine and numerous other digital datasets [e.g., 5, 30, 31]. Lunar GIS databases are available to facilitate mapping, data processing and analysis, and mission support activities (see http://webgis.wr.usgs.gov/pigwad/-maps/the_moon.htm, and especially the lunar data download site at http://webgis.wr.usgs.gov/pigwad-/down/moon_dl.htm).

Summary: Clementine data for mature and immature lunar soils provide information on the shape and position of the 1-micron band and the strength of the 1- and 2-micron bands. Analyses of the UVVIS and NIR data will provide better discrimination of the presence of high- and low-calcium pyroxenes, olivine, ilmenite and Fe-rich glass and plagioclase in lunar soils. These data thus provide a viable tool for characterizing and mapping lunar geologic units at ~high spatial resolution (≤200 m/pixel).

References: [1] Eliason et al. 1999, PDS Vol. USA_NASA_PDS_CL_4001 to 4078. [2] Gaddis et al., 2007, PDS Volumes USA_NASA_PDS_CL_5001 through 5078. [3] Cahill et al., 2004, LPS XXXV, abs. # 1469. [4] Staid et al., 2003, LPS XXXIV, abs. #1767. [5] Gaddis et al., 2006, LPS XXXVII, abs. #2135. [6] Rencz, A.N. (ed.), 1999, Man. Rem. Sens., 3rd Ed., V. 3, 707 pp. [7] Pieters and Englert (eds.), 1993, Rem. Geochem. Anal.: Elem. And Min. Comp., Cambridge Univ. Press. [8] Pieters et al., 1993, J. Geophys. Res. 98, 17,127. [9] Nozette et al., 1994, Science, 266, 1777. [10] Cloutis and Gaffey, 1991, J. Geophys. Res., 96, 22809. [11] Burns, 1993, Min. App. Of Crystal Field Theory, Cambridge Univ. Press. [12] Bell et al., 1976, Proc. Lun. Sci. Conf. 7th, 2543. [13] Wilcox et al., 2006, J. Geophys. Res., 111, E09001, doi:10.1029/2006JE002686. [14] Blewett et al., 2005, J. Geophys. Res., 110, E04015, doi:10.1029/2004JE002380. [15] Lucey et al., 2006, Rev. Min. Geochem., 60, 83. [16] Fischer and Pieters, 1994, Icarus 111, 475. [17] Lucey et al., 2000, J. Geophys. Res., 105, E8 20377. [18] Grier et al., 2001, J. Geophys. Res., 106, E12, 32847. [19] Hawke et al., 2007, LPS XXXVIII, abs. # 1133. [20] Gillis and Lucey, 2004, LPS XXXV, abs. #2158. [21] Pieters et al., 1994, Science, 266, 1844. [22] Lucey et al., 1995, J. Geophys. Res., 103, 3679. [23] LeMouelic et al., 2000, Jour. Geophys. Res., v. 105, 9445. [24] Wilcox et al., 2005, Jour. Geophys. Res., v. 110, doi:10.1029/2005JE002512. [25] Pieters et al., 2001, J. Geophys. Res., 106(E11), 28,001–28,022. [26] Zellner et al., 2002, J. Geophys. Res., 107(E11), 5102, doi:10.1029/2001JE001800 [27] Lucey, 2004, Geophys. Res. Lett., 31, L08701, doi:10.1029/2003GL019406. [28] Staid and Pieters, 2001, J. Geophys. Res. 106, 27887. [29] Li and Mustard, 2000, J. Geophysical Res., Vol. 105, 20,413-20,450. [30] Hare et al., 2007, Lunar Expl. Arch. Wkshp., Tempe, AZ, March 2007. [31] Skinner et al., 2005, LPS XXXVI, abs. #2344.

REMOTE SENSING STUDIES OF COPERNICUS RAYS: IMPLICATIONS FOR THE CALIBRATION OF THE LUNAR STRATIGRAPHIC COLUMN. B.R. Hawke[1], T.A. Giguere[1,2], L.R. Gaddis[3], B.A. Campbell[4], D.T. Blewett[5], J.M. Boyce[1], J.J. Gillis-Davis[1], P.G. Lucey[1], C.A. Peterson[1], M.S. Robinson[6], and G.A. Smith[1], [1]Hawaii Institute of Geophysics and Planetology, University of Hawaii, Honolulu, HI 96822, [2]Intergraph Corporation, P.O. Box 75330, Kapolei, HI 96707, [3]U.S. Geological Survey, Astrogeology Program, 2255 N. Gemini Drive, Flagstaff, AZ 86001, [4]Center for Earth and Planetary Studies, National Air and Space Museum, Washington, D.C. 20560, [5]NovaSol, 733 Bishop Street, Honolulu, HI 96813, [6]School of Earth and Space Exploration, Box 871404, Tempe, AZ 85287-1404.

Introduction: The nature and origin of lunar rays have long been the subjects of major controversies. We have been investigating the origin of lunar crater rays in support of the new Lunar Geologic Mapping Program. In an effort to better understand the processes responsible for the formation of lunar rays, we have utilized a variety of remote sensing data to study selected rays. Clementine UV-VIS images were used to produce high-resolution FeO, TiO_2, and optical maturity (OMAT) maps for the various rays utilizing the methods presented by Lucey et al. [1, 2]. Near-IR spectra and 3.8- and 70-cm radar maps were also utilized [3, 4]. Our preliminary finding resulted in a model for lunar ray formation [5, 6]. It was found that lunar rays are bright because of compositional contrast with the surrounding terrain, the presence of immature debris, or some combination of the two. The purpose of this report is to present the results of studies of Copernicus rays, to assess the implications for the calibration of the lunar stratigraphic column, and to reevaluate the ages of large craters in Mare Imbrium.

The Origin of Copernicus Rays in Mare Imbrium: Copernicus is a large bright-rayed crater, 93 km in diameter, located at 9.5º N, 20.0º W on the lunar nearside, and has long been used as a stratigraphic marker for lunar geology [7, 8, 9]. Continuous ejecta deposits occur up to a crater diameter away from the rim crest of Copernicus, while the ray system extends radially for more than 500 km [9]. We have investigated the Copernicus rays that extend north across the surface of Mare Imbrium with particular emphasis on four major rays. Two of these rays (Rays 1 and 2) extend north of Copernicus, and two (Rays 3 and 4) extend to the northeast. The albedo of the rays varies from moderate to high, and all exhibit numerous secondary craters which range in diameter from 200 m to 7.0 km.

The rays north of Copernicus (Rays 1 and 2) exhibit moderate to strong returns in the 3.8-cm depolarized radar image mosaic. The highest values are associated with secondary crater clusters. These areas have greater abundances of 1- to 40-cm-sized fragments in the upper 0.5 m of the regolith. Portions of Rays 1 and 2 exhibit slightly enhanced backscatter in the depolarized 70-cm radar image. The strongest enhancements are associated with secondary crater clusters. These enhancements have an excess of meter-sized blocks within 5-10 m of the surface.

The Copernicus rays in Mare Imbrium exhibit lower FeO and TiO_2 values than do the adjacent mare deposits. The background mare flows have FeO values that range between 17 and 19 wt.% and TiO_2 concentrations that range between 4 and 6 wt.%. The rays north of Copernicus have FeO abundances that vary from 12 to 16 wt.% and TiO_2 values that range from 2 to 4 wt.%. The FeO and TiO_2 concentrations generally show a negative correlation with the albedo values exhibited by the ray surfaces. FeO abundances generally increase along a given ray as a function of distance from Copernicus. The measured FeO value (8.0 wt.%) for the Copernicus ejecta blanket can be used to calculate the amount of highland-rich primary ejecta in the rays north of Copernicus. The calculated abundances of primary ejecta range from 20% to 60%.

The optical maturity (OMAT) images of the Copernicus rays indicate that relatively high OMAT values are associated with secondary crater chains and clusters. The highest values are exhibited by steep slopes on the crater interiors. Apparently, downslope movement on the interior crater walls constantly adds fresh material to the regolith. Ray surfaces away from the interiors of secondary craters display much lower OMAT values. These OMAT values are slightly higher than those exhibited by fully mature background mare surfaces near the rays. The rays of Copernicus in Mare Imbrium have not reached full optical maturity.

In summary, the Copernicus rays in Mare Imbrium display relatively low FeO and TiO_2 values because of the presence of variable amounts of highland-rich primary ejecta. The rays exhibit relatively low OMAT values except for areas with secondary crater clusters. Still, the rays are not fully mature. The Copernicus rays are bright largely due to contrast in albedo between the ray material containing highland-rich primary ejecta and the adjacent dark mare surfaces.

Implications for the Copernican-Eratosthenian Boundary: The working distinction between the Eratosthenian (E) and Copernican (C)

Systems is that Copernican craters have visible rays whereas Eratosthenian-aged craters do not [7, 11, 12]. Since compositional rays can persist for 3 Ga or more, the mere presence of bright rays is not a reliable indicator that a crater was formed during the C Period [6, 9, 13, 14, 15]. It is clear that a new method is required to distinguish C- from E-aged craters. It has been suggested that the OMAT parameter be used to define the C-E boundary [6, 14, 15]. With increasing age, the OMAT values for ejecta and rays decrease and eventually become indistinguishable from the background value, which is the optical maturity index saturation point [2, 15]. The time required for a fresh surface to reach the optical maturity index saturation point could be defined as the Copernican Period. Surfaces that have reached full optical maturity would then be of Eratosthenian (or greater) age. Grier and co-workers [14, 15] noted that if the ejecta of Copernicus were slightly more mature, it would be indistinguishable from the background in an OMAT image. Our results for the Copernicus rays in Mare Imbrium are consistent with these findings. Hence, the saturation of the optical maturity index may occur at about 0.8 Ga, which is the commonly accepted age of Copernicus [16, 17, 18].

A Reevaluation of Lunar Crater Ages: Because of the new definition of the C-E boundary, we have investigated the ejecta and rays associated with a number of large craters in Mare Imbrium. Our purposes were to determine the compositions and maturity states of the rays and to assess the ages of the parent craters in light of the new criteria.

Aristillus, Autolycus, and Theaetetus are located north of the Apollo 15 site. They have been mapped as Copernican craters based on the presence of rays [8, 10, 12]. The high-albedo rays of Aristillus, Autolycus, and Theaetetus contain highland material and are bright because of compositional contrast with the surrounding mare terrain. The rays and ejecta of these craters have reached full optical maturity. Hence, Aristillus, Autolycus, and Theaetetus are older than Copernicus and should be mapped as Eratosthenian-aged craters.

Timocharis (D=34km) and Euler (D=28 km) were mapped as Copernican-aged craters by Carr [19] and Wilhelms and McCauley [8] because they exhibit bright ejecta and rays. However, Wilhelms [20] recommended that they be assigned an Eratosthenian age. Portions of the ejecta deposits of Euler and Timocharis are bright because they contain FeO-poor highlands material. The OMAT data indicate that the ejecta and rays of both craters have reached full optical maturity. Hence, Euler and Timocharis should be mapped as Eratosthenian-aged craters. Unlike Euler and Timocharis, Lambert (D=30 km) excavated only FeO-rich mare material and does not exhibit bright rays. The OMAT image shows that Lambert ejecta is fully mature. Lambert was correctly mapped as an Eratosthenian crater by previous workers [8,19,20].

Pytheas (D=20 km) has been mapped as a Copernican-aged crater [8,19,20] because it exhibits bright ejecta deposits. FeO and TiO_2 maps indicate that the high-albedo portions of the Pytheas ejecta blanket contain abundant highland material. The OMAT data indicate that these highlands-rich deposits are fully mature and are bright only because of compositional contrast with the adjacent mare terrain. Since the Pytheas ejecta and rays have reached full optical maturity, it should be assigned an Eratosthenian age. An Eratosthenian age for Pytheas is confirmed by crater size-frequency values.

Delisle (D=25 km) and Diophantus (D=18 km) have been mapped as Eratosthenian-aged craters because they lack well-defined rays [e.g.,8]. It is not possible to determine the true degree of maturity of the Diophantus ejecta deposit because it is largely covered by immature ejecta from small, superposed craters such as Diophantus C as well as Aristarchus and Copernicus rays. However, those portions of the Delisle ejecta blanket not covered with fresh, small crater ejecta appear to be fully mature.

References: [1] Lucey P. *et al*. (2000*) J. Geophys. Res*., 105, 20,297. [2] Lucey P. *et al.* (2000) *J. Geophys. Res.,* 105, 20,377. [3] Zisk S. *et al*. (1974) *Moon*, 10, 17. [4] Campbell B. and Hawke B. (2005) *J. Geophys. Res*., 110, E09002. [5] Hawke B. *et al*. (2006) *LPSC 37*, #1133. [6] Hawke B. *et al*. (2004) *Icarus*, 170, 1. [7] Shoemaker E. and Hackman R. (1962) *The Moon-Sym. 14 of the I.A.U*., 289. [8] Wilhelms D. and McCauley J. (1971) U.S.G.S. Map I-703. [9] Pieters C. *et al*. (1985*) J. Geophys. Res*., 90, 12,393. [10] Page N. (1970) U.S.G.S. Map I-666. [11] Ryder G. *et al*. (1991) *Geology*, 19, 143. [12] Wilhelms D. (1987) U.S.G.S. Prof. Pap., 1348. [13] McEwen A. *et al*. (1993) *J. Geophys. Res*., 98, 17,207. [14] Grier J. and McEwen A. (2001) *Accretion of Extraterrestrial Material Throughout Earth History*, 403. [15] Grier J. *et al*. (2001) *J. Geophys. Res*., 106, 32,847. [16] Eberhardt P. *et al*. (1973) *Moon*, 8, 104. [17] Bogard D. *et al*. (1994) *GCA*, 58, 3093. [18] Stoffler D. and Ryder G. (2001) *Space Sci. Rev*., 96, 9. [19] Carr M. (1965) U.S.G.S. Map I-462. [20] Wilhelm D. (1980) U.S.G.S. Prof. Pap., 1046-A. [21] Neukum G. and Konig B. (1976) *Proc. Lunar Sci. Conf*., 7th, 2867.

GEOLOGY OF MTM QUADRANGLES -40277, -40272, -45277, AND -45272, EASTERN HELLAS PLANITIA, MARS. Leslie F. Bleamaster III[1,2], and David A. Crown[1], Planetary Science Institute, [1]corporate address - 1700 E. Ft. Lowell Rd., Suite 106, Tucson, AZ 85719; [2]mailing - 3635 Mill Meadow Dr., San Antonio, TX 78247, lbleamasPSI@satx.rr.com.

Introduction: Geologic mapping studies at the 1:1M-scale are being used to characterize geologic processes that have shaped the highlands surrounding the Hellas impact basin and, in particular, to evaluate landforms and deposits resulting from modification of highland terrains by volatile-driven degradation. Specific research objectives for geologic mapping of MTM quadrangles -40277, -40272, -45277 and -45272, located in eastern Hellas Planitia, include: 1) to reconstruct fluvial systems that dissect the Hellas rim, 2) to characterize the extensions of Dao and Harmakhis Valles onto the basin floor and to identify, if present, sediments contributed to Hellas Planitia from the rim, 3) to investigate the nature of the boundary between the east rim and Hellas Planitia in order to infer its mode of origin, age, and history of modification, and 4) to use small-scale surface morphology and small crater populations to examine finely layered deposits, local erosion, and burial/mantling/exhumation of surfaces. This mapping study builds on previous mapping in eastern Hellas [1-10] and facilitates comparisons between the geologic history of the east rim, the remainder of the rim, and Hellas Planitia.

Mapping Region: The map area includes the terminal portions of Dao and Harmakhis Valles and their floor deposits, dissected and channeled plains materials, and deposits associated with the Hellas basin floor. Following the mapping precedents of [3 and 8], materials in MTM -40277, -45277, and -45272 (and -40272 [8]) quadrangles have been divided into two major geologic assemblages: the Hellas rim assemblage (3 units) and the Hellas floor assemblage (3 units). The contact between these assemblages occurs at a prominent topographic break near the -5800 meter contour. In addition, valles and channel materials (7 units), and crater materials (3 units) have been defined. At 1:5M-scale, materials within this region above -5800m were mapped as the Hesperian/Noachian dissected unit, member 1; below -5800m, materials were mostly mapped as the Hesperian smooth interior unit [3]. Mapping at 1:1M-scale by Price [8] subdivided the dissected unit (rim assemblage) into Hesperian smooth plains (unit Hps) and Hesperian/Noachian hummocky plains (unit HNh), but did not evaluate any of the floor assemblage.

Hellas rim assemblage. Using THEMIS IR and VIS data, we have evaluated the contacts of units Hps and HNh mapped by Price [8] and have extended these unit boundaries westward from MTM -40272 to the rim/floor boundary. These two areally expansive units (new designations of HNps and Nph, respectively) surround the distal portions of the Dao and Harmakhis Valles canyon systems. The hummocky plains (unit Nph) display 10s to 100s of meters of relief and are located more near the rim/floor assemblage boundary and within high-standing inselbergs along the floor. Nph is bound by elevations –5200m and –5800m. Outcrops of finely layered materials are exposed in local high standing mesas, knobs, and surfaces near -5700±100m within the hummocky plains. The smooth plains (unit HNps) superpose unit Nph and are correlated with the locations of small-scale surface channels. The exposure, elevation, and spatial concentration of the layered deposits with unit contacts between units Nph and HNps (Fig. 1) suggest that the isolated layered outcrops most likely represent remnants of a once laterally continuous deposit of the smooth plains (unit HNps) that was part of a more widespread depositional shelf in eastern Hellas [11]. Removal of the upper smooth plains surface exposes the hummocky plains either by down cutting from channels, scarp retreat and aeolian erosion, and/or

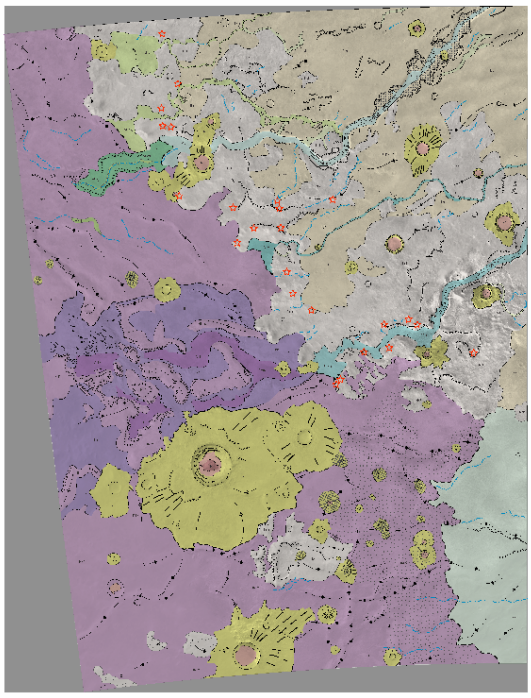

Figure 1. Geologic map of MTM quads –40277, -45277, -45272, and –40272. Rim/floor assemblage boundary runs from the upper left to lower right. Red stars represent finely layered outcrops.

collapse from loss of volatiles. Although it is unclear if the smooth plains channels are responsible for emplacing the smooth plains (i.e., bank-full deposits) or if they simply cut the smooth plains (most likely both circumstances exist), the small-scale channels within the smooth plains likely represent the first stage in canyon development and hummocky plains exposure [11].

In the SE corner of the map area, the division between the rim and floor assemblages is not distinct. Here, it is expressed as a much less pronounced facies transition between the channeled plains (unit AHpc, an expansive unit to the east) and the floor. The rim to floor gradient is more gradual than the sharp margin in the north; however, the -5800m contour still marks a significant morphologic change. Some ridge trends trace across this gradational boundary, but east of the contact, the surface is smooth and displays superposed channels (unit AHpc), whereas to the west prominent channels are lacking and several small to medium-sized craters mark a distinct morphological difference.

Hellas floor assemblage. Hellas floor materials are moderately to heavily cratered, deformed by wrinkle ridges, and are locally dissected by the farthest extensions of Dao and Harmakhis Valles. With the exception of a lobe extending from the mouth of Dao Vallis (unit AHv_t), there is a general lack of distinct depositional margins/contacts in the vicinity of channel and canyon mouths that cross the rim/floor assemblage boundary. This leaves several hypotheses about the origin of the eastern Hellas floor materials: 1) they are composed of far reaching deposits from Dao and Harmakhis Valles with contacts west of the map area, 2) they are not comprised of significant materials delivered by Dao and Harmakhis Valles, but rather consist of planitia-wide deposits, or 3) both the floors of the canyons and Hellas received materials from the rim, but have undergone significant Amazonian softening (aeolian infill, mid-latitude mantling), which has masked any original genetic and/or temporal relationships between canyon floor and Hellas floor materials.

Relatively deep sinuous depressions extend from the mouth of Harmakhis Vallis and meander around several high standing plateaus. These depressions do not preserve primary channel features but do maintain a characteristic planform shape indicative of fluvial processes, supporting hypothesis 3 as described above. The subdued topography of these depressions and the surrounding plateaus suggests burial by meters to 100s of meters of material. The deepest portions of these depressions exhibit the smoothest materials, perhaps indicating the greatest degree of burial (unit AHfs). These farthest extensions of Harmakhis Vallis may or may not represent ancient surface connections between the Harmakhis head valley to the northeast and its terminus located within the map area.

The scarp-bound plateaus in this region preserve trends consistent with wrinkle ridge trends to the north and south of the sinuous depressions. There are no topographic expressions of any wrinkle ridges across the depressions, suggesting that topography associated with the wrinkle ridges and plateaus was established prior to the excavation of the channel-like features. Thus the surfaces of the plateaus and the surrounding plains most likely represent the same surface (unit HNfis). South of this plateau region are several large craters with commingled ejecta blankets. Some ejecta blankets display radial striations, lobate margins, and dark albedo materials. A variety of degradation states are evident, consistent with various ages of the impact events; however, the exposed surface is dominated by armored ejecta blankets with few superposed pristine craters suggesting that this surface was buried and has since been exhumed in a relatively uniform manner. To the east, near the contact between units HNfis and AHpc, an anomalous zone of semi-exhumed craters exists. This zone represents the sub-surface bridge between the rim Nph units and floor Nph inselbergs and the thinnest preservation of unit HNfis. Several crater rims merge with both pronounced and subdued topography associated with the regional wrinkle ridges, making this region older than the deformation, and potentially the oldest area within the map area.

Valles and Channel materials. The larger, more mature, canyon segments of Dao and Harmakhis Valles also dissect the rim and floor assemblages; the lower reaches of Dao Vallis preserve several episodes of channel/canyon development showing abandoned truncated channels (units Hch_1 and $AHch_2$). Where the canyons are wide and more fully developed, Amazonian/Hesperian valley fill superposes their floors (units AHv_D and AHv_H).

References. [1] Crown D.A. et al. (1992) Icarus, 100, 1-25. [2] Mest S.C. and Crown D.A. (2001) Icarus, 153, 89-110. [3] Leonard G.J. and Tanaka K.L. (2001) USGS Geol. Invest. Ser. Map I-2694. [4] Tanaka K.L. and Leonard G.J. (1995) JGR, 100, 5407-5432. [5] Greeley R. and Guest J.E. (1987) USGS Geol. Invest. Ser. Map I-1802B. [6] Mest S.C. and Crown, D.A. (2002) USGS Geol. Invest. Ser. Map I-2730. [7] Mest S.C. and Crown, D.A. (2003) USGS Geol. Invest. Ser. Map I-2763. [8] Price K.H. (1998) USGS Geol. Invest. Ser. Map I-2557. [9] Mest S.C. and Crown, D.A. (2006) USGS Sci. Invest. Map 2934. [10] Crown D.A. and Greeley R. (2007 in press), USGS. [11] Crown D.A. et al. (2005) JGR, 110, E12S22.

GEOLOGIC MAP OF MTM 35337, 40337, AND 45337 QUADRANGLES, DEUTERONILUS MENSAE REGION OF MARS. Frank C. Chuang and David A. Crown, Planetary Science Institute, 1700 E. Fort Lowell Rd., Suite 106, Tucson, AZ 85719 (e-mail: chuang@psi.edu).

Introduction: Deuteronilus Mensae, a gradational zone along the dichotomy boundary in the northern mid-latitudes of Mars, includes the transition from the rugged cratered highlands of Arabia Terra to the northern lowland plains of Acidalia Planitia. Within Deuteronilus Mensae, polygonal mesas are prominent along with features diagnostic of Martian 'fretted' terrain, including lobate debris aprons, lineated valley fill, and concentric crater fill [1-3]. Lobate debris aprons, as well as the valley and crater fill deposits, are considered to be geomorphic indicators of ground ice [4-8] and their concentration in Deuteronilus Mensae is of great interest because of their potential association with Martian climate change. The morphologic and topographic characteristics of the Deuteronilus Mensae region record a diverse geologic history [9-10], with significant modification of the ancient highland plateau and resurfacing of low-lying regions. Recent geologic mapping of Deuteronilus Mensae and regional studies of lobate debris aprons and other ice-rich flow features have revealed insights into highland plateau degradation, including the significance of surface collapse [11-12].

Data and Methods: Digital files in raster and vector format produced by the U.S. Geological Survey (USGS), along with some non-USGS data, were used in the geological mapping of the Deuteronilus Mensae region in conjunction with ArcGIS™ Geographic Information Systems (GIS) software. The geology was mapped primarily on a Viking MTM base mosaic, supplemented with a THEMIS daytime IR mosaic. The contacts and structures were digitized and saved in an ArcGIS "geodatabase." The individual geodatabase components were then imported into Adobe Illustrator CS using a MAPublisher 7.0 software plug-in. The locations of individual craters, along with other information for crater count age dating, were saved as a point shapefile in ArcGIS.

Geologic Map: Deuteronilus Mensae was first mapped at 1:5M scale using Mariner 9 data and later at 1:15M scale with Viking Orbiter data [13-14]. We have mapped 3 Mars Transverse Mercator (MTM) quadrangles (35337, 40337, and 45337; 32.5-47.5ºN, 20-25ºE) that transect the dichotomy boundary in Deuteronilus Mensae (Fig. 1). A total of 17 geologic units were identified, which can be grouped into 4 material types (from oldest to youngest): Plateau, Plains, Impact Crater, and Surficial materials. Plateau materials consist of the continuous ancient highland plateau and polygonal mesas and small knobs scattered within the plains. Plains materials consist of relatively flat expanses of smooth-to- hummocky deposits in the lowland plains north of the continuous highland margin. Impact Crater materials consist of rim, floor, and ejecta deposits of impact craters in a variety of preservation states, and include the central peak materials of an ancient impact structure. Surficial materials consist of Smooth-to-Hummocky Fill deposits within the floors of impact craters, plateau depressions, and other low-lying regions near Cerulli impact crater, and Lobate Debris Apron materials, which cover much of the surface area in the mapping region and surround and extend beyond the bases of impact crater walls, mesas, escarpments, and other features that have significant relief. For a complete description of the geologic history, see [15].

Key Mapping Results: 1) Within the highland plateau, three prominent large, elongated, closed depressions 300-500 m deep contain numerous polygonal blocks and rounded knobs that have different sizes and abundances, indicating progressive stages of highland degradation and provides a potential formation mechanism for the polygonal mesas and fretted valleys in the region [12]. 2) Analyses of MOLA profiles from the dichotomy boundary to the northern extent of polygonal mesas show elevation differences within some far boundary mesas. The differences could be due to progressive erosion of the plateau to the north, a less-resistant, upper layer that has been removed, a general downsloping of the plateau into the lowlands, or any combination of these. 3) Distinct geomorphologic evidence for an ancient ocean or standing bodies of water along the dichotomy boundary in the map region was not apparent.

Acknowledgments: This work was supported by NASA PG&G Grant NNG04GI85G.

References: [1] Sharp R.P. (1973) *JGR, 78*, 4073-4083. [2] Carr M.H. (1996) *Water on Mars, Oxford Univ. Press*, 221 p. [3] Carr M.H. (2001) *JGR, 106*, 23571-23593. [4] Squyres S.W. (1978) *Icarus, 34*, 600-613. [5] Squyres S.W. (1979) *JGR, 84*, 8087-8096. [6] Squyres S.W. (1989) *Icarus, 79*, 229-288. [7] Lucchitta B.K. (1984) *JGR, 89*, B409-B418. [8] Squyres S.W. and Carr M.H. (1986) *Science, 231*, 249-252. [9] McGill G.E. (2000) *JGR, 105*, 6945-6959. [10] McGill G.E. (2002) *USGS Geol. Invest. Ser. Map I-2746*, 1:1M scale. [11] Crown D.A. et al. (2006) *LPSC 37*, abstract #1861. [12] Chuang F.C. and Crown D.A. (2007) *LPSC 38*, abstract #1455. [13] Lucchitta B.K. (1978) *USGS Misc. Invest. Ser. Map I-1065*, 1:5M scale. [14] Greeley R. and Guest J.E. (1987) *USGS Misc. Invest. Ser. Map I-1802B*, 1:15M scale. [15] Chuang F.C. and Crown D.A. (2007) *USGS Sci. Invest. Ser. Map*, submitted (available for download: http://www.psi.edu/pggroup/mapping.htm).

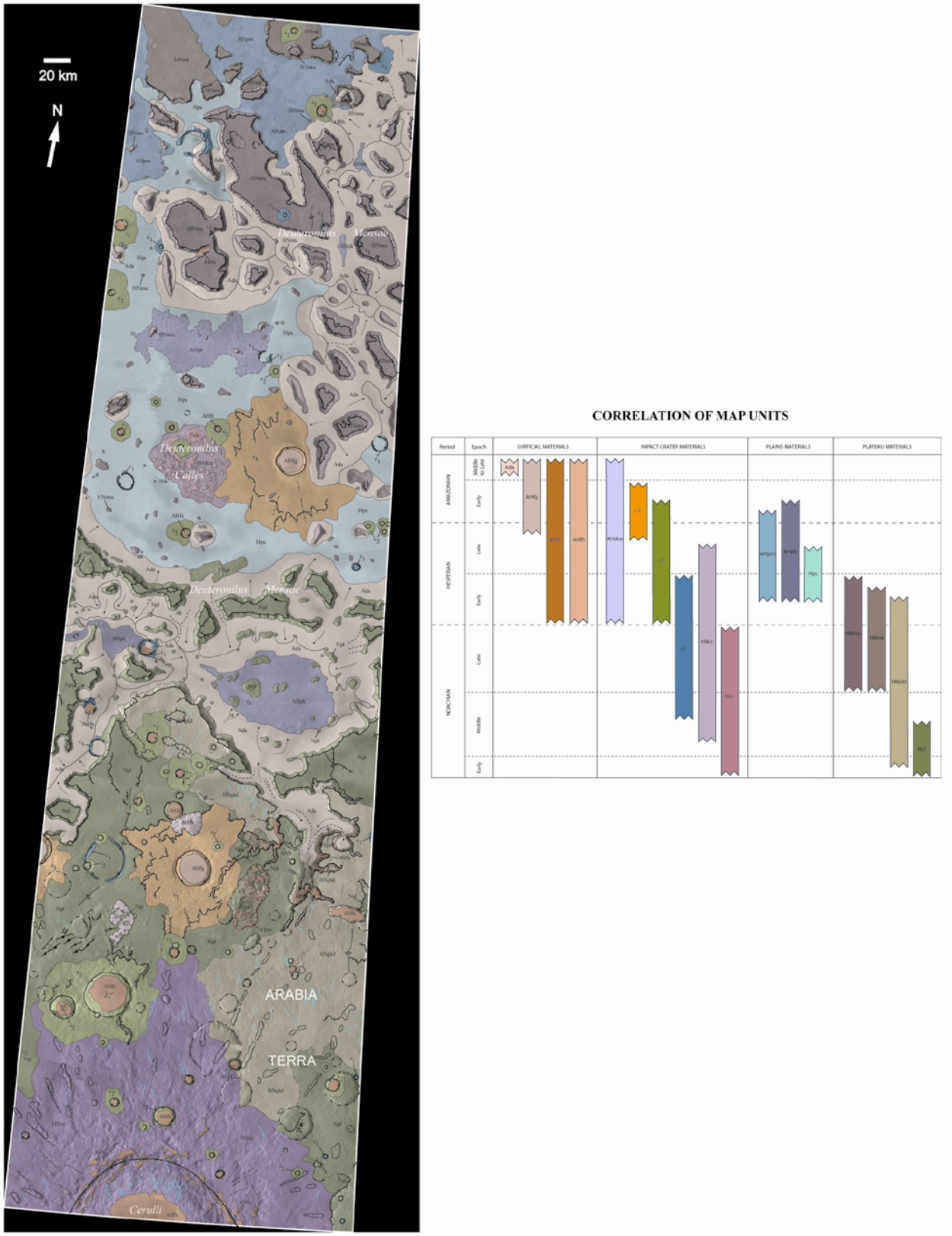

Figure 1. Geologic map of MTM Quadrangles 35337, 40337, and 45337, Deuteronilus Mensae region of Mars and accompanying chart showing the Correlation of Map Units. See [15] for more details.

MAPPING MARGARITIFER TERRA: MTMS -15017, -20002, -20007, -20017, -20022, -25002, -25007. C. M. Fortezzo[1], K. K. Williams[2], and J. A. Grant[3], [1]Northern Arizona University, Flagstaff, AZ, 86001. cmf@nau.edu, [2]Earth Sciences Department, Buffalo State College, Buffalo, NY 14222. williakk@buffalostate.edu, [3]Center for Earth and Planetary Studies, National Air and Space Museum, Washington, DC, 20013-7012.

Introduction: As part of a continuing campaign to better understand the relationship between valleys and resurfacing events through mapping, we are mapping seven 1:500,000-scale MTM quads in the Margaritifer Terra region. Results from this mapping will also help constrain the role and extent of past water in Margaritifer Terra. The MTMs are grouped in two different areas (Figure 1, red boxes with black text) within the region and compliment the completed mapping in four quads (Figure 1, red boxes with hatch pattern) that are currently in the review process [1-5].

Three western quads focus on Jones crater and the Himera, Samara and Loire Valles systems (central portion of Figure 1). The four eastern quads focus on the headward regions of Paraná Valles and the valleys on the western flank of Newcomb crater (southeastern area of Figure 1).

Datasets: For these maps, we used MDIM 2.1 and MOLA 128 pix/deg datasets as the initial mapping base and have processed THEMIS daytime and nighttime infrared images. We rubbersheet the daytime IR images using MDIM 2.1 as the control and are using them as a mapping base with ~95% coverage. THEMIS daytime and nighttime infrared band 9 images were processed using the ISIS-based THEMIS processing tools (them-proc.mars.asu.edu) and overlain in ArcMap. THEMIS daytime IR three-band RGB (8-7-5, 9-6-4, and 6-4-2) decorrelation stretch images are being used for mineralogy information [6]. Regional-scale map bases are supplemented with processed and georeferenced THEMIS visible and MOC narrow angle images where available. Several HiRISE images provide detailed textural information where available.

Methods: We have imported and registered all pertinent raster and vector data using ESRI's ArcMap GIS software. Using this digital environment, we have begun digitizing lines (e.g., contacts, structures, etc.) and polygons (e.g., units and craters). Arc extensions provide robust tools for (1) analyzing spatial relationships across multiple data layers, (2) attributing and updating digital linework, (3) building and analyzing vector topologies, and (4) importing new data as they are released. To inspect and quantify stratigraphic relations, we are compiling crater counts in ESRI's ArcView GIS software to make use of crater counting tools [7] specifically developed for planetary mappers [8].

Current Work: Work on the seven quads began by concentrating on the Newcomb-Paraná area

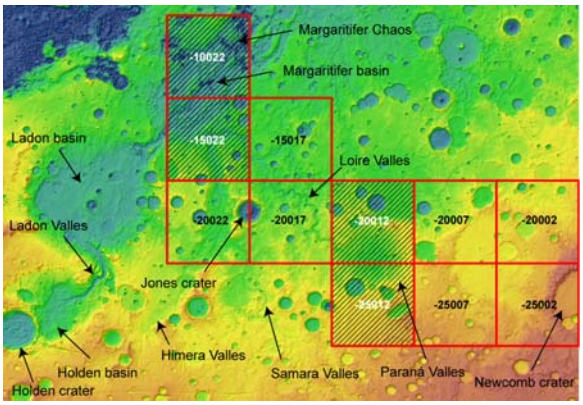

Figure 1: Shaded relief overlain by MOLA 128 pix/deg of Margaritifer Terra. Arrows point to the locations of prominent features. The red boxes indicate individual MTM quads. Red boxes with black numbers are the 7 quads currently being mapped and boxes with a hatch pattern and white numbers indicate quads under review.

(MTMs -20002, -20007, -25002, and -25007; Figure 2) in order to determine the relative ages of resurfacing events in upper Paraná Valles and to examine how valleys either incise or are mantled by resurfacing deposits within the Newcomb-Paraná region.

In this mapping area, as was demonstrated in the adjacent two western quadrangles (MTM -20012 and -25012) [1-5], Noachian cratered plains dissected by fluvial erosion are resurfaced by two separate events. In addition to dissection of the ancient highland terrain unit, troughs and valleys are also found in the first resurfacing unit. The second resurfacing episode infills craters, embays valleys and troughs, and appears smooth in THEMIS IR images.

The valleys, valley networks and troughs in the area dissect the ancient Noachian highland terrain, the first resurfacing event, and craters in the mapping area. Centers of deposition along the paths of these valleys are usually impact basin interiors or small, flat areas adjacent to the outer flanks of the map-centered large impact basin. This ~350 km diameter ancient impact has multiple inlets flowing into its eastern and southern flanks. The interior of the basin is basically horizontal (slope <0.01); the outlet is only ~200 meters lower than the main input. On the basin floor are several areas of positive relief chaotic terrain similar to that of a basin west of Paraná Valles [1-5]. There is also a paucity of

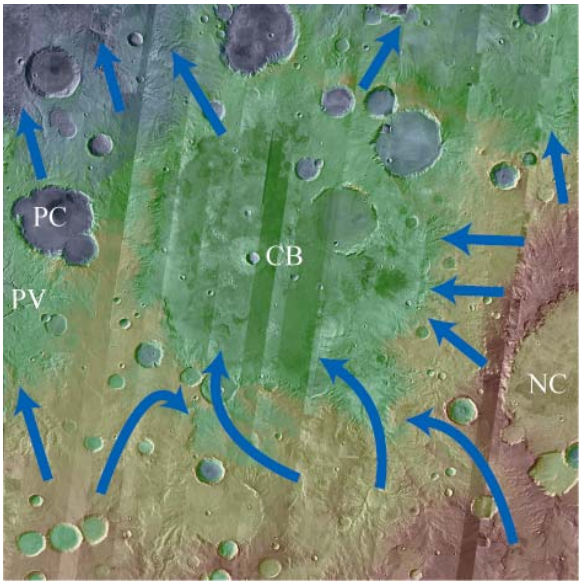

Figure 2: MOLA topography overlain on THEMIS daytime IR strips for the southeast portion of Margaritifer Terra. Blue arrows indicate flow direction of numerous valley networks in the area. NC = Newcomb crater; CB = crater basin; PC = Peta crater; and PV = Paraná Valles.

geomorphic evidence of fluvial erosion in this basin. These observations lead to the hypothesis that this was an extensive area of fluid ponding and (possibly) infiltration into the Martian regolith.

The western edge of Newcomb crater is characterized by a plateau area flanked by dense fluvial dissection. The plateau area does not appear to be a large enough contributing area to feed the valley networks with overland flow, and the valley networks are consistent with the geometry described for terrestrial sapping valleys [9]. The radial pattern of valleys in this area may relate to the groundwater flow through the system of fractures created by the impact that formed Newcomb crater with some contribution from overland flow.

The western 3 quads (MTMs -15017, -20022, and -20017; Figure 3) cover Himera and Samara Valles to the west, Jones crater, and Loire Valles to the east (Figures 1 and 3). Current work in this area involves counting craters and demarcating initial units. This work now involves three undergraduate students.

Future Work: For both areas, geologic linework advances as the science tasks are continued.

In the Newcomb-Paraná area, crater counting techniques designed for calculating the ages of narrow, linear features [10, 11] will be used to establish comparative ages of the valley networks relative to each other. This analysis will be performed on the Paraná Valles network and on the network on the western flank of Newcomb crater, and the results of each area will be compared to determine their ages relative to each other. We will compute the cumulative crater densities for sub-basins within the valley networks and compare them against each other to further constrain the role and persistence of water in the region.

In the Jones crater area, review of Viking Orbiter images led to the hypothesis that the drainage history of the Jones-Loire area may have been affected by emplacement of Jones crater [12]. These images showed that ejecta from Jones crater partially buried parts of Samara and Loire Valles and totally obscured portions of Samara Valles [12]. We will test the hypothesis that a second order pathway once connected Samara Valles with Loire Valles east of the third ring of the Ladon basin using higher resolution MOC and THEMIS images, MOLA topography and the 1:500,000 map.

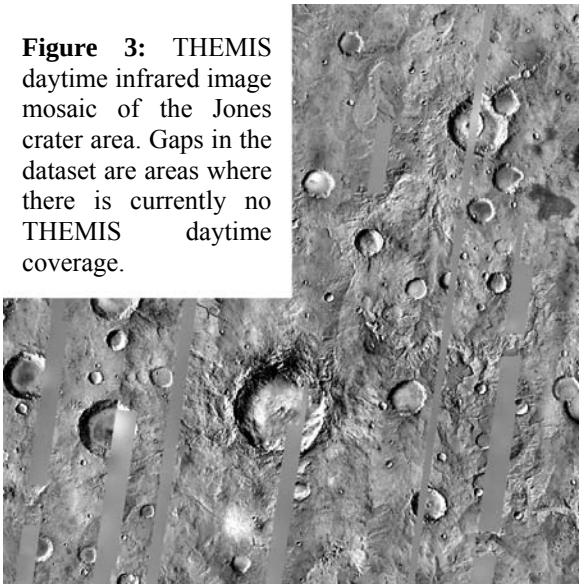

Figure 3: THEMIS daytime infrared image mosaic of the Jones crater area. Gaps in the dataset are areas where there is currently no THEMIS daytime coverage.

References. [1] Grant J.A. and D.A. Clark (2002) Planetary Mappers Meeting (abst.). [2] Williams, K.K. and J.A. Grant (2003) Planetary Mappers Meeting (abst.). [3] Fortezzo, C.M. and J.A. Grant (2004) Planetary Mappers Meeting (abst.). [4] Grant, J.A., K.K. Williams, and C.M. Fortezzo (2005) Planetary Mappers Meeting (abst.). [5] Wilson, S. et. al. (this volume) Planetary Mappers Meeting (abst). [6] Rogers, D. et. al., (2003) *J. Geophys. Res.*, 108. [7] Hare, T. et al. (2006) *LPSC XXXVII,* 2398 (abst.). [8] Barlow, N. (2006) *LPSC XXXVII,* 1337 (abst.). [9] Laity, J.E. and M.C. Malin, (1985), *Geo. Soc. Am. Bull*, 96, 203-217. [10] Tanaka, K.L. (1982) *NASA Tech. Memo.*, 85127, 123-125. [11] Wichman, R. and P.H. Schultz (1987) *NASA Tech. Memo.*, 89810, 474-475. [12] Grant, J.A. (1987) *NASA Tech. Memo*., 89871, 1-268.

MAPPING HESPERIA PLANUM, MARS. Tracy K.P. Gregg[1] and David A. Crown[2], [1]Department of Geology, 876 Natural Sciences Complex, University at Buffalo, Buffalo, NY 14260, tgregg@geology.buffalo.edu; [2]Planetary Science Institute, 1700 E. Ft. Lowell Rd., Suite 106, Tucson, AZ 85719, crown@psi.edu.

Introduction: Hesperia Planum, characterized by a high concentration of mare-type wrinkle ridges and ridge rings [1-4], encompasses > 2 million km^2 in the southern highlands of Mars (Fig. 1). The most common interpretation is that the plains were emplaced as "flood" lavas with total thicknesses of <3 km [4-10]. The wrinkle ridges on its surface make Hesperia Planum the type locale for "Hesperian-aged ridged plains" on Mars [e.g., 9], and recent investigations reveal that wrinkle-ridge formation occurred in more than one episode [4]. Hesperia Planum's stratigraphic position and crater-retention age [e.g., 9, –11, 12] define the base of the Hesperian System. However, preliminary results of geologic mapping reveal that the whole of Hesperia Planum is unlikely to be composed of the same materials, emplaced at the same geologic time. To unravel these complexities, we are generating a 1:1.5M-scale geologic map of Hesperia Planum and its surroundings (Fig. 1). To date, we have identified 4 distinct plains units within Hesperia Planum and are attempting to determine the nature and relative ages of these materials (Fig. 2) [13-15].

Hesperia Planum Plains Materials: Using images from the Thermal Emission Imaging System (THEMIS) [16], we have been able to broadly divide the "Hesperian ridged plains materials" identified using Viking Oribiter images [9] into 6 distinct geologic units. MOLA data reveal that the east and west boundaries of the continuous topographic basin that defines Hesperia Planum [cf. 9] closely follow the 2-km elevation contour, and most of what has been geologically defined as Hesperia Planum [cf. 1, 7, 9] is contained within that contour line. In contrast, highland plains occur in isolated outcrops surrounded by highlands material (Fig. 3). Units with the descriptor "highlands" are found at elevations above 2 km [16].

Geologic units within Hesperia Planum can be broadly classified as those associated with Tyrrhena Patera, and those that are not (Fig. 2). Crown and others [15] discuss the characteristics and relative ages of the Tyrrhena Patera materials [see also 17-21]. The plains materials to the south and southeast of Tyrrhena Patera are heavily affected by fluvial, ice, and possibly lacustrine processes [17, 22, 23], making interpretations of the original nature of the materials difficult. "Modified plains materials" contain mare-type wrinkle ridges, but the ridges are not morphologically crisp; they appear to have been modified by erosional processes, locally revealing layers within the plains. "Dissected plains materials" also contain mare-type wrinkle ridges and have locally been dissected by channels. Within dissected plains materials, small channels surrounded by lobate deposits are observed. Available images do not yet allow an unequivocal interpretation for these channel features: they may be lava flows, fluvial features, or debris flows.

The region of Hesperia Planum located to the east of Tyrrhena Patera (Fig. 2) is the typical "Hesperian ridged plains" [7, 9]. Aside from Tyrrhena Patera, no obvious volcanic vents have been found within Hesperia Planum [cf. 4, 13, 18, 20-22]. Lava flows can be seen at available image resolutions in the Tyrrhena Patera lava flow field [18] that post-dates the ridged plains, but they are not readily apparent within the ridged plains. Within these "ridged plains materials," we have thus far identified four distinct plains units [14], suggesting that a range of depositional and/or erosional processes have operated across Hesperia Planum through time [cf. 22].

Mapping Progress: Units have been identified and are being mapped across the region. Preliminary crater size-frequency distributions have been calculated using Barlow's crater database for craters ≥5 km in diameter

References: [1] Scott, D.A. and M. Carr (1978) *USGS Misc. Series I-1083*. [2] Chicarro, A.F., P.H. Schultz and P. Masson (1985) *Icarus 63*:153. [3] Watters, T. and D.J. Chadwick (1989), *NASA Tech. Rpt. 89-06*:68. [4] Goudy, C., R.A. Schultz and T.K.P. Gregg, *J. Geophys. Res. 110*: E10005 10.1029/2004JE002293. [5] Potter, D.B. (1976) *USGS Misc. Series I-941*. [6] King, E.A. (1978) *USGS Misc. Series I-910*. [7] Greeley, R. and P. Spudis (1981) *Rev. Geophys. 19*:13. [8] Scott, D.A. and K. Tanaka (1986) *USGS Misc. Series I-1802A*. [9] Greeley, R. and J. Guest (1987) *USGS Misc. Series I-1802B*. [10] Leonard, J.G. and K. Tanaka (2001) *USGS Misc. Map Series I-2694*. [11] Tanaka, K.L., 1986, Proc. LPSC 17th, JGR Suppl. 91, E139-E158. [12] Tanaka, K. (1992), in *Mars*, U. Arizona Press, p. 345. [13] Gregg, T.K.P. and D.A. Crown, 2007, *Lun. Planet. Sci. Conf. 38th*, Abstract #1190. [14] Crown, D.A., D.C. Berman and T.K.P. Gregg, 2007, *Lun. Planet. Sci. Conf. 38th*, Abstract #1169. [15] Jones, T.K., T.K.P. Gregg and D.A. Crown, 2007, *Lun. Planet. Sci. Conf. 38th*, Abstract #2156.

[16] Christensen, P.R. and others, 2004, *Space Sci. Rev. 110:*85-130. [17] Mest, S. and Crown, D.A. (2001) *Icarus 153*:89. [18] Greeley, R. and D.A. Crown (1990) *J. Geophys. Res. 95*:7133. [19] Gregg, T.K.P., D.A. Crown and R. Greeley (1998) *USGS Misc. Series I-2556*. [20] Gregg, T.K.P. and M.A. Farley (2006) *J. Volcanol. Geotherm. Res. 151*:81-91. [21] Farley, M.A., T.K.P. Gregg and D.A. Crown (2004) *USGS Open File Rpt. 2004-1100*. [22] Ivanov, M.A. et al., 2005, JGR 110, E12S21. [23] Crown, D.A., L.F. Bleamaster III and S.C. Mest, 2005, *J. Geophys. Res. 110, E12S22*, doi:10.1029/2005JE002496.

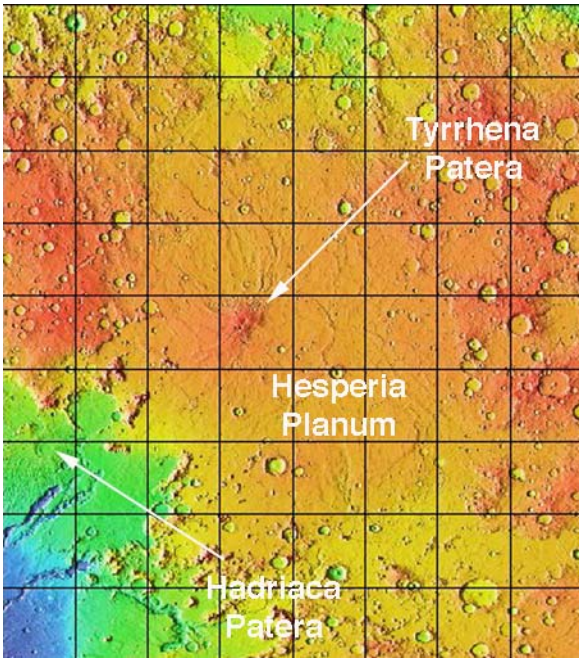

Figure 1. Gridded MOLA data (128 pixels/degree) of the area being mapped at 1:1.5 million scale. Reds are topographic highs (Tyrrhena Patera summit is ~3 km above mean planetary radius) and blues are lows.

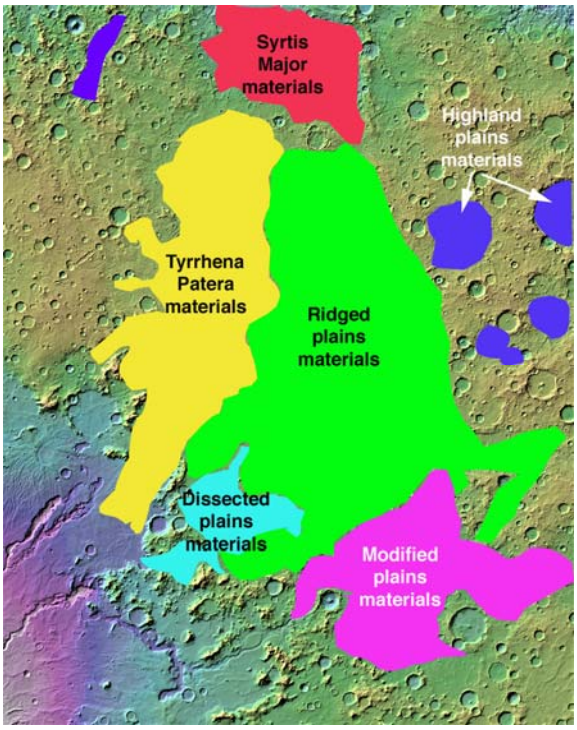

Figure 2. Rough boundaries of identified plains materials within Hesperia Planum. Portions of these materials were originally mapped as "Hesperian-aged ridged plains" at 1:15 million [9].

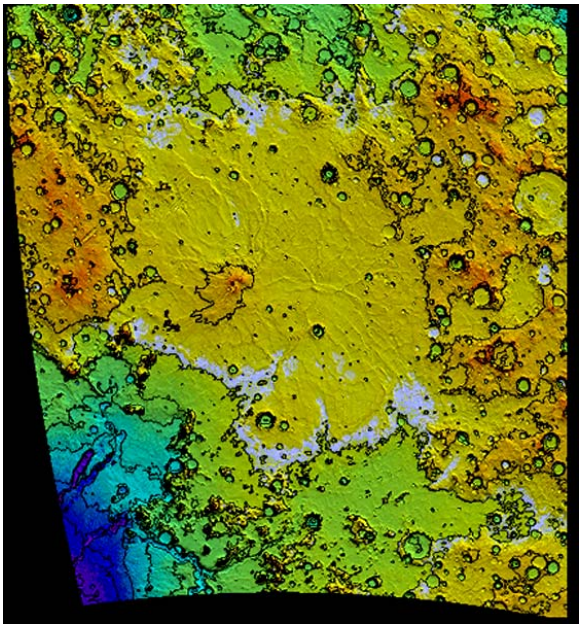

Figure 3. Hesperia Planum with 1-km-interval contour lines. The boundary of Hesperia Planum [9] roughly corresponds with the 2-km elevation line [22].

HYDROLOGIC AND VOLCANIC EVOLUTION OF ATHABASCA VALLES, MARS: THE FIRST STEP TO GEOLOGIC MAPPING AT 1:500,000 SCALE. L. Keszthelyi[1], W. Jaeger[1], K. Tanaka[1], [1]U.S. Geological Survey, Astrogeology Team, 2255 N. Gemini Dr., Flagstaff, AZ 86001.

Introduction: The "Follow-the-Water" Mars exploration strategy espoused by NASA places a great deal of emphasis on the most recent examples of large-scale aqueous flow on Mars. The Cerberus region, which includes Athabasca Valles, has long been recognized as one of the geologically youngest areas on the planet with large-scale fluvial and volcanic activity [e.g., 1-10]. The fact that Athabasca Valles was seriously considered as a landing site for the MER mission and the Beagle 2 lander is one indication of the level of interest in this location [11,12].

Understanding the recent activity at Athabasca has implications for adjacent regions and times. For example, the lava and water from the Cerberus Fossae extended through Marte Vallis into western and perhaps northern Amazonis Planitia [e.g., 5, 8, 10, 13, 14]. Thus, the recent resurfacing processes in Athabasca may have also operated across much of the northern plains in the more distant past [e.g., 15].

Work Plan: This project has been divided into five tasks to be completed over three years. We are near the end of the 1st year. The tasks are (1) combine the relevant Mars data sets into a single georegistered GIS project, (2) choose the geologic units to be mapped, (3) determine the spatial and temporal nature of the contacts between these units at key locations, (4) extrapolate the contacts across the entire region, and (5) publish a peer-reviewed journal article and a set of 4 USGS MTM quadrangle maps.

Task 1: A GIS project containing the following datasets has been assembled: Viking MDIM, MOLA, all available MOC images, and all available THEMIS VIS images. THEMIS IR data were initially processed for inclusion but we are now moving to simply use the mosaics provided by the THEMIS team. While slightly lower in spatial resolution, the mosaic is much easier to work with than the individual images. A slight delay has been introduced by the processing upgrade from ISIS2 to ISIS3. The tools to update the pointing (and thus locations) of the MOC and THEMIS data are just now coming on line. The other more significant delay is that we are awaiting the June 8th release of MRO CTX data which we have good reason to expect to be extremely valuable for mapping this region. CTX data ingestion is expected to be straightforward because all the necessary tools are available (and tested) in ISIS3.

Task 2: Partly based on new MRO data, but relying largely on work for this project, we have determined what geologic unit to classify the floor of Athabasca Valles. It is a lava flow [16-19]. We have also determined the other major units (the equivalents of units HBu_2, HNn, AHEe, AEc_2 and AEc_3 from [20]). The ejecta from Persbo crater will also be mapped separately. While further refinement will be inevitable as the actual linework of the map starts (we expect to be able to subdivide AEc_3), Task 2 is largely complete.

Task 3: In completing Task 2, the detailed localized studies have been completed. This has been accomplished using both new MRO data and older MGS and MO data. As noted above, the key finding is that Athabasca Valles is draped by a recent lava flow. No exposures of fluvial sediments have been identified.

Task 4: The actual drawing of lines on the basemaps will begin later this summer and continue through the next fiscal year.

Task 5: The last year of this project will be dedicated to publication of the maps and journal articles.

Preliminary Results: The basic geologic history that we have found is as follows: (1) Long lobate lava flows from the Elysium volcanic rise covered the region, (2a) wrinkle ridges formed, (2b) the Persebo impact, (3a) Athabasca Valles was cut by fluids (water or lava) from the Cerberus Fossae, (3b) minor extensional fracturing of the floor of Athabasca Valles, (4) Athabasca Valles is filled by a large fluid flood lava flow, (5) the lava flow drains out leaving a thin draping, (6) a light toned mantle is deposited, (7) the Zunil impact and the formation of a field of secondary craters, (8) wind erosion of the light-toned mantle except where protected by crater ejecta and local topography. Very little time may have passed between (3) – (6).

References: [1] Tanaka, KL (1986) *JGR*, 91, E139-158. [2] Greeley, R and JE Guest (1987) *USGS Misc. Inv.* Map I-1802-B. [3] Plescia, JB (1990) *Icarus, 88*: 465-490. [4] Plescia, JB (1993) *Icarus*, 104: 20-32. [5] Plescia, JB (2003) *Icarus*, 164, 79-95. [6] Berman DC and WK Hartmann (2002) *Icarus*, 159: 1-17. [7] Burr, DM et al. (2002a) *GRL*, 29: 2001GL013345. [8] Burr, DM et al. (2002b) *Icarus* 159, 53-73. [9] Rice, J.W. et al. (2002) LPSC 33 Abstract #2026. 10] Tanaka, KL et al. (2003) *JGR*, 108: 2002JE001908. [11] Golombek, MP et al. (2003) *JGR* 108, CiteID 8072. [12] Bridges, JC et al. (2003) *JGR*, 108, 2001JE00182003. [13] Fuller, ER, and JW Head (2002) *JGR* 107, CiteID 5081. [14] Keszthelyi, L et al. (2004) *Geochem. Geophys. Geosys*., 5, 2004GC000758. [15] Tanaka, KL et al. (1992) *U.S. Geol. Surv. Misc. Invest. Ser*., Map I-2147. [16] Jaeger, WL et al. (2007) LPSC 38, Abstract #1995. [17] Jaeger, WL et al. (2007) LPSC 38, Abstract #2066. [18] Jaeger WL et al. (2007) Mars7, Abstract #3394. [19] Jaeger WL et al. (in revision) Science. [20] Tanaka, KL et al. (2005) *U.S. Geol. Surv. Sci. Inv. Map* 2888.

Figure 1. Mosaic of MRO CTX images in the mapping area over the Viking MDIM 2.1 basemap. All processing was completed in ISIS3 but the CTX images have not yet been controlled. There is already almost complete CTX coverage of the Athabasca Valles channel system (which runs diagonally NE-SW across the mosaic). Much of the Cerberus Fossae fissures (in the NE) and the Cerberus Palus basin (in the SW) are also imaged. The link between Cerberus Palus and the eastern part of Elysium Planitia (called Lethe Vallis) is covered by the southernmost CTX image. The contacts between each of the main geologic units have been at least sampled by CTX.

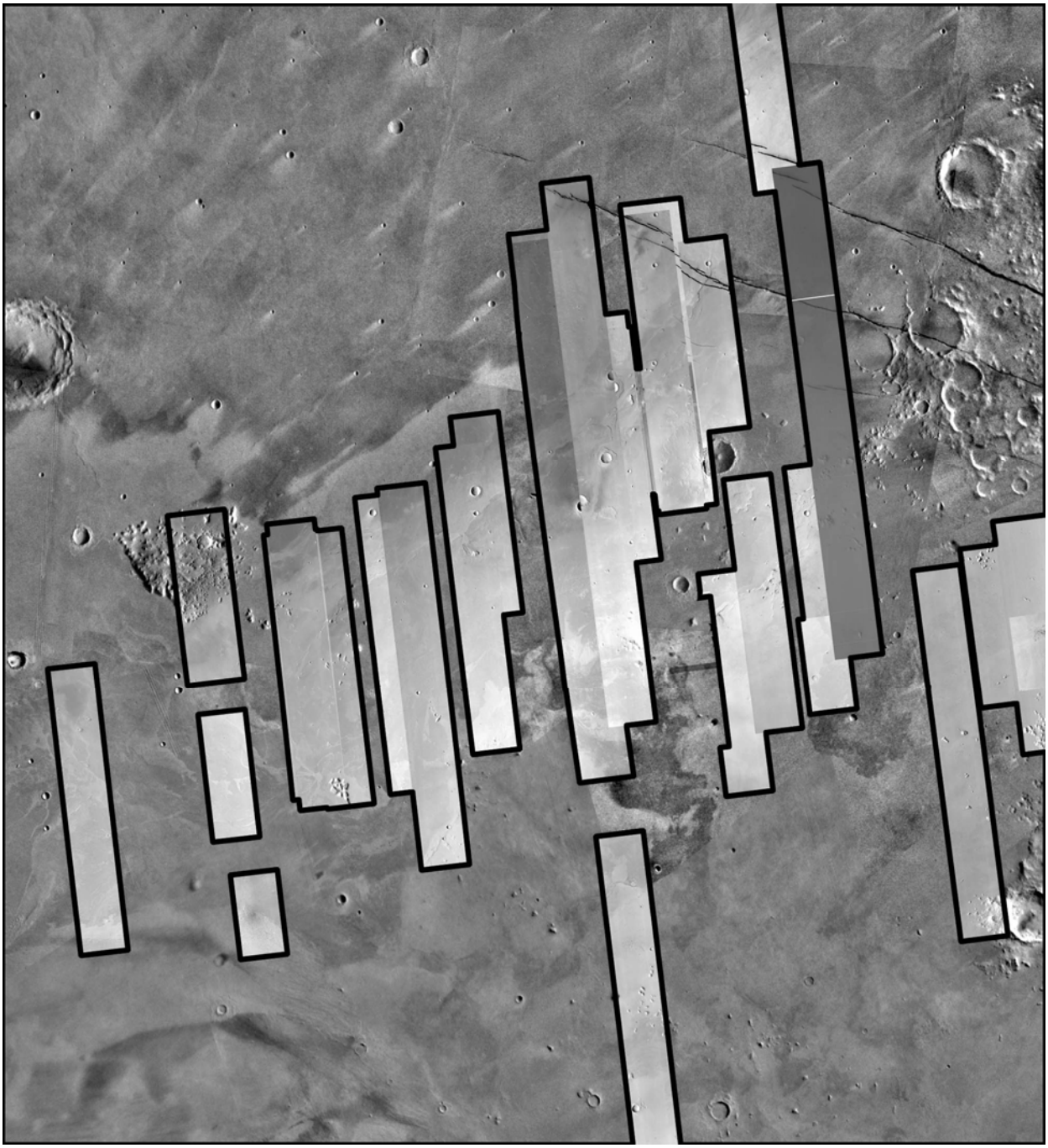

Geologic Mapping of the Martian Impact Crater Tooting. Pete Mouginis-Mark, HIGP/SOEST, Univ. Hawaii, Honolulu, HI 96822. <pmm@higp.hawaii.edu>

Introduction: Tooting crater is ~29 km in diameter, is located at 23.4°N, 207.5°E, and is classified as a multi-layered ejecta crater [1]. Tooting crater formed on virtually flat lava flows within Amazonis Planitia where there appears to have been no major topographic features prior to the impact, so that we can measure ejecta thickness and cavity volume [2]. To date, we have: (1) Produced a 30-image THEMIS VIS mosaic of Tooting crater with extensive help from Ryan Luk at Arizona State University. (2) Finished a first draft of the geologic map of Tooting Crater (Figure 1). (3) In collaboration with Alfred McEwen and Livio Tornebene of the HiRISE Team, we have obtained five 25-cm resolution HiRISE images of Tooting crater that dramatically show some of the errors of our previous studies, and show the importance of dewatering of the ejecta blanket [3].

Science Questions: We are trying to resolve several science issues that have been identified during this mapping, including:

1) What is the relative importance of dewatering of the ejecta (both within the crater cavity and within the ejecta blanket)? HiRISE images indicate that dewatering has been responsible for the formation of several flows on the crater rim and inner walls, and desiccation of the wet ejecta may also be responsible for the formation of extensive pitted material on the crater floor.

2) Do the ejecta layers lie on top of each other, so that the layers closest to the primary are the youngest? Or are the outermost ejecta layers on top of layers more proximal to the parent crater? Resolving this stratigraphic relationship has fundamental implications for understanding the process that creates the ejecta blanket of multi-layered impact craters on Mars.

3) We want to distinguish the distal ramparts of the ejecta layers as separate morphologic units, as they may offer unique insights into the formation of the ejecta layers as deceleration features [4]. However, they are probably made of the same material as the rest of the ejecta layers. Their identification as a separate unit could help with the interpretation of the ejecta flow processes [4 – 6].

Plans for Year 2:

a) Complete a draft geologic map of Tooting crater (i.e., refine Figure 1), and submit this map to the U.S. Geological Survey for preliminary review.
c) Publish a research paper (either in *JGR-Planets* or *Meteoritics and Planetary Science*) on the HiRISE contributions to our understanding of impact melt at Tooting crater.
d) Start the accompanying map text.
e) Map the distribution of secondary craters from Tooting crater. This will form a second map, to be included with the 1:200K geologic map, and will be produced at a scale of 1:1M.

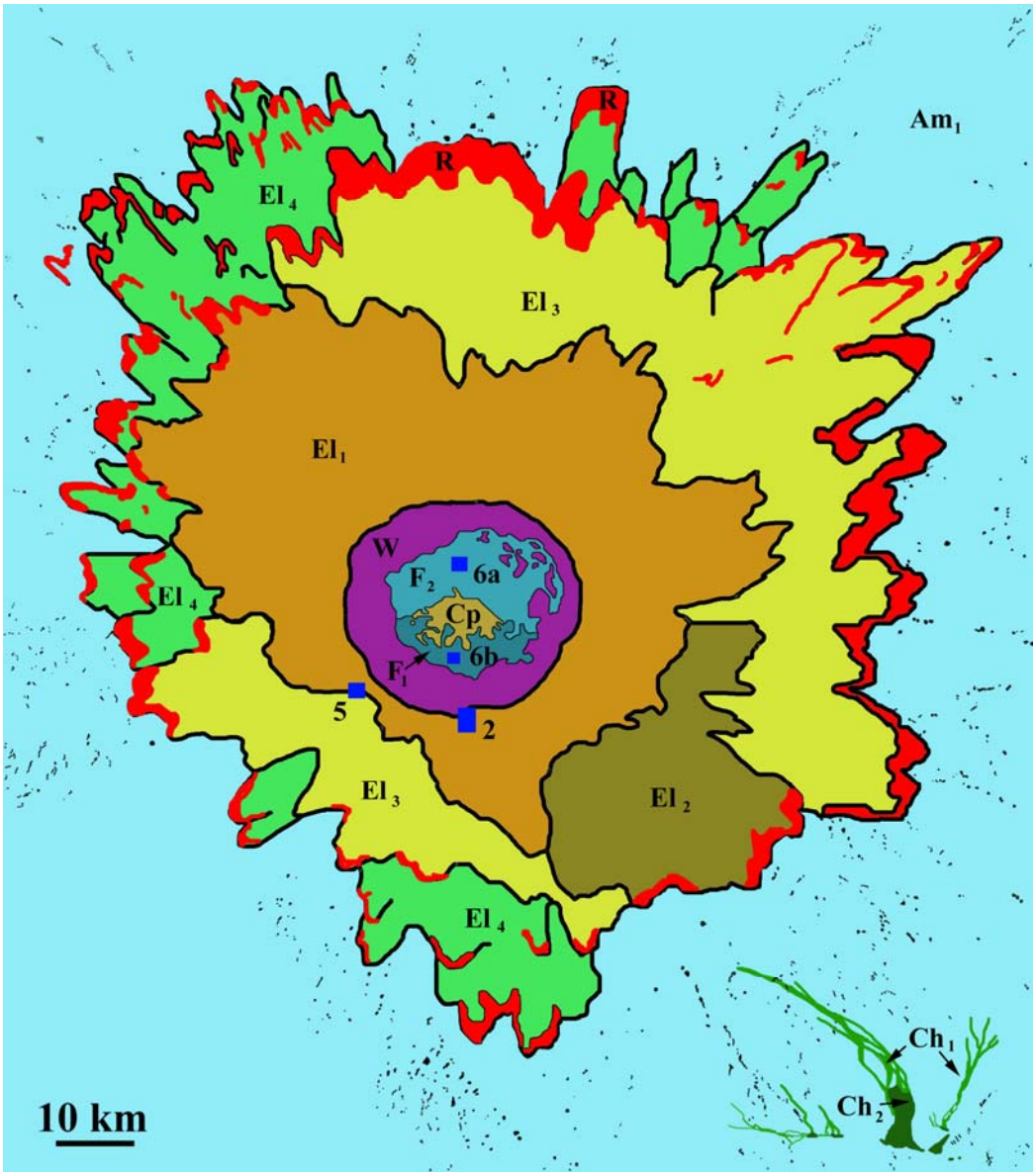

Figure 1: First draft of the Tooting crater geologic map. Individual secondary craters are shown as black dots surrounding the crater. Blue boxes mark the locations of HiRISE images studied in detail.

References: [1] Barlow N. G. et al. (2000). Standardizing the nomenclature of Martian impact crater ejecta morphologies. *Journal of Geophysical Research* 105: 26,733 - 26,738. [2] Mouginis-Mark, P.J. and H. Garbeil (2007). Crater geometry and ejecta thickness of the Martian impact crater Tooting. In press: *Meteoritics and Planetary Science*. [3] Mouginis-Mark, P.J., L.L. Tornabene, J.M. Boyce, and A.S. McEwen (2007). Impact melt and water release at Tooting crater, Mars. *7th Int. Conf. On Mars. Abs #3039.* [4] Mouginis-Mark P.J. and Baloga S.M. (2006). Morphology and geometry of the distal ramparts of Martian impact craters. *Meteoritics and Planetary Science* 41: 1469 – 1482. [5] Baloga, S.M., S.A. Fagents, and P.J. Mouginis-Mark (2005). Formation of rampart ejecta deposits around Mars impact craters. *Journal of Geophysical Research* 110, E10001, doi: 10.1029/2004JE002338. [6] Barnouin-Jha O. S., Baloga S., and Glaze L. (2005). Comparing landslides to fluidized crater ejecta on Mars. *Journal of Geophysical Research* 110, E04010, doi: 10.1029/2003JE002214.

Geologic Mapping of the Olympus Mons Caldera. Pete Mouginis-Mark, HIGP/SOEST, Univ. Hawaii, Honolulu, HI 96822. <pmm@higp.hawaii.edu>

The second year of this mapping has focused on trying to understand the mode of formation of the different units within the Olympus Mons caldera. In collaboration with Ryan Luk at Arizona State University, we have produced a new THEMIS VIS mosaic of the summit caldera that will be used for all the formal mapping. This new mosaic (Fig. 1) is a great improvement over the earlier images that we were using because it contains many of the THEMIS VIS images that were obtained in Years 4 and 5 of the mission (i.e., since the start of this mapping), and we have used it for our preliminary mapping.

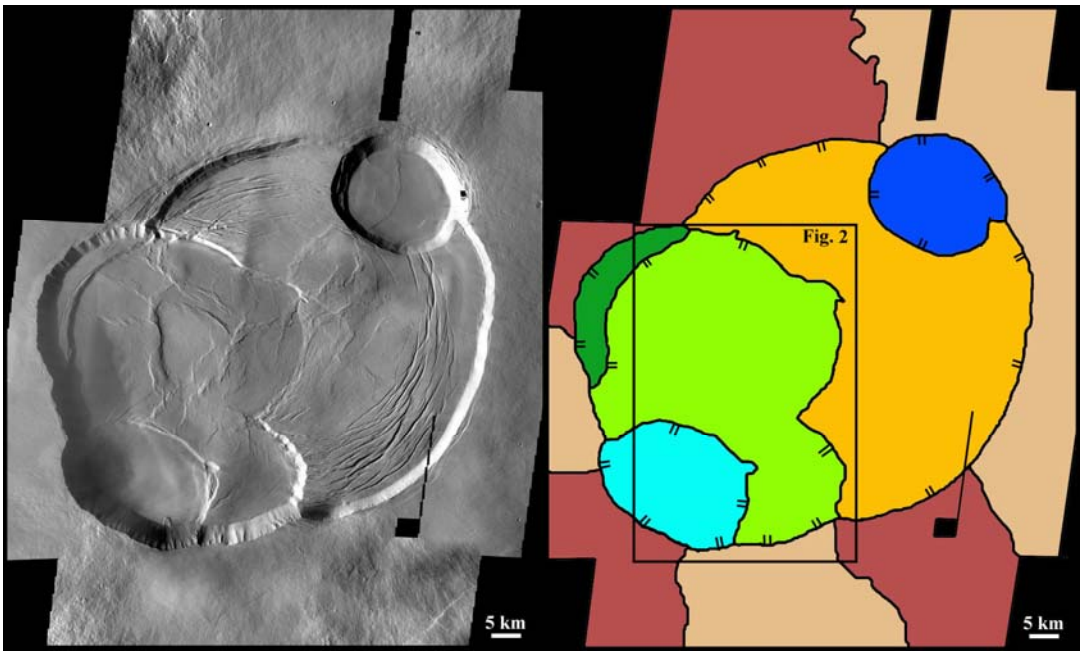

Figure 1: (Left): Latest version of the THEMIS VIS base image of the Olympus Mons caldera, produced in collaboration with Ryan Luk at Arizona State University. (Right) Major units and depressions within the area to be mapped. Rim units are difficult to precisely identify due to varying illumination conditions, but are currently sub-divided into undifferentiated lava flows (light tan) and individual lobate flows (darker peach color). Note that the central crater (in bright green) probably comprises several discrete collapse features. In order to better identify the resurfacing of this unit, initial attention has focused on mapping the collapse and compressional features in this part of the caldera. Rectangle illustrates location of Fig. 2.

As can be seen from Figure 1, there is a large segment of the western caldera floor that comprises (probably) three or four separate collapse events that have now been almost totally buried under more recent lava flows. A science goal of this mapping is to determine more of the details of this burial process, because it would help to constrain the volume of each eruption within the caldera. This segment of the caldera floor is unusual because it contains a large number of collapse pits and numerous compressional features (Fig. 2). The final map will include the distribution of these features on all segments of the caldera floor because it is believed that they are indicators of the post-fill modification of the caldera floor. The collapse pits seem to be preferentially located within a few kilometers of the boundary with the oldest segment of the caldera (i.e., the

largest crater that occupies most of the eastern side of the caldera). The compressional features are more enigmatic. In particular, there appears to be several generations of ridges on the caldera floor. Some of these ridges form broad swells that have then had narrow (<200 m wide) ridges superimposed upon them. There are also several broad, generally flat and horizontal, segments of the floor that lack any ridges. Even at MOC resolution (<4 m/pixel), there are no clear signs of lava flow fronts of volcanic vents in this part of the caldera floor (Fig. 2c), so that the exact mode of origin for the caldera floor has yet to be identified.

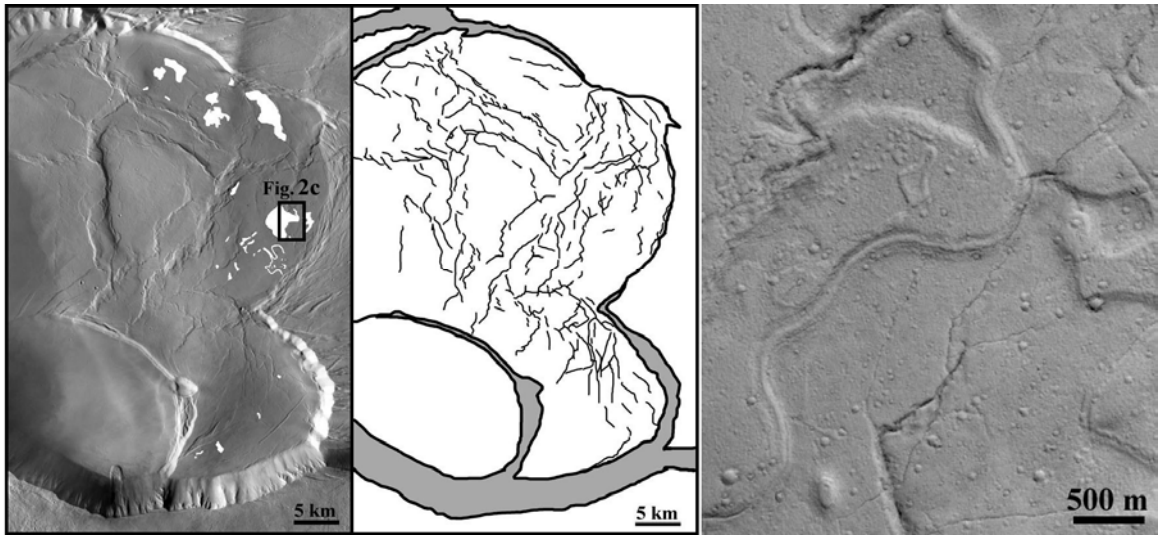

Figure 2: Distribution of collapse features (white outlines in image at left) and compressional features (center), mapped from the new THEMIS VIS mosaic (see Figure 1 for location). Notice that almost all of the collapse features are located on the eastern side of the complex, where the basal unit (the earlier part of the floor) is probably closest to the surface. The wall material of the different collapse features is shown in mid-tones. MOC image (Figure 2c at right) is denoted by the black rectangle in left image.

Outstanding Issue: At the summer 2006 Mappers' Meeting, we discussed whether the features that comprise the caldera should be called "pit craters." This formal naming is needed because there are several specific differences that will be referred to on the map, and there is the need to compare the different collapse features. However, the IAU prefers a more generic name, such as "patera." This does not seem to be acceptable to this PI, as the collapse features are clearly part of the entire caldera. In the terrestrial community, these features would be called "craters," except that this standard terrestrial nomenclature only applies to features that are less than 1 km in diameter. Larger features on Earth would be called "calderas," but this does not seem to be appropriate for Olympus Mons, where we would have to have "calderas within a caldera." This PI prefers to have formal names, with each feature being called a "crater."

Publication derived from this mapping:

Mouginis-Mark, P.J., A.J.L. Harris and S.K. Rowland (2007). Terrestrial analogs to the calderas of the Tharsis volcanoes on Mars. In: *The Geology of Mars: Evidence from Earth-based Analogs*, ed. Mary Chapman. Cambridge University Press, pp. 71 - 94.

FINAL MAP RESULTS OF THE OLYMPIA CAVI REGION OF MARS (MTM 85200): GEOLOGIC UNITS AND HISTORY. J. A. Skinner, Jr. and K. Herkenhoff, Astrogeology Team, U.S. Geological Survey, 2255 N. Gemini Drive, Flagstaff, AZ 86001 (jskinner@usgs.gov).

Introduction. Our recently-completed, 1:500K-scale geologic map of MTM 85200--the Olympia Cavi region--provides details of geologically-recent Martian processes. The quadrangle includes dunes of Olympia Undae, the deep depressions of Olympia Cavi and the narrow troughs of Boreales Scopuli. A >1000 m high scarp located at ~85° N (termed herein the "boreal scarp") elevates higher-latitude troughs above the lower-latitude depressions and dune fields. In this paper, we present the regional geologic history of materials in MTM 85200 and environs using excerpts from the completed map.

Surface Morphologies. A variety of kilometer-, meter- and sub-meter-scale surface landforms and texture are apparent in MOLA, MOC narrow and wide angle, THEMIS VIS, HRSC, and HiRISE data sets. Within MTM 85200, these include (1) asymmetric, trough-parallel surface troughs and swales, (2) linear hummocks located south of the boreal scarp, (3) multiple, overlapping, eolian dune-forms, (4) darks streaks and mantles of variable albedo, and (5) small-scale impact craters. Based on cross-cutting relationships, these features span the entire exposed sequence of layered rocks within the north polar plateau (**Fig. 1**). Along with unit descriptions, their occurrence and range of formational mechanisms assist in unraveling the geologic history of Planum Boreum.

Unit Descriptions. Linework was digitized at 1:75,000 using MOLA 115 m/px DEM, the most continuous, highest-resolution, geo-registered base map. We used a late summer 1976 mosaic of Viking Orbiter 1 and 2 images as a temporal "control" to show the extent of the residual ice cap [2]. Geologic units of MTM 85200 are located in the Borealis province [1]. We apply Amazonian epochs to units based on the stratigraphic work of other workers [3-7]. Units are described below from youngest to oldest.

Planum Boreum 2b unit (ABb_{2b}) – Very high-albedo material that forms the uppermost surface of Planum Boreum. Dominates polar flats and extends into spiral troughs, mostly south of the boreal scarp. Drapes all other polar units. Forms rugged patches at lower latitudes and elevations and on trough margins. No impact craters observed. Interpretation: Extent of the 1976 residual water-ice cap [2]. Unit thickness ranges from several-meters-thick down to thin coatings interfingered with adjacent units (**Fig. 1**). Subjacent units are only locally exposed. Buried contacts are inferred.

Olympia Undae 2 unit ($ABou_2$) – Low-albedo, closely-spaced, crescent and transverse dune-forms in both Olympia Planum and Cavi. Where frosted, unit detected by high-albedo hummocks and mottles. Unit overlies Olympia Undae 1 unit, Planum Boreum 1 unit, and Olympia Cavi 1 unit. Inferred time transgressive contact with both Planum Boreum 2a and 2b units (**Fig.1**). Interpretation: Wind-blown sand and silt of basaltic composition (including weathering products). Accumulated primarily through erosion of the Olympia Cavi 1 unit, with secondary contributions from other plateau units.

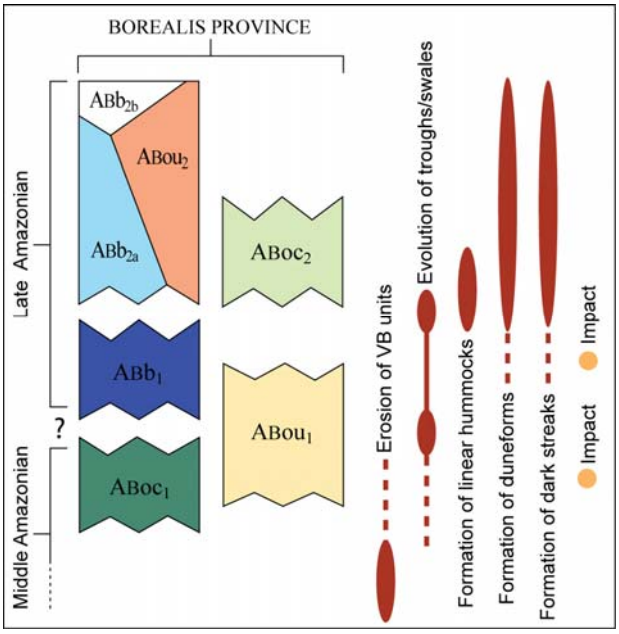

Figure 1. Schematic correlation of map units and associated major geologic events that affected the materials of MTM 85200.

Olympia Cavi 2 unit ($ABoc_2$) – Forms the flat floors of Olympia Cavi located south of the boreal scarp. Medium- to low-albedo. Smooth at MOLA scale. Decameter-scale features include hummocks, pits, and undulations. Overlain by the Olympia Undae 2 unit near the base of northward-facing trough walls. Interpretation: Residuum formed through the sublimation of ice-rich mantles, lag deposits, or mass-wasting slough from higher-standing layered units.

Planum Boreum 2a unit (ABb_{2a}) – Forms on trough floors and on the shallowly-sloping, north-facing trough walls and polar flats. Moderately-smooth at MOLA scale. High-albedo with local low-albedo patches and mottles. Lower boundary commonly diffuse and is drawn using a downward transition to smooth-surfaced, evenly-layered material. Thickest at steeply-sloped, southward-facing trough walls. Some very low-angle unconformities are observed. Interpretation: Dust and ice layers of laterally-variable thickness. Texture and appar-

ent layer subparallelism formed either by deposition of ice-rich lithic layers or erosion of the unit's layers. Actively accumulating on decadal time scales. Time-transgressive contact with residual ice (unit ABb_{2b}) and polar dunes.

Planum Boreum 1 unit (ABb_1) – Outcrops occur on southward-facing trough walls. Unit forms the bulk of the polar plateau and has maximum single exposures of ~800 m; total unit thickness is >1800 m. Has characteristic parallel, even layers of alternating high- and low-albedo. Layers meter-scale and form ~100-meter-thick packages. Unconformities are common, mostly south of the boreal scarp. Lower boundary defined by transition to low-albedo, slab-like material. Interpretation: Dust and ice layers of laterally-continuous thickness. Layering reflects varying dust-ice ratios. Deposited from atmospheric fall-out and/or surface saltation. Rhythmic nature relict of climatic alternations caused by orbital cyclicity, regional volcanic activity, and/or large-scale planetary impact. Forms the bulk of the polar plateau.

Olympia Cavi 1 unit ($ABoc_1$) – Occurs on southward-facing trough and depression walls of Olympia Cavi. High- and low-albedo, slab-like, cross-bedded, cliff-forming, thickly-bedded layers. Very low-albedo layers grade into sand sheets and dunes. Maximum apparent thickness in any single exposure is ~400 m. Interpretation: Layers of dust and sand, perhaps indurated with varying amounts of ice, salt, or other cementing agents. Outcrop morphology may be evidence of low-grade diagenesis, perhaps via compaction and/or chemical induration/alteration. Cliff-forming layers may have a higher proportion of ice or another cementing agent.

Olympia Undae 1 unit ($ABou_1$) – Occurs in northern Olympia Planum. Contains irregularly-shaped, low amplitude swales, commonly abutted by dunes on their windward edges. Small, discontinuous patches of closely-spaced ripples and meter-scale, crescent-shaped ridges common. Overlain by the Planum Boreum 2a and 2b units and Olympia Undae 2 unit. Interpretation: Moderately-resistant, eolian-scoured substrate. Localized sand ripples are inactive. Crescent-shaped ridges are the preserved bases of dunes, indurated perhaps by salt-cementation.

Geologic History. We reconstruct the geologic evolution of the units in MTM 85200 using morphologic, geologic, and stratigraphic observations (**Fig. 1**) as well as past investigative results of other authors. Crater paucity impedes accurate relative age dating and an understanding of when Planum Boreum began to form [e.g., 4-6]. Superposition of these materials on Vastitas Borealis (VB) units clearly shows that the earliest possible start was during the Early Amazonian [1, 3]. Based on past work, we suggest the unit $ABoc_1$ began to accumulate during the Middle Amazonian [1, 3-7], after a prolonged episode of lowland surface degradation [8] (**Fig. 1**), evidenced by lowland pedestal–type craterforms [e.g., 1, 9]. Unit $ABoc_1$ was deposited as massive, overlapping, cross-bedded dunes whose thickness appears to be >400 m based on the minimum apparent thickness of outcrops. Dunes may have contained minor ice and fine-grained lithic components. The unit rooted the Middle Amazonian polar plateau into buried, volatile-rich rocks of the VB units, though it is unclear how unit $ABoc_1$ rocks may interfinger with subjacent lowland plains materials. Unit $ABoc_1$ may have sourced from eroded Scandia materials, Chryse outflow sediments, or other regional units [1, 7].

During the Middle (or Late?) Amazonian, unit $ABoc_1$ dune rocks were eroded into irregularly-shaped hillocks <400 m high, based on a capping unconformity. Eroded detritus may have been dispersed across the adjacent lowland plains as dune fields, some of which may be exposed today (as unit $ABou_2$). This erosional event was followed by deposition of the units $ABou_1$ and ABb_1, locally interrupted by erosional or depositional hiatus (forming unconformities). We suggest the unit $ABou_1$ unit is stratigraphically equivalent to lower portions of unit ABb_1, perhaps representing a planated and partly-buried sequence of layered rock. Unit ABb_1 may have started accumulating during the most recent major decrease in solar insolation (estimated at ~5 Myr [7, 10]).

During the Late Amazonian, Planum Boreum 1, which was locally >1800 m thick, underwent planum-wide erosion, though there is some evidence for depositional hiatus. A resumption of rhythmic layer accumulation deposited unit ABb_{2a}. The temporal extent of the unit ABb_1 erosional episode is not known. Unit ABb_{2a} may have begun accumulating during the most recent high obliquity cycle (estimated at ~20 Kyr [7, 10]). The original extents of units ABb_1 and ABb_{2a} are not precisely known; it is possible both units were severely eroded from previous extents. Time-transgressive contacts between units ABb_{2a}, $ABou_2$ and ABb_{2b} allude to these materials forming (in part) simultaneously, perhaps by localized erosion and re-deposition of layered materials. These observed interfingerings and time-transgressive contacts are potential evidence for current large-scale erosion of the much of the quadrangle surface.

References. [1] Tanaka et al. (2005) *USGS SIM 2888*, 1:15M scale. [2] Herkenhoff (2003) *USGS I-2753*, 1:500K scale. [3] Cutts et al. (1976) *Science* 194, 1329-1337. [4] Tanaka and Scott (1987) *USGS I-1802-C*, 1:15M scale. [5] Thomas et al. (1992) in Mars, 767-795. [6] Herkenhoff and Plaut (2000) *Icarus* 144, 243–253. [7] Tanaka (2005) Nature 437, 991-994. [8] Tanaka et al. (2003) *JGR* 108, (E4), 8043. [9] Skinner et al. (2006) *LPSC* 37, abs. #1476. [10] Laskar et al. (2002) *Nature* 419, 374-377.

GEOLOGY OF THE SOUTHERN UTOPIA PLANITIA HIGHLAND-LOWLAND BOUNDARY PLAIN: CURRENT UNDERSTANDING AND FIRST YEAR MAPPING PLAN. J. A. Skinner, Jr., K. L. Tanaka, T. M. Hare., and D. B. Christensen. Astrogeology Research Program, U. S. Geological Survey, 2255 N. Gemini Drive, Flagstaff, AZ 86001 (jskinner@usgs.gov).

Introduction. Mars' highland-lowland boundary (HLB) scarp spans >4000 m of elevation and >60º of latitude, borders at least three known giant impact basins (Utopia, Chryse, and Isidis), and transects, underlies, or bounds almost every currently-identified geologic unit. Modern (post-Viking Orbiter) data sets reveal that the HLB is generally accompanied by a geologically and stratigraphically complex plain of material along its down-slope margin (*i.e.*, the highland-lowland "boundary" plain) [1-6]. In southern Utopia Planitia, the boundary plain forms bench-like platforms that contain depressions, pitted cones (some organized into arcuate chains and thumbprint terrain), isolated domes, lineated depressions, buried circular depressions, ring fractures, polygonal fractures, and other locally- to regionally-dispersed landforms. Because the origins of these features are not well-understood, the objective of our mapping project is to clarify the geologic evolution of the southern Utopia Planitia HLB by identifying the geologic, structural, and stratigraphic relationships of surface materials in MTMs 10237, 15237, 20237; 10242, 15242, 20242; 10247, 15247, 20247 (**Fig. 1**).

Current Understanding. The southern Utopia HLB extends >1500 km westward from northern Nepenthes Mensae to the topographic saddle that separates the Isidis and Utopia Planitiae. The map area contains 20% Noachian highland materials, 60% Hesperian boundary plain materials, and 20% Amazonian lowland plain materials. These three geologic provinces and the transition between each hold important geologic and stratigraphic information. Yet, a coherent geologic and stratigraphic framework for interpreting these features based on the most modern data sets is currently lacking.

Highlands - Past geologic maps delineated the southern margin of the southern Utopia Planitia HLB as assemblages of Noachian and Hesperian basement and regolith materials that were eroded by fluvial activity, mass-wasting, impacts, and other geologic processes [3-5]. Remnants of the Utopia impact massifs and/or ejecta blanket are not generally detected aside from cursory morphologic inference [*e.g.*, 6]; these have been either deeply buried or eroded beyond recognition.

Boundary plain - The southern Utopia boundary plain is divided into the Early Hesperian Utopia Planitia 1 unit and the Late Hesperian Utopia Planitia 2 unit [3]. These two units cover the majority of our selected quadrangles. The boundary plains units and their contained morphologies are interpreted to be evidence of temporally and spatially pervasive deposition and/or modification of the dichotomy boundary during the Hesperian, prior to the Early Amazonian emplacement of Vastitas Borealis units [3,6]. The transition between these two HLB units is demarcated by isolated and scalloped depressions of Amenthes Cavi, which are unique to the southern Utopia boundary plain and well-covered by our selected MTM quadrangles. Among the suggested origins of boundary plain landforms are (1) marginal marine erosional platforms [7-10], (2) surficial cryoturbation vestiges [11], (3) highland detritus of varying thickness and origin [12-13], and (4) soft-sediment deformation products [6].

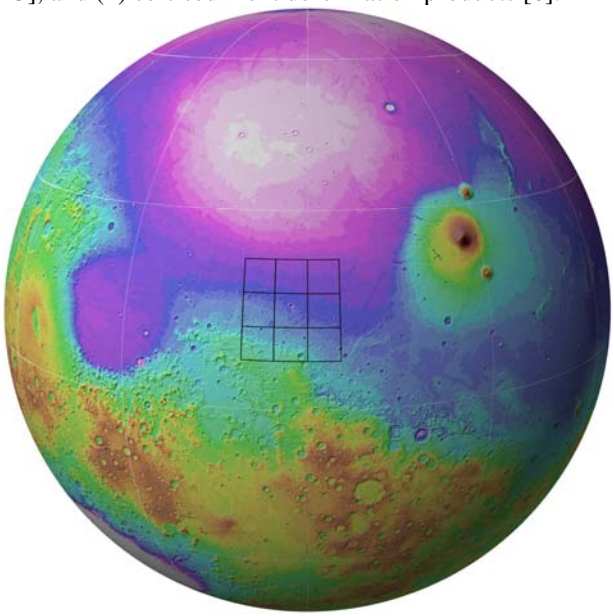

Figure 1. Mars globe centered at 120º E, 10ºN showing the nine quadrangles that cross the southern Utopia Planitia HLB. Orthographic projection of MOLA shaded-relief image.

Lowlands – The four units that previously comprised the Vastitas Borealis Formation [14-15] were recently re-interpreted as only two stratigraphically-discrete geologic units (*e.g.*, the Vastitas Borealis marginal and interior units) based on well-defined crater counts and other stratigraphic relationships [3, 11]. The Vastitas Borealis units, which are variably pockmarked with eroded and/or exhumed impact craters, extend northward from the southern Utopia Planitia boundary plain into the broader lowland basins. These materials are generally interpreted as laterally-gradational, sedimentary sequences derived from the erosion of highland, boundary, and lowland terrains, locally to regionally interfingered with volcanic materials [3, 7, 9-11]. While the most recent lowland plains surface formed during the Early Amazonian [3, 14-16], it is unclear to what degree

the exposed surface represents combined depositional and modificational processes.

Mapping Method. Our base maps include full-coverage image and topographic data sets, including the Viking MDIM 2.1 (231 m/px), MOLA 1/128 px/degree (463 m/px) digital elevation model, the THEMIS IR mosaic (231 m/px), and the MOC WA mosaic (231 m/px) along with various supplemental map layers and ancillary information (*e.g.* topographic high-pass filters and internet-hotlinked THEMIS VIS and IR footprints). We use ArcGIS® as our map environment and will continually update metadata over the life of the project in order to improve documentation during the mapping stages and to ease production of a final map product.

We are using both "classical" and updated planetary mapping methods [3, 17-19]. Because many of the materials that form the southern Utopia Planitia HLB are likely to be dispersed sedimentary sequences [3-6, 11], daytime and nighttime thermal data provide critical information for defining unit boundaries (where not covered by dust), particularly as such sequences may laterally grade into other materials. Where possible, particularly in the wall-rock of high-standing, eroded highland materials adjacent to the HLB scarp, we are examining bedding locations, paying close attention to the character and continuity of such features as they may hint at subsurface layering.

Year 1 Work Plan. The beginning of our Year 1 work plan has focused on (1) creating/updating crater inventories and (2) surveying, comparing, and contrasting morphologic features that dominate the region. Firstly, we are logging crater locations, diameters, and ejecta characteristics. This task also provides a cursory examination of the regional geology using "exploratory" methods during the early stages of mapping. Crater densities (and "curves") provide a means to infer both the age and resurfacing history of any given surface, particularly when used to supplement cross-cutting information. We are currently locating all craters within the selected mapping quadrangles that are ≥ 2 km diameter. In addition, we are tabulating the erosional state of crater ejecta ("high," "medium," or "low") as a preliminary proxy for superposition (*e.g.*, a "low" erosional state may signify the effects of post-impact modification) [20]. Secondly, we are surveying and then comparing and contrasting morphologic features that dominate the region. We began this effort by using landform assessments of past mapping efforts [3-5] and topical studies [6, 11-13], including highland-transitional landforms such as knobs, mesas, mass-wasting fans, and channels, and lowland-transitional landforms such as lobate margins, pitted cones, and depressions. We are also using thermophysical characteristics to identify potentially unique geologic surfaces. Of particular interest in this early part of the study is to characterize, without preconception, a distinct thermophysical transition from the boundary plain into the lowland plain. This transition is dominated by south-facing, overlapping, (relatively) lower thermal inertia, thin lobes that appear to have been emplaced around (relatively) higher thermal inertia surfaces and knobs [3, 6]. This area coincides with a general increase in regional crater onset diameters (the diameter at which crater ejecta transitions from ballistic to lobate) [6], perhaps indicating a local shallowing of subsurface water and/or ice.

Year 1 Anticipated Results. Total Year 1 efforts will consist of (1) processing and geo-registration of pertinent data sets, (2) cataloging of craters ≥ 2 km in diameter and assignment of a preliminary "high," "medium," or "low" ejecta erosional state, (3) geology, geomorphology, and structure mapping, (4) and nomenclature updates and refinements. These efforts will result in, by the close of Year 1, a preliminary assessment of quad-scale geomorphologies (and any clustered variability thereof) and stratigraphic characteristics of regional surfaces. Relative ages and units will be resolved using the crater inventory as well as the observed erosional state of the ejecta. We will use this information to delineate preliminary geologic units to stratigraphically correlate map units. Year 2 efforts will focus on testing and revamping Year 1 map results with intent to submit map for review by the beginning of Year 3.

References. [1] McGill, G.E., (2005) *USGS I-2811*, 1:1M scale. [2] Irwin, R.P., *et al.*, (2004) *J. Geophys. Res. 109*. [3] Tanaka *et al.*, (2005) *USGS SIM 2888*, 1:15M scale. [4] Scott, D.H. and Carr, M.H., (1978) *USGS I-1083*, 1:25M scale. [5] Greeley, R. and Guest, J.E., (1987) *USGS I-1802-B*, 1:15M scale. [6] Skinner, J.A. Jr. *et al.*, (2007) *Icarus*, *186*, 41-59. [7] Head, J.W. III, et al. (1999) *Science*, *286*, 2134-2137. [8] Thomson, B.J. and Head, J.W. III, (2001) *J. Geophys. Res.*, *106*, 23,209-23,230. [9] Parker, T.J., *et al.*, (1989), *Icarus*, *82*, 111-145. [10] Parker, T.J., *et al.*, (1993) *J. Geophys. Res.*, *98*, 11,061-11,078. [11] Tanaka, K.L. *et al.*, (2003a) *J. Geophys. Res.*, *108*, (E4). [12] McGill, G.E., (1989) *J. Geophys. Res.*, *94*, 2753-2759. [13] Buczkowski, D.L. *et al.*, (2005) *J. Geophys. Res.*, *110*, E03007. [14] Scott, D.H. *et al.*, (1986-87) *USGS I-1802-A/B/C*, 1:15M scale. [15] Tanaka, K.L., (1986) *J. Geophys. Res.*, *91*, E139-158. [16] Head, J.W. III et al. (2002) *J. Geophys. Res.*, *107*, (E1). [17] Wilhelms, D.E., (1990) in *Planetary Mapping* (R. Greeley and R.M. Batson (eds.)), Cambridge U. Press. [18] Hansen, V.L. (2000) *EPSL*, *176*, 527-542. [19] Skinner and Tanaka (2003) *LPSC XXXIV*, abs. #2100. [20] Barlow, N.G. (2006) *LPSC XXXVII*, abs. #1337.

NEW GLOBAL GEOLOGIC MAP OF MARS. K. L. Tanaka[1], James M. Dohm[2], Trent M. Hare[1], R. P. Irwin, III[3], E. J. Kolb[4], and J. A. Skinner, Jr.[1], [1]U.S. Geological Survey, Flagstaff, AZ (ktanaka @usgs.gov), [2]U. Arizona, Tucson, AZ, [3]Smithsonian Inst., Washington, DC, [4]Arizona State U., Tempe, AZ

Introduction. We recently received a NASA Planetary Geology and Geophysics grant to remap the global geology of Mars at 1:20M scale (printed), which will employ the lower resolution mapping data sets in Table 1 and digital tools and approaches using the latest Geographic Information Systems technology. Our work plan runs for five years (2007 to 2011; the Viking-based global map at 1:15M scale and more recent northern plains map at 1:15M scale each took ~six years to complete). Our team includes additional colleagues who will contribute mapping of particular features and regions, perform detailed crater counts, and provide additional analyses of the mapping results. Along the way, we will present our progress, including preliminary results and updated thinking about geologic and stratigraphic schemes for Mars. We will encourage input from the planetary geology community during the course of the project as the results of concurrent studies by others will help us to improve our global geologic map in various ways.

Table 1. Mars geologic mapping data sets. *MOLA = MGS Mars Orbiter Laser Altimeter; THEMIS = ODY Thermal Emission Imaging System; HRSC = MEX High Resolution Stereo Color camera; CTX = MRO Context Camera; IR = infrared, VIS = visual range.*

Data	Type	Resolution (m/pixel)	Current coverage
MOLA	Altimetry	460 (115 at poles)	global
THEMIS IR	Infrared images	100	global
HRSC	Color, stereo images	10 to 30	extensive
THEMIS VIS	Visual range images	18 to 40	patchy
CTX	Visual range images	6	little

Issues that can be addressed. Our newly-funded global mapping project will achieve a better understanding of the global geology of Mars. In particular, we will focus on the following science objectives.

1. Update global stratigraphy. Each previous global map of Mars has resulted in constructions and formal definitions of global stratigraphic and chronologic schemes, first with the establishment of the Noachian, Hesperian, and Amazonian Periods from Mariner 9-based mapping [1], and later with the subdivision of the periods into Early, Middle, and Late epoch divisions using Viking images [2-3]. A "pre-Noachian epoch" was introduced in the northern plains map [4], based on the recognition of quasi-circular depressions indicative of primordial, buried crustal material underlying the oldest determined exposed Noachian surface materials [5]. Another major stratigraphic revision was the re-assignment of the beginning of the Amazonian Period to the surface age of the Vastitas units of [4] (those units are roughly equivalent to the Vastitas Borealis Formation of [2]). These units are much more geologically and spatially significant and broadly coeval than the lava flows of Amazonis Planitia previously used as the basal Amazonian stratigraphic marker, which are now perceived to have a complex stratigraphy [4]. Global mapping will provide us with the proper perspective to consider whether any other significant revisions to the unit-based stratigraphic divisions ought to be made, such as to represent younger deposits related to climate cycling [4, 6-7], as well as re-evaluation of each Martian epoch.

Furthermore, discrepancies exist in crater size-frequency distributions at the most critical diameter range, between ~1 and 20 km, where the distributions are most at odds [8]. Discrepancies also exist at larger diameters [cf. 9-10]. Our work will provide an extensive database of crater size-frequency data as a function of geologic units in these critical diameter ranges. The new mapping and crater statistics, when applied judiciously (with proper consideration to resurfacing) will result in an improved scheme of Martian epochs defined by crater densities. In turn, ages and rates of geologic activity can be estimated [e.g., 8], which can be useful for scientific and mission-related applications.

2. Update global tectonic history. Global structural mapping will permit refinement of the tectonic history for Mars, as follows:

(a) Contractional history. Viking-based mapping of wrinkle ridges recognized few ridges in the northern plains and indicated stress sources primarily due to Late Noachian and Early Hesperian global contraction and local compression caused by outflow channel erosion and Tharsis tectonism [11]. MOLA shaded-relief and detrended maps and THEMIS day IR images permit identification and mapping of wrinkle ridges previously unrecognized in Viking images [4]. Furthermore, some wrinkle ridges located in the northern

plains may have been active more recently than previously interpreted, perhaps during the Late Hesperian and Early Amazonian [4]. Remapping and relative-age dating of wrinkle ridges will better constrain lithospheric stress history, particularly in the highlands.

(b) Extensional history. We do not expect significant alteration to the line mapping of extensional structures such as graben and rifts because much of the original printed maps have been digitally renovated, including improved spatial registration [12]. This renovation improved the positioning of previously mapped tectonic structures, which enabled their accurate registration to more recent global data sets (e.g., MOLA DEM and MDIM 2.1) [12]. We do, however, anticipate some refinement in the constraints to dating of these features as they relate to newly-defined geologic units and their boundaries. We can also more adeptly assess relative-age information for globally-mapped tectonic features through the application of digital tools, improved mapping, and more detailed crater counting of the map units that constrain their ages. Impact craters and their preservation states can be more precisely delineated and characterized using THEMIS IR images rather than with panchromatic, visible-range Viking images.

3. Analysis of fluvial valleys, paleolakes, oceans, and surficial mantles. Our global mapping will provide the broadest context to search for geologic associations that various climatic/hydrologic scenarios predict. We can document the relative timing and spatial relations of major fluvial, mass wasting, and potential glacial erosion vs. age of emplacement of sedimentary and other possibly related units. For example, a significant gap in time between valley network activity and plains emplacement would suggest non-fluvial materials, whereas contemporary deposits would be consistent with a fluvial origin or perhaps a combined fluvial and volcanic suite where magma/volatile interactions have occurred.

The relative-age relationships between fluvial erosion and extensive mantling (sedimentary or volcanic) events will help to characterize the activity during waning stages of activity, perhaps when the supply of water was episodic. In areas where extensive eolian deflation has not occurred, mantle deposits can be dated relative to fluvial activity by simple cross-cutting and burial relationships. In addition, catastrophic floods sourced from chaos within highland material may have ponded in the northern plains as transient oceans and/or lakes, perhaps causing the punctuated development of short-lived (tens of thousands of years?) regional to global hydrologic cycles and climatic perturbations [13-14]. The latter may have caused environmental conditions (and, thus, geologic conditions) at the surface to deviate, perhaps significantly, to an unusually warm and wet Mars [e.g., 13-16]. Despite such assertions, geologic evidence for a paleo-ocean remains inconclusive [e.g., 16], perhaps because the large amount of time since their putative existence has allowed for thorough erosional masking. Oceans may also have formed by elevation-controlled surface runoff [17] or ground-water discharge [18-19], hypotheses that can be tested with a global map and the MOLA data set. Alternatively, topographically-controlled groundwater basins may have inhibited the delivery of highland recharged groundwater to a putative northern ocean. We can also assess the timing and distribution of features potentially related to precipitation and ground-water recharging hypotheses that involve sapping [e.g., 19] and tapping of Tharsis and east Hellas aquifers that led to catastrophic discharges evident in the carving of outflow channels [20-21].

4. Other volatile-related processes. These processes include deposition and exhumation of ice and dust mantles [6], volatile-exchange and weathering in near-surface materials (including formation of phyllosilicates and hydrous sulfates [22-23]), and cryoturbation and soft-sediment deformation [24]. Global examination of such processes will help us understand the volatile history within the near surface and its relation to geologic and climate history.

References: [1] Scott D.H. and Carr M.H. (1978) *USGS Map I-1083.* [2] Scott D.H. et al. (1986-87) *USGS Maps I-1802-A, B, C.* [3] Tanaka K.L. (1986) *JGR 91, suppl.,* E139-E148. [4] Tanaka K.L. et al. (2005) *USGS Map SIM-2888.* [5] Frey H.V. (2004) *LPS XXXV,* Abstr. #1382. [6] Mustard J.F. et al. (2001) *Nature 412,* 411-414. [7] Head J.W. et al. (2003) *Nature 426,* 797-802. [8] Hartmann W.K. and Neukum G. (2001) *Space Sci. Rev. 96,* 165-194. [9] Barlow N.G. (1988) *Icarus 75,* 285-305. [10] Frey H.V. et al. (2002) *GRL 29,* 1384. [11] Tanaka K.L. et al. (1991) *JGR 96,* 15617-15633. [12] Skinner J.A., Jr. et al. (2006) *LPS XXXVII,* Abst. #2331. [13] Baker V.R. et al. (1991) *Nature 352,* 589-594. [14] Fairén A.G., et al. (2003) *Icarus* 165, 53-67. [15] Parker T.J. et al. (1993) *JGR 98,* 11061-11078. [16] Carr M.H. and Head J.W. (2003) *JGR 108,* 5042. [17] Craddock R.A. and Maxwell T.A. (1990) *JGR 95,* 14265-14278. [18] Tanaka K.L. et al. (2003) *JGR 108,* 8043. [19] Grant J.A. (2000) *Geology 28,* 223-226. [20] Harrison K.P. and Grimm R.E. (2004) *GRL 31,* doi:10.1029/2004GL020502. [21] Crown D.A. et al. (2005) *JGR 110,* doi:10.1029/2005JE002496. [22] Bibring J-P. et al. (2006) *Science 312,* 400-404. [23] Wyatt M.B. et al. (2004) *Geology 3,* 645-648. [24] Skinner J.A. Jr. and Tanaka K.L. (2007) *Icarus 186,* 41-59.

RECENT GEOLOGIC MAPPING RESULTS FOR THE POLAR REGIONS OF MARS. K.L. Tanaka[1] and E.J. Kolb[2], [1]Astrogeology Team, U.S. Geological Survey, Flagstaff, AZ 86001, ktanaka@usgs.gov, [2]Arizona State University, Tempe, AZ 85287, eric.kolb@asu.edu.

Introduction: The polar regions of Mars include the densest data coverage for the planet because of the polar orbits of MGS, ODY, and MEX. Because the geology of the polar plateaus has been among the most dynamic on the planet in recent geologic time, the data enable the most detailed and complex geologic investigations of any regions on Mars, superseding previous, even recent, mapping efforts [e.g., 1-3]. Geologic mapping at regional and local scales is revealing that the stratigraphy and modificational histories of polar materials by various processes are highly complex at both poles. Here, we describe some of our recent results in polar geologic mapping and how they address the geologic processes involved and implications for polar climate history.

North polar stratigraphy: The exposed geologic record for the north polar region appears largely limited to the Amazonian Period, as redefined by [3]. The north polar plains are made up of the *Vastitas Borealis units*, perhaps emplaced as fluvial sediments and (or) periglacially reworked material at the beginning of the Amazonian following cessation of outflow-channel discharges from the Chryse region [3].

Thereafter, the *Scandia region unit* was emplaced in the form of circular plateaus and irregular hilly complexes of Scandia Tholi and Cavi and planar deposits that have since eroded into knobs and mesas, forming Scandia Colles. This unit may have once covered ~1.5 x 10^6 km^2 of the plains north of Alba Patera to Planum Boreum to an average thickness of 100 m. We interpret that the material represents deposits related to mud-diapir-like processes, possibly redistributed by wind. In this scenario, the north polar gypsum discovered by the OMEGA instrument [4] may relate to Alba Patera magmatism [5].

Possibly coeval with and following formation of the Scandia region unit was emplacement of evenly to wavy-bedded material forming the *Rupes Tenuis unit* [6]. This material forms the base of much of Planum Boreum. West of Chasma Boreale, along the Rupes Tenuis scarp, the unit includes more than 20 beds and is >1000 m thick. A number of large impact craters on the unit indicate that it is a fairly ancient polar deposit. In spite of the unit's great thickness, it appears to be completely eroded back to an abrupt margin. Possibly correlative is the mantle material that forms the bases of >1800 pedestal craters in surrounding plains [7].

Perhaps during much of the Amazonian, dark, (possibly made up of weathered basalt [8]) dune fields migrated across the circum-polar plains mainly north of 70ºN where dunes are presently common. We map the current dune fields as the *Olympia Undae unit,* after the largest dune field. This unit also includes rippled surfaces as seen in MOC images that may form an underlying, indurated sand sheet. Some of the present dune fields originate from steep scarps exposed on the margins of Abalos Mensa, from Boreum and Tenuis Cavi at the head of Chasma Boreale, and from reentrants of Olympia Cavi into Planum Boreum. The bases of the scarps include dark, cross-bedded bright and dark layered material mapped as the *Planum Boreum cavi unit* [9]. Some of the dunes of Olympia Undae are embayed by the young mid-latitude mantle [10] and the youngest polar layered deposits (Planum Boreum unit 2).

The Planum Boreum cavi unit grades upwards into *Planum Boreum 1 unit,* which forms the majority of what are commonly referred to as "polar layered deposits" (however, other polar deposits are also layered, thus the term is now ambiguous). The unit includes dozens of unconformities as seen in MOC images, which may be related to changing patterns of spiral-trough development and (or) local variations in topographically controlled depositional environments [11]. Correlation of layer sequences exposed in various troughs is challenging, but rhythmic sequences of layers ~30-m-thick have been detected [12]. Deformation within this unit is rarely observed, such as near Udzha crater [13].

Within Chasma Boreale and troughs and adjacent plains of Planum Boreum, several dark layers form a sequence as much as 200 m thick and forms the *Planum Boreum 2 unit.* This unit is sculpted with yardangs and within Chasma Boreale is embayed by dozens of bright layers of the *Chasma Boreale unit*, which also includes yardangs. In turn, the youngest layered deposit, *Planum Boreum 3 unit*, consists of several layers as much as a few tens of meters thick that unconformably overlie older Planum Boreum units. In turn, the residual ice cap forms the *Planum Boreum 4 unit,* which rests unconformably on underlying materials [14]. The basal layer of the upper unit appears to be made up of a sandy, dark layer, which is the source of veneers of material that appear to contribute to erosion of the spiral troughs and related undulations [15].

South polar stratigraphy: In contrast to the north polar region, the south polar region exposes a geologic record that extends into the Noachian Period. Here, the oldest rocks form the *Noachis Terra unit* and consist of impact breccia and melt, volcanic materials, and eolian and other sediment of the southern cratered highlands. Many impact craters within the highland terrain have undergone degradation and removal, and some unusual remnants, perhaps modified by volcanism, form the rounded massifs of the *Sisyphi Montes unit* [16]. Also, outpourings of likely volcanic material during the Late Noachian through Early Hesperian formed the *Aonia Terra*, *Malea Planum*, and *Terra Cimmeria* units.

Throughout the Hesperian, the nearly circum-polar deposits of the Dorsa Argentea province were emplaced, forming a complex sequence consisting of lobate plains and superposed sinuous ridges, high-standing rugged terrain, and depressions. These unusual characteristics have led to various interpretations [see 2 and references therein]. We divide the Dorsa Argentea province into eight units that differ markedly from those mapped by [1]. The province includes: (1) a thick basal sequence of layered deposits exposed within the pits of Cavi Angusti and Sisyphi Cavi, (2) a high-standing rugged member that includes pitted cones and ridges, (3) five units of plains materials, and (4) a thick, fine-grained friable planar deposit that caps mesas and plateaus of Cavi Angusti. We suggest that the deposits and structures are best explained collectively by cryovolcanic eruptions and discharges of volatile-rich, fluidized slurries formed by the mixing of subsurface volatiles with fine-grained, unconsolidated crustal material and perhaps cryoclastic ash. This activity may have arisen from instabilities in Hesperian aquifers and triggering events caused by seismic shaking, fracturing, intrusions, and loading by polar deposition [2].

The *Planum Australe 1 unit* forms the majority of Planum Australe, the south polar plateau, reaching a maximum thickness of ~3 km within the plateau's thickest region, Australe Mensa. The unit is exposed along plateau margins and within canyons, and its basal layer sequences are perhaps Early Amazonian in age. A regional unconformity identified in the chasmata of Promethei Lingula and the curvilinear canyons of Australe Scopuli divides the Planum Australe 1 unit into the lower and upper members. The erosion associated with the unconformity was primarily wind and sublimation driven, and occurred after approximately one-third of the Planum Australe 1 unit stratigraphy was emplaced. The unconformity's orientation and outcrop expression indicates the chasmata formed by down-cutting of Planum Australe 1 unit surface depressions formed where the unit overlies uneven substrate [17] and marks the initiation of curvilinear canyon formation within Australe Scopuli [18].

The *Planum Australe 2 unit* unconformably buries eroded Planum Australe 1 surfaces. The unit was emplaced after the canyons had largely reached their current form and after the plateau margins underwent extensive removal from Argentea, Promethei, and Parva Plana. The unit is <300 m thick and is comprised of layers that are slightly thicker than those of Planum Australe 1 unit.

The *Planum Australe 3 unit* crops out mostly in a series of narrow, shallow (<~200 m) curvilinear Australe Mensa canyons between 270°E and 30°E and on the floors of canyons that cut the southernmost sections of Australe Scopuli [19]. The unit is ~300 m thick and is comprised of 6-7 uniformly thick, conformable layers; individual layers have undergone differential erosion, resulting in an outcrop profile of cliffs and terraces. The characteristic low-to-intermediate albedo of the individual layers suggests they are relatively dust rich. The unit unconformably overlies the Planum Australe 1 and 2 units.

The *Planum Australe 4 unit* delineates the residual ice cap, the bright, <~10 m-thick veneer centered between 225°E through 45°E and poleward of ~82°S. The upper member consists of the high-albedo CO_2-dominated sections [20] of the residual ice cap and constitutes the majority of the deposit's areal extent. The lower member is a thin basal layer consisting of water ice [21-22] that forms the moderate-albedo margins of the residual ice cap. The unit unconformably overlies the Planum Australe 1 through 3 units.

Synthesis of polar geology: Polar deposits include atmospheric volatile and dust precipitates and aeolian dunes and sheets made up of basaltic fines that have undergone some moderate cementation and weathering and extensive aeolian reworking. Our mapping studies generally indicate that the availability of dust, sand, and volatiles controlled by climate conditions and geologic activity and the variable circum-polar wind patterns controlled by topography and weather conditions have resulted in a complex history of accumulation and erosion at Planum Boreum and Planum Australe. Both climate-related cycles operating at differing time scales as well as unique geologic and climatic events have driven these processes. However, we find no compelling evidence for glacial-like deformation and for basal melt-water discharge of polar deposits.

References: [1] Tanaka K.L. and Scott D.H. (1987) *USGS Map I-1802-C*. [2] Tanaka K.L. and Kolb E.J. (2001) *Icarus 154,* 3-21. [3] Tanaka K.L. et al. (2005) *USGS Map SIM-2888*. [4] Langevin Y. et al. (2005) *Science 307,* 1584-1586. [5] Tanaka K.L. (2006) *4th Mars Polar Sci. Conf.* Abs. #8079. [6] Tanaka K.L. et al. (2006) *LPSC XXXVII,* Abs. #2344. [7] Skinner J.A., Jr. (2006) *LPSC XXXVII,* Abs. #1476. [8] Wyatt M.B. et al. (2004) *Geology 32,* 645-648. [9] Byrne S. and Murray B.C. (2002) *JGR 107,* 5044. [10] Mustard J.F. et al. (2001) *Nature 412,* 411. [11] Fortezzo C. and Tanaka K.L. (2006) *4th Mars Polar Sci. Conf.* Abs. #8079. [12] Milkovich S.M. and Head J.W. (2005) *JGR 110,* doi:10.1029/ 2004JE002349. [13] Tanaka K.L. (2005) *Nature 437,* 991. [14] Skinner J.A., Jr. et al. (2006) *4th Mars Polar Sci. Conf.* Abs. #8083. [15] Rodriguez J.A.P. et al. (2006) *LPSC XXXVII,* Abs. #1437. [16] Rodriguez J.A.P. and Tanaka K.L. (2006) *4th Mars Polar Sci. Conf.* Abs. #8066. [17] Kolb E.J. and Tanaka K.L. (2006) *Mars* 2, 1-9. [18] Kolb E.J. and Tanaka K.L. (2006) *4th Mars Polar Sci. Conf.* Abs. #8085. [19] Kolb E.J. and Tanaka K.L. (2006) *LPSC XXXVII,* Abs. #2408. [20] Bibring et al. (2006) Nature 428, 627. [21] Byrne S., and Ingersoll A.P. (2003) Science 299, 1051. [22] Titus T.N., Keiffer H.H., and Christensen P.R. (2003) Science 299, 1048.

MARGARITIFER TERRA QUADRANGLES -20012 AND -25012: REVIEWED AND RESUBMITTED.

S. A. Wilson[1], J. A. Grant[1] and C. M. Fortezzo[2], [1]Center for Earth and Planetary Studies, National Air and Space Museum, Smithsonian Institution, Washington, DC 20560, [2] Department of Geology, Northern Arizona University, Flagstaff, AZ 86011.

Introduction: Valley networks and associated landforms in Margaritifer Terra (Figure 1), located southeast of Valles Marineris, reflect a complex history involving water transport, storage, and release [1-6]. Margaritifer Terra straddles a depression known as the Chryse trough [7], with the Uzboi-Ladon-Margaritifer (ULM) northward-flowing, mesoscale outflow system draining the west side of the trough [2], and the Samara and Paraná-Loire valley systems draining the east side of the trough [3-5]. Both valley systems merge in Margaritifer basin near the head of Ares Vallis [5] (Figure 1).

Mars Transverse Mercator (MTM) -20012 and -25012 (latitude 17.5ºS to 27.5ºS between 345ºE and 350ºE) are two of multiple quadrangles in a series of 1:500,000-scale study areas on Mars sponsored by NASA Planetary Geology and Geophysics Program grants (NAG5-4157, NAG5-10390). These two quadrangles cover a portion of Margaritifer Terra (Figure 1) centered on the collection basin between Loire Valles to the west and Paraná Valles to the east (Figures 2 and 3).

Map Status and Results: MTM quadrangles -20012 and -25012 were submitted, reviewed, updated and resubmitted in June, 2007. MTM quadrangles -10022 and -15022 are submitted and in review. The results from mapping quadrangles -20012 and -25012 are emphasized here (Figures 2 and 3).

The degraded Ladon and Holden multi-ringed impact basins [8] are the oldest features in Margaritifer Terra (Figure 1), followed by evolution of the cratered upland surface (Nm and Npld in Figures 2 and 3). Subsequently, widespread resurfacing events occurred [4, 5]. The first two resurfacing events, which are not in the map area, date to the early to middle Noachian with the second event ending at an N5 age of around 1000 (number of craters >5 km in diameter per 1,000,000 km^2). The third resurfacing event (HNsp), which began in the late Noachian (N5 age ~300), was coincident with waning highland volcanism. From the late Noachian extending into at least the early [5] or middle to late [9] Hesperian, valley networks (HNvn), dissected terrain (HNspd), fans (Hspf), positive-relief chaotic terrain (Hct$_p$) and depositional sinks formed. The initial collapse of the Margaritifer Chaos in the Margaritifer basin occurred at this time, as well as chaos to the northwest of the basin (Figure 1). A final, more localized resurfacing event (AHsp) began in the middle Hesperian (N5 age ~130), typically embaying many of the valleys and channels [4, 5]. Whereas the older resurfacing events (including HNsp) created widespread plains that may be related to a variety of processes, the final resurfacing event (AHsp) emplaced materials we favor as volcanic rather than sedimentary in origin based on the presence of wrinkle ridges, occasional lobate morphology [5], confinement to topographic basins, and a paucity of valleys.

The duration of valley formation is uncertain; some drainages along the ULM valley system may have extended into the Hesperian (N5 ~150), and late-stage flows may have been concurrent with local volcanic activity into the early Amazonian (N5 ~40) adjacent to the ULM system in quadrangles -10022 and -15022 (Figure 1). Additional mapping of the Samara and Paraná-Loire Valles and adjacent drainages is underway (Figure 1), and should help place further constraints on the timing and extent of valley formation.

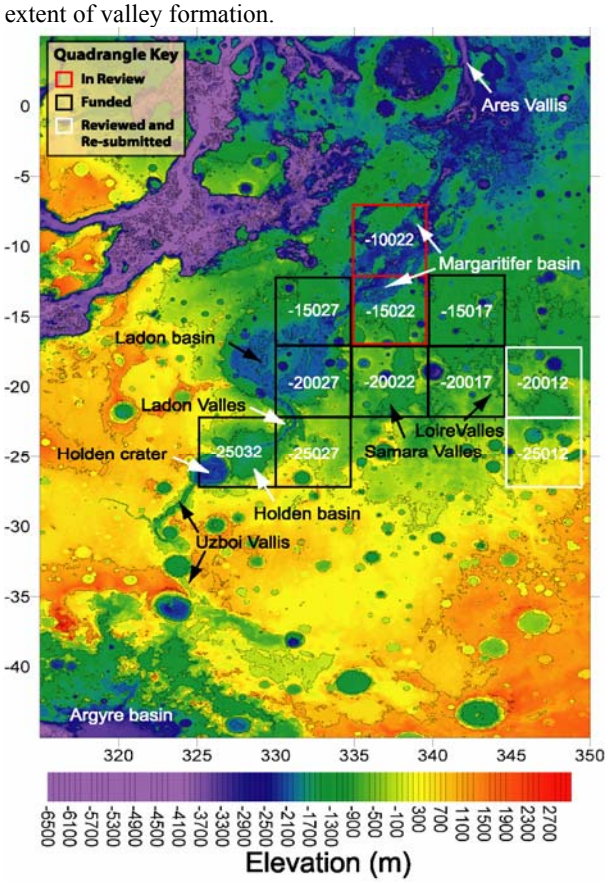

Figure 1. MOLA Topography of Margaritifer Terra. Reviewed and re-submitted MTM quadrangle maps (white boxes), funded maps (black boxes) and maps under review (red boxes) are shown. Contour interval is 1 km and north is towards the top of the image.

Ongoing Mapping in Margaritifer Terra: Mapping in Holden crater in SW Margarititfer Terra is underway as part of a new project. Impact megabreccia is unconformably overlain by distal alluvial fan and/or lacustrine sediments that were deposited during two or more Noachian-age phases of aqueous activity. A lower and mechanically

weak, light-toned, layered, phyllosilicate-bearing unit exhibits few resolvable blocks and laterally continuous (on a kilometer scale), meter to sub-meter thick beds. This light-toned, layered unit was likely deposited in a distal alluvial or lacustrine environment. Dark-toned layers with little or no phyllosilicates drape the lower sequence and were emplaced during later, relatively short-duration, high-magnitude flooding as a confined Uzboi Vallis lake overtopped the Holden rim (Figure 1). The diverse stratigraphy exposed in Holden crater provides a rare opportunity to evaluate the changing potential for habitability during the Noachian Period.

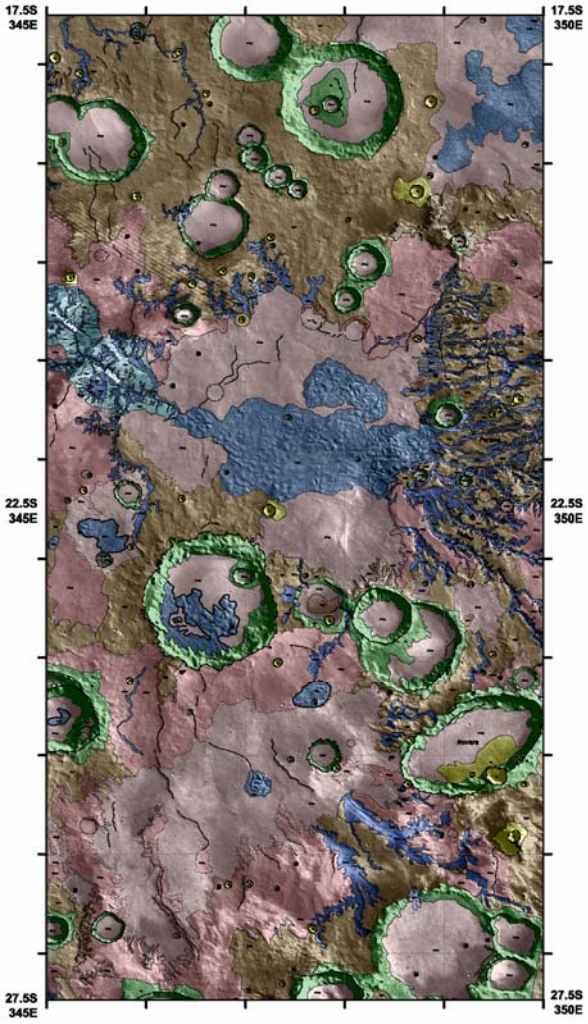

Figure 2. Completed 1:500,000 map of MTM -20012 and -25012 covering the headward reaches of the Paraná-Loire Vallis systems. Mapped units are described in Figure 3.

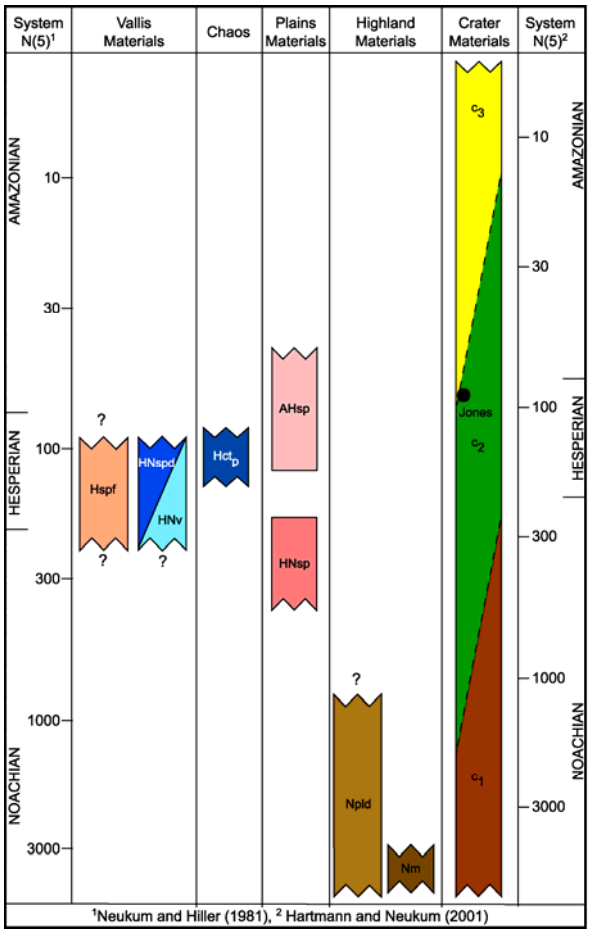

Figure 3. Correlation of mapped units in Figure 2. Relative ages are expressed as the number of craters larger than 5 km-in-diameter per 1,000,000 km^2 and were derived via comparison to [10] and [11] on the left side and right side, respectively. The oldest materials in the map are heavily cratered mountainous material (*Nm*) and dissected highland material (*Npld*). The Noachian/Hesperian smooth plains resurfacing unit (*HNsp*) was emplaced before the valley networks (*HNv*) and associated degraded surfaces (*HNspd*), the positive-relief chaotic terrain (*Hct$_p$*), and the fan (*Hspf*). The Amazonian/Hesperian smooth plains resurfacing unit (*AHsp*) typically embays valleys, channels and older materials. Craters mapped as c_3, c_2, and c_1, are well-preserved, moderately preserved and heavily degraded, respectively.

References: [1] Saunders, S.R., 1979, USGS Map I-1144. [2] Parker, T.J., 1985, MS Thesis, Cal. State Univ., LA. [3] Grant, J.A., 1987, NASA Tech. Memo. **89871**, 1-268. [4] Grant, J.A., 2000, *Geology*, **28**, 223-226. [5] Grant, J.A., and Parker, T.J., 2002, *J. Geophys. Res*., **107**, 10.1029/2001JE001678. [6] Hynek, B.M., and R.J. Phillips, 2001, *Geology*, **29**, 407-410. [7] Phillips, R.J., et al., 2001, *Science*, **291**, 2587-2591. [8] Schultz, P.H., et al., 1982, *J. Geophys. Res*., **87**, 9803-9820. [9] Rotto, S., and K.L. Tanaka, 1995, USGS Map I-2441. [10] Neukum, G. and Hiller K., 1981, *J. Geophys. Res*., **86**, 3097-3121. [11] Hartmann, W.K. and Neukum, G., 2001, *Space Science Rev*., **96**, 165-194.

GEOLOGIC MAPPING OF THE MEDUSAE FOSSAE FORMATION ON MARS (MC-8 SE). J. R. Zimbelman, CEPS/NASM, Smithsonian Institution, Washington, D.C. 20013-7012 (zimbelmanj@si.edu).

Introduction: This report summarizes the status of a mapping project supported by NASA grant NAG5-11743 (the no-cost extension of which ended in April of 2006), and the current plans for new mapping of the Medusae Fossae Formation (MFF) on Mars through a proposal that was selected for funding by the Planetary Geology and Geophysics program in March of 2007. Money has not yet been received for this new grant, but here we present the areas identified in the proposal for mapping during the next three years.

MC-8 SE: Mapping in the eastern portion of MFF was initiated at 1:500K scale using the best available Viking images, then mapping commenced at 1:4M scale to provide a broader context. As THEMIS daytime IR coverage became steadily more complete, a map-projected base of daytime IR images was used for mapping at 1:2M scale, which we concluded was the best scale for portraying the MFF geology on the new base materials [1]. During the no-cost extension of the old grant, mapping proceeded to the point of completing a 1:2M scale map for the MC-8 SE quadrangle (0° to 15°N lat., 202.5° to 225°E long.) (Fig. 1, which includes a 0.5° margin around the quadrangle). Little change in the

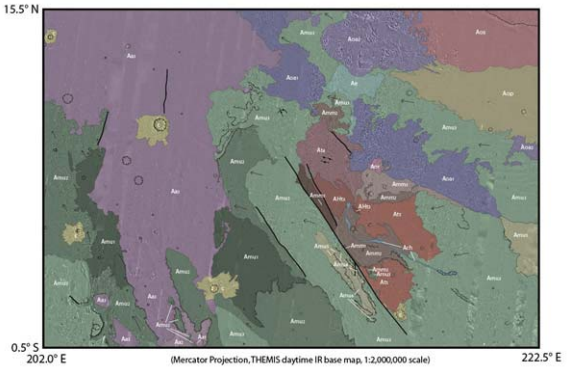

Figure 1. 2007 version of the MC-8 SE geologic map. See Fig. 2 for correlation of geologic units.

unit locations or designations (Fig. 2) are present on the new map, relative to the mapping and stratigraphy presented at the 2006 Mappers meeting, but structural mapping has been added in the new map. As a result of the mapping, we have identified six subunits to the upper member of MFF and three subunits to the middle member of MFF, expanding on the units as designated by Scott and Tanaka [2]. Conclusive evidence for the origin of the enigmatic

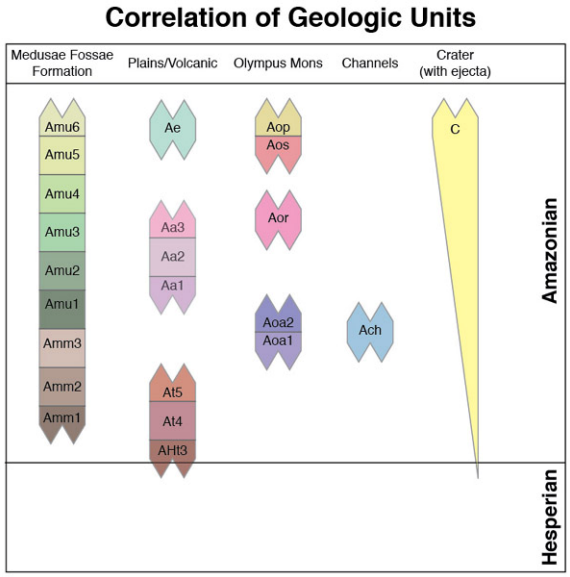

Figure 2. Correlation chart of the geologic units identified from mapping of MC-8 SE (Fig. 1). All units are derived from those as originally identified by Scott and Tanaka [2].

MFF materials remains elusive, but considerable progress has been made in evaluating the numerous hypotheses of formation that have been proposed for MFF. Our results to date have either an ignimbrite or an aeolian origin as the hypotheses with the greatest likelihood of being a part of the MFF story. We are optimistic that new data, such as the spectacular images now being returned by the High Resolution Imaging Science Experiment (HiRISE) (Fig. 3), plus results from the SHARAD and MARSIS radar sounders, will provide new evidence to aid in distinguishing between the two most viable hypotheses of origin.

MC-16 NW: A proposal to extend the mapping of MFF materials on THEMIS daytime IR base maps was selected for funding in March of 2007. Money for the new work has not yet been received, but here we present the main goals for the new mapping. MC-16 NW (0° to 15°S lat., 180° to 202.5°E long.) was identified for mapping because it includes large exposures of material previously identified [2] as upper (u-MFF) or middle (m-MFF) members of MFF (Fig. 4). This quadrangle also has large exposures of cratered highlands material, and we intend to devote particular attention to the contacts with these ancient materials in an effort to obtain better constraints on the likely emplacement of the MFF materials.

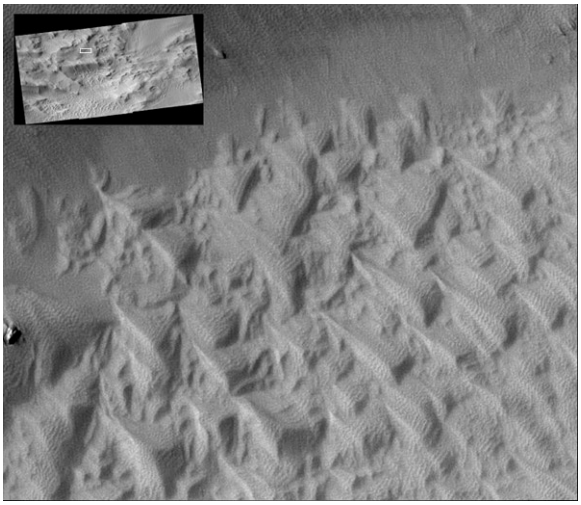

Figure 3. HiRISE image of MFF material in MC-8 SE. TRA_0001865_1905, 25 cm/p, center at 10.2°N, 211.5°E, NASA/JPL/U of A.

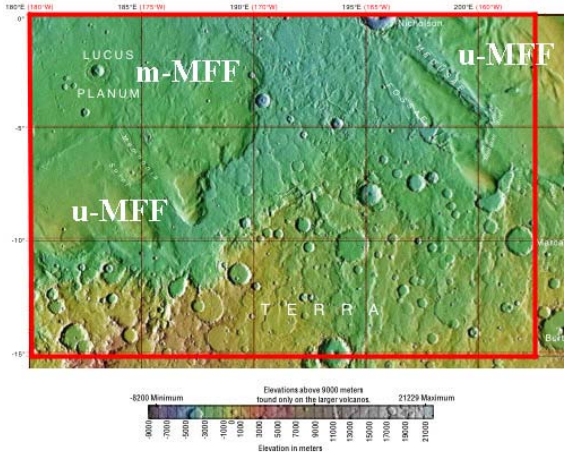

Figure 4. MC-16 NW quadrangle, on color-coded MOLA shaded relief base. u-MFF is upper member, m-MFF is middle member.

MC-23 NW: Previous mapping was carried out in areas where the upper and middle members of MFF have been dominant. MC-23 NW (0° to 15°S lat., 135° to 157.5°E long.) includes large exposures of the lower member (l-MFF) of MFF (Fig. 5), the unit showing the largest degree of erosion of all MFF materials [2, 3]. Unusual deposits superposed on the central peak of Gale crater (5°S, 138°E) will be investigated as a possible outlier of MFF material. HiRISE data will once again be crucial in refining the interpretation of the heavily eroded MFF materials, which are apparently sufficiently competent to maintain m-scale blocks during erosion (Fig. 6). We will most likely proceed first with mapping of MC-23 NW before starting work on MC-16 NW, in order to obtain initial interpretations of the lower member of the MFF materials, which has not yet been investigated through detailed mapping utilizing the recent data sets.

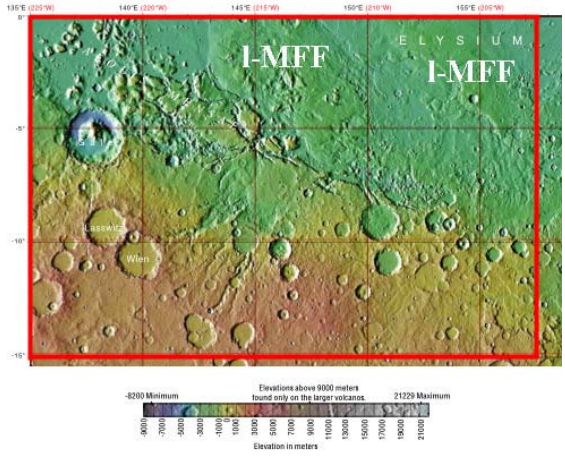

Figure 5. MC-23 NW quadrangle, on color-coded MOLA shaded relief base. l-MFF is lower member.

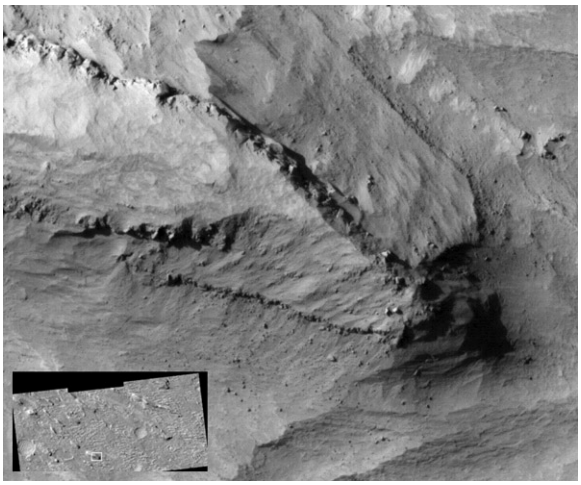

Figure 6. HiRISE image of the upwind nose of a yardang in MFF material just north of MC27-NW. TRA_000828_1805, 27 cm/p, center at 0.5°N, 142.5°E, NASA/JPL/U of A.

References: [1] Zimbelman, J.R. (2006) Planetary Geology Mappers Meeting Abstracts, Zimbelman_medusae_edited_final.pdf. [2] Scott D.H. and Tanaka K.L. (1986) USGS Map I-1802-A, 1:15,000,000 scale. [3] Greeley R. and Guest J. (1987) USGS Map I-1802-B, 1:15,000,000 scale.

Remote Geologic Mapping of Lunar Crater Volcanic Field, Nye County, Nevada: A Test for Planetary Geologic Reconnaissance. J.M. Dohm[1], K.L. Tanaka[2], J.A. Skinner, Jr.[2], L.A. Crumpler[3], and T.M. Hare[2], [1]Dept. of Hydrology and Water Resources, University of Arizona, Tucson, AZ, 85721 jmd@hwr.arizona.edu; [2]Astrogeology Team, U. S. Geological Survey, Flagstaff, AZ 86001; [4]New Mexico Museum of Natural History, Albuquerque, NM

Introduction: Geologic mapping of Mars and other planetary bodies in the solar system has recorded their evolutionary histories. Often cited geologic maps of Mars [1], for example, portray an episodically dynamic planet with magmatic, tectonic, water/ice, and wind activity throughout its recorded history, a picture supported by recent missions. Information obtained from these and future missions will continue to improve upon past mapping efforts by adding additional layers of information for further comparative analyses (increased perspectives at varying scales, including enhancing the geologic detective work and ultimately resulting in the identification of prime targets for further in situ investigation [2]). This includes testing and revising existing working hypotheses, as well as generating new ideas that stimulate further scientific inquiry.

Importantly, though the published geologic map information is often cited, the accuracy of the information and the utility of the mapping approaches that yield such information have not been field evaluated, except for the spatially limited reaches of Mars Sojourner (tens of meters) and the Mars Exploration Rovers, Opportunity and Spirit (tens of thousands of meters). For example, in question are the accuracies of unit assignments to outcrops, relative-age determinations of stratigraphic units and structures, and overall histories detailed by the mapping. While there have been numerous consistencies among existing geologic information (largely Viking-based) and diverse data sets recently acquired from the Mars Global Surveyor, Mars Odyssey, Mars Express, and Mars Reconnaissance spacecrafts (e.g., centers of tectonism correlate with MOLA-based topographic rises [3]), there has also been greater detail that has been unveiled, underappreciated during Viking-era mapping efforts (e.g., geologically recent and possibly currently active hydrologic activity [4,5]). The immense amount of new orbital- and field (lander and rover)-based information, which will add greater detail, and therefore ultimately improve upon the geologic maps and related interpretation, forms the basis for a new global mapping investigation of Mars currently underway [6, this meeting].

In order to optimize geologic mapping reconnaissance during this golden age of exploration and discovery, we have undertaken a timely investigation to assess remote planetary geologic mapping with grant support from the Mars Fundamental Research Program. We are using existing Mars-like terrestrial data sets (topography and visible and thermal infrared images at appropriate resolutions) to simulate Viking, Mars Global Surveyor, and Mars Odyssey data sets useful for performing remote mapping investigations of the test sites that can be evaluated through existing well-documented, field-based geologic information. Our team of planetary geologists is experienced in both terrestrial field mapping and remote mapping of planetary bodies including Mars. Our initial test focused on part of the San Francisco Volcanic Field of northern Arizona [7]. Below, we report on our second test.

Geologic and Physiographic Setting of the Second Test Site: Part of the Lunar Crater Volcanic Field, Nye County, Nevada, was geologically mapped during the second test using an approach similar to that used for planetary bodies such as Mars [8,9], in order to test the feasibility and accuracy of planetary geologic mapping. The volcanic field (Figs. 1 and 2) provides a suitable test site, as many features have analogs on the Moon and Mars, vegetation is minimal, and satellite data is available that approximates the quality and resolution of those of Mars. The test site includes cinder cones, maars, and basalt flows of Tertiary (Oligocene and Miocene) and Quaternary age. Intervals of relative quiescence and erosion separate episodes of volcanism. Variations in morphology, degree of weathering, and superposition and cross-cutting relations among volcanic constructs, flows (volcanic, fluvial, and alluvial), drainages, and tectonic structures provide a basis for determining relative age. Basement structural control is indicated by vent (cones and craters) alignments and their associated lava flows emplaced along normal faults and fissures, as well as drainage patterns. Magmatic differentiation at depth, which is based on petrographic analysis of basalts and pyroclastics, produced subalkaline basalts, alkali-olivine basalts, and basanitoids, the latter of which comprise the youngest flows in the field [10].

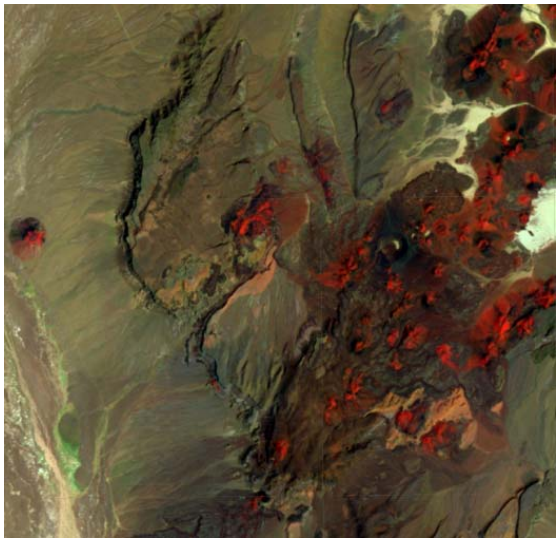

Figure 1. Landsat TM false-color image mapping test area, part of the Lunar Crater Field, Nevada; ~20 km wide; north at top.

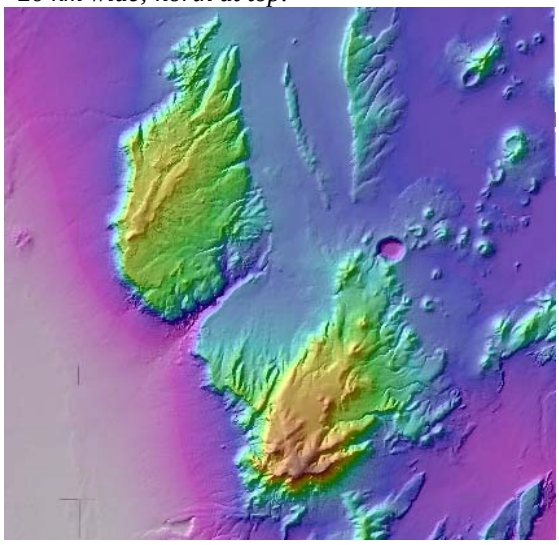

Figure 2. Color shaded-relief image of mapping test area; ~20 km wide; north at top.

Approach: We used image and topographic data that simulate those typically used to map the geology of Mars. Map units and stratigraphic relations are based primarily on morphology and superposition and cross-cutting relations, similar to the approach used for Mars [8,9]. Without prior knowledge of the volcanic field, each investigator mapped the test site separately and remotely.

Summary: Quantifiable stratigraphic and structural mapping information for comparative analysis among the published field-based information and the results of each mapper included: (1) total number of polygons, (2) total length of a specific contact type (e.g., certain, uncertain), (3) total number of faults, (4) total fault length, (5) total number of polygons and total area of (a) stratigraphically young mantling materials, (b) stratigraphically young volcanic materials, and (c) stratigraphically old materials, (6) total area and number of features interpreted to be vent structures, and (7) fault-length density with respect to (i) mantling materials (e.g., alluvial and fluvial deposits), (ii) stratigraphically young volcanics, (iii) vent structures, and (iiii) stratigraphically old materials. Such an analysis provides us with useful information, including the reliability of identifying and interpreting map units, structure, and superposition relations among map units and structure. In addition, such information provides the basis for assessing the approaches and primary focuses of individual mappers. A significant variation in total number of mapped tectonic structures, for example, indicates that mapping emphasis and experience directly bears on mapping results (one mapper may focus on stratigraphy and resurfacing from fluvial activity while another on stratigraphy and tectonic deformation). Findings of this investigation, including consistencies and inconsistencies among the ground-truth and remote-based mapping information, lessons learned, and underlying implications on the overall utility of planetary geologic mapping, will be presented at the mappers' meeting.

References: [1] Scott, D.H., Tanaka, K.L. (1986) *USGS Misc. Inv. Ser. Map, I-1802-A* (1:15,000,000). [2] Dohm J.M., et al. (2004) *Planet. Space Sci.* 2, 189-198. [3] Anderson, R.C., et al. (2001) *J. Geophys. Res.* 106, 20,563-20,585. [4] Ferris et al. (2002) *Geophys. Res. Lett.* 29, 10.1029/2002GL014936. [5] Miyamoto, H., et al. (2004). *J. Geophys. Res.* 109, doi:10.1029/2003JE002234. [6] Tanaka et al. (2007) *Abstracts, Seventh Intl. Conf. Mars*. [7] Tanaka et al. (2004) *Abstracts, PGM meeting*. [8] Dohm, J.M., et al. (2001) *USGS Map I-2650*. [9] Tanaka, K.L., et al. (2005) *USGS Map SIM-2888*, scale 1:15,000,000. [10] Scott, D.H., Trask, N.J. (1971) *USGS Prof. Pap. 599-1*.

GEOSCIENCE DATA VISUALIZATION SYSTEMS APPLIED TO PLANETARY GEOLOGICAL MAPPING. J. W. Head[1], Prabhat[2], A. S. Forsberg[3], A. T. Basilevsky[1,4], M. A. Ivanov[1,4], J. L. Dickson[1], C. I. Fassett[1], J. S. Levy[1], G. A. Morgan[1], and P. Senthil Kumar[1,5], [1]Dept. of Geological Sciences, Brown University, Providence, RI 02912 (james_head@brown.edu), [2]Center for Computation and Visualization, Brown University, Providence, RI 02912, [3]Dept. of Computer Science, Brown University, Providence, RI 02912, [4]Vernadsky Institute of Geochemistry and Analytical Chemistry, RAS, Moscow, Russia, [5]National Geophysical Research Institute, Hyderabad 500007, India (senthilngri@yahoo.com).

Introduction and Background: Traditional methods of planetary geological mapping have relied on photographic hard copy and light-table tracing and mapping. In the last several decades this has given way to the availability and analysis of multiple digital data sets, and programs and platforms that permit the viewing and manipulation of multiple annotated layers of relevant information. This has revolutionized the ability to incorporate important new data into the planetary mapping process at all scales.

We are currently investigating important new technological developments in computer visualization display in order to assess their importance and utility in planetary geological analysis and mapping [1,2]. At a fundamental level, there is a poor understanding of how computer visualization display qualities (e.g., level of immersion, stereoscopic vs. monoscopic viewing, field of view, large vs. small display size, etc.) influence performance on scientific analysis and geological mapping. We are exploring four different environments: 1) conventional desktops (DT), 2) semi-immersive Fishtank VR (FT) (i.e., a conventional desktop with head-tracked stereo and 6DOF input), 3) tiled wall displays (TW), and 4) fully immersive virtual reality (IVR) (e.g., "Cave Automatic Virtual Environment", or Cave system). While we have completed some formal studies demonstrating that fully immersive Cave environments are superior to desktop systems [e.g., 3], there is still much to learn and understand about how the varying degrees of immersive displays affect task performance. It is clear that the new availability of ultra-high-resolution datasets presents challenges in terms of handling and visualization. But due consideration must also be given to the final medium on which these phenomenal images are displayed. For example if a HiRISE image has 20Kx40K pixels, and the researcher is using a 1280x1024 desktop monitor to explore the image, the researcher will waste a lot of time in image zooming/panning to balance the analysis-driven need for both detail as well as context. If higher-resolution media, such as an IBM Bertha display 3840x2400 or a tiled wall with multiple projectors is used, we have found through four months of weekly meetings that they definitely improve the efficiency of analysis and mapping.

ADVISER: System Description: We are developing ADVISER (ADvanced VIsualization for Solar system Exploration) [1,2] as a tool for taking planetary geologists virtually "into the field" in support of several scientific themes and are assessing its application to geological mapping. The project aims to create a field experience by integrating multiple data sources and presenting them as a unified environment to the scientist. Additionally, we are developing a virtual field kit, tailored to supporting research tasks dictated by scientific and mapping themes. Technically, ADVISER renders high-resolution topographic datasets (8192x8192 samples) in stereo at interactive frame-rates (25+ frames-per-second). The system is based on a state-of-the-art terrain rendering system [4]. The system is highly interactive; for example, vertical exaggeration, lighting geometry and contour lines can be modified by the user in real time. High-resolution image data can be overlaid on the terrain and other data can be rendered in this context. A detailed description and case studies of ADVISER are available [1,2].

In our previous work we have exported many of the ADVISER functions to a desktop environment and made comparisons of the utility and productivity of the two media [1,2]. We are now beginning to explore the middle ground between Desktop displays (DT) and Cave displays (IVR) in terms of both 1) availability to a wide range of users, and 2) utility for scientific analysis and geological mapping. In our preliminary assessment we have found that the most effective capabilities in the middle range include the semi-immersive "fishtank display" (FT) and high-resolution tiled-wall displays (TW) and we are currently beginning to explore and evaluate this hardware spectrum "middle ground".

Application to Science Analysis and Mapping: ADVISER was originally designed for a Cave [1] because we believed the Cave's large-scale stereo display was most appropriate for doing "virtual fieldwork", but we are adapting its functionality to run on conventional desktop systems for two reasons: 1) to make it more generally accessible, and 2) to help us learn about the relative value of the information that can be gathered from both systems. While the Cave and desktop represent possibly two extreme ends of the VR spectrum, there are other intermediate systems, such as a Geowall (see http://www.geowall.org) which utilize a 1-wall stereo display. Such systems are less expensive than the Cave and are potentially better suited for wider deployment.

The desktop system has a high-end nVidia graphics card; 2GB RAM and a Pentium 4 processor. A video game controller (Logitech dual-action gamepad) is used to provide navigational input to the program. Our Cave system is an 8'x8'x8' cube with four projection surfaces (three walls and the floor). Four linux machines (identical in performance to the desktop machine) provide data for the Cave. Users utilize a handheld 3D tracked input device to navigate. Our 3D input device has a joystick and is simple to use. To navigate, the user simply points in the direction he/she wants to fly and pushes the joystick forward or backward to move relative to that direction. The user can push the joystick to the left and right to rotate his/her position in the virtual world. A collision detection algorithm is used to prevent the user from going underneath the surface.

A 200 dpi IBM Bertha display at Brown enables us to conduct desktop-based exploration sessions and a 9-projector, active stereo, tiled-wall display with an effective resolution of 2400x1800 is available next to the Cave in the Center for Computation and Visualization. In our past ADVISER geoscience research activities, we exclusively used the Cave and desktop environments for exploration. Recent commercial demand for high-definition and high quality display has helped improve our capabilities in this area. While Caves in general provide for a better immersive experience, desktops are brighter and crisper than our current Cave, but their dis-

play area is relatively small. Our current tiled wall is a middle ground and has bright, crisp images on a large display surface. Fishtank VR is most similar to a regular desktop system, but adds head-tracked stereo viewing, and typically 3D tracked input devices. The effect is comparable to looking into a fishtank (its namesake) where objects appear in stereo, but the working volume is physically small, effectively producing a diorama-like "world in miniature." The exploration of this middle-ground has been shown to be very useful, particularly in terms of tiled displays for group discussion and analysis, and in geological mapping on Venus and on Mars.

Testing the Different Platforms: We are developing the ADVISER system primarily to assist graduate-level geoscience research, but its basic function of interactively navigating 3D terrains also serves as an educational tool. We have tested the desktop and Cave systems in Geological Sciences 5 (Mars, Moon and the Earth), an introductory geosciences course at Brown University. Students learn about scientific study and analysis, how the Earth works, where the Earth fits into the solar system, the themes in the formation and evolution of planets, and how this information relates back to better understanding of the Earth. The course consists of lectures, reading assignments, homework, and laboratory exercises.

Students learn that geologists study the Earth and its evolution through field work and analysis of the geological record at various points on the Earth's surface. Geologists then integrate these individual data points about the Earth's surface by means of more synoptic analyses, often aided by the perspectives seen from image and topographic data acquired from Earth orbit. In contrast, planetary geoscientists commonly work in the reverse order, since the distances and times involved in acquiring data dictate that the first data from individual moons and planets comes from flybys and orbital spacecraft. Later, in some cases, more detail comes from the deployment of a few landers and rovers and, in the case of the Moon, human explorers. Consequently, there is a huge difference today between the local analysis of the Earth and the remote analysis of other planets. For example, while Earth geoscientists employ the 3D in-situ strategies described above in analyzing their data, most planetary geoscience analysis is done using either static or interactive 2D visualizations.

To help do fieldwork in remote places, immersive virtual reality (IVR) systems let one or more people visit a computer generated world. Thanks in part to the video game industry and other new technologies, VR worlds can be explored interactively and contain amazing detail. The experience can be similar to an interactive stereo IMAX film, with wide field-of-view display and a strong sense of spatial relationships between visual features. Geoscientists use IVR to recreate and interact with distant places by using both remotely obtained data such as topography and images of the surface as well as simulated data (like atmospheric conditions varying with time) as a foundation of a visual world (Figs. 1-2).

For three years, Geo 5 students have used ADVISER to complete a laboratory exercise about the geological history of Mars. In this exercise groups of three students first pose questions about the geology of Mars and subsequently "virtually" visit Mars's surface using ADVISER. During their "visit" the students search for evidence pertaining to their questions. After three years of successfully running and customizing the lab, this past year we formally collected information from students about the educational experience [3]. In general students highly prefer a Cave-like system to a conventional desktop display for learning about geology and topography datasets. This preference is indicated by their ratings and choice of Cave as the preferred medium for future exploration. Both Cave and desktop media are preferred, however, to a standard 2D image-based investigation. Students report positively about the insights gained from the Lab exercise [4], an indication that 3D visualization is a valuable tool in teaching students about topographic and geologic datasets, and thus has a high potential in future applications to geological mapping.

Summary and Directions: We are striving for interdisciplinary collaborations that span the space science and computer science disciplines by 1) working very closely and iteratively with our computer science colleagues and collaborators, 2) involving interdisciplinary science partners within space science and the NASA community (geosciences, atmospheres, multiple instruments, the international community), and 3) bringing the new technological developments to the attention of this entire spectrum. Planetary geological mapping is an important part of these applications. We have explored these capabilities and have tested them in classroom laboratory situations and in individual seminar sessions dedicated to geological mapping projects. We find that each of the platforms has unique capabilities and that science analysis and geological mapping are enhanced by their use. In the coming year we are completing several test mapping cases on different planetary bodies and we will be tabulating and presenting the advantages and disadvantages of each of these media in scientific analysis and geological mapping.

References: [1] Head, III, J.W. et al. (2005) Photogrammetric Engineering and Remote Sensing (PE&RS), Vol. 71:10. [2] Forsberg, A. et al. (2006) IEEE Computer Graphics and Applications, 26:4, pp. 46-54. [3] Prabhat et al. (2007) Lunar and Planetary Science 38, #1297. [4] Hwa, L.M. et al. (2005) IEEE Transactions on Visualization and Computer Graphics, 11: 4, pp. 355-368.

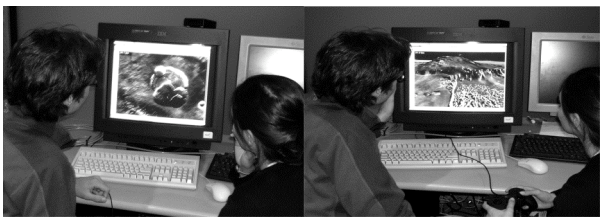

Fig. 1. Students explore Olympus Mons at a conventional desktop system. A videogame-like controller lets the students navigate around the volcano. A view from the top of the caldera is on the left, and a perspective view closer to the flanks of the volcano is on the right.

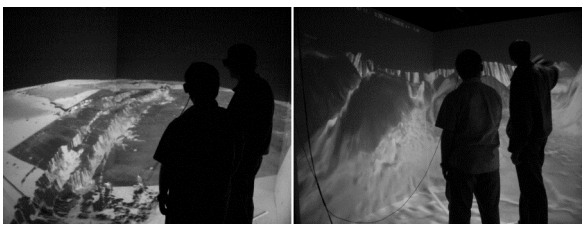

Fig. 2. Students fly through Valles Marineris in a Cave. A 3D wand input device lets the students interactively fly freely around the terrain in search of important geological features.

Acknowledgments: The NASA Applied Information Systems Research Program and the NASA Planetary Geology and Geophysics Program are gratefully acknowledged.